INFORMATION TO USERS

UMI

Classification, Biomass Estimation, and Carbon Dynamics of a Northern Forest using SIR-C/X-SAR Imagery

by

Kathleen Mary Bergen

A dissertation submitted in partial fulfillment
of the requirements for the degree of
Doctor of Philosophy
(Natural Resources and Environment)
in The University of Michigan
1997

Doctoral Committee:

Professor Charles E. Olson, Jr., Chair
Professor Burton V. Barnes
Professor Gary W. Fowler
Assistant Professor Johnathan Levine
Assistant Professor Mark Wilson
Associate Research Scientist M. Craig Dobson

UMI Number: 9721945

Copyright 1997 by
Bergen, Kathleen Mary

UMI
300 North Zeeb Road
Ann Arbor, MI 48103

Dedicated to
Jack and Katie
John, Keith, and Kenton
for always being there
and
Craig, Josef, Leland, and Paul
for their generous friendship and help
throughout our work together

ACKNOWLEDGEMENTS

ABSTRACT

CLASSIFICATION, BIOMASS ESTIMATION, AND CARBON DYNAMICS OF A NORTHERN FOREST USING SIR-C/X-SAR IMAGERY

by
Kathleen M. Bergen

Chair: Charles E. Olson, Jr.

Because of the significance of C resident in forest trees, efforts are being directed to better quantify the amount and distribution of this component of the global C cycle. The need for information over large areas has lead to the implementation of remote sensing instruments such as synthetic aperture radar (SAR). This dissertation addresses all of the stages needed to derive the parameters fundamental to assessing C storage and change using a primarily SAR-based methodology. These include: 1) ground reference data, 2) forest classification, 3) biomass estimation, and 4) C estimation. The imagery used is multi-temporal SIR-C/X-SAR imagery of the NASA Michigan Forests Test Site (MFTS) in the Hiawatha National Forest in northern Michigan.

Ground data was collected and analyzed for 70 forest test stands. These data include stand structural and biomass statistics used for image classification and construction of biomass, C, and ANPP (above-ground net primary production) estimation functions. A hierarchical structural methodology is used to classify SIR-C/X-SAR scenes to Level II (forest community). Overall unbiased accuracies are compared and results show that multi-temporal (97%) may show improvement over single-date (April 90%, Sept. 95%, and Oct. 98%), and definitely shows good improvement over pooled (April 90%, Sept. 77%) classifications. Empirical biomass estimation algorithms are developed for each structural type and when combined with the classified image, above-ground biomass is mapped in the image domain at 5.79×10^9 kg in 51,448 ha's. Finally, three components of C storage and change are estimated: (1) C stored in above- and below-ground living vegetation(3.22×10^9 kg), (2) C gain from ANPP (0.75 to 1.31 kg/m^2/yr), and (3) C removed by forest harvesting (6.02×10^6 kg).

Results confirm that it is possible to successfully develop a multi-stage approach to estimate C storage and change using SIR-C/X-SAR imagery as the major data set. This provides a new method for estimating these parameters at the landscape level. The method improves on previous ones by incorporating actual (as opposed to potential) vegetation cover, plus the amount of vegetation, and results in quantifications which are significantly closer to measured calibration values.

TABLE OF CONTENTS

LIST OF TABLES

LIST OF FIGURES

LIST OF APPENDICES

CHAPTER 1

INTRODUCTION AND BACKGROUND

1.1 Introduction

The past several decades have seen a scaling-up of ecological research. Where 20 years ago over 50% of quantitative ecology was carried out on plot scales of a meter square and global geography was primarily descriptive, current large portions of the ecology research agenda are being directed to rigorous quantification and modeling of Earth system states and processes on scales from regional to global (Shugart et al., 1992). This focus builds on knowledge gained from intensive small scale research and combines it with new data and techniques to assess a larger picture.

The impetus for this scaling up may be attibuted to the convergence of several factors. Beginning in the 1950s there have been a series of environmental problems whose potential mitigation has required the understanding and quantification of how processes operate over larger regions. The pesticide DDT, acid rain, global climate change, desertification, and loss of habitat and biodiversity are several of the major issues which have shaped the ecology science agenda and its funding in recent years.

At the same time, advances have been made in both the theory and the tools to enable study of these issues at a much larger scale and with a more intensively quantitative focus. On the theory side are the maturing of a working body of knowledge in spatial analysis, electromagnetics, modeling, ecology, and earth systems science. These are combined with rapidly increasing computing power, more and better digital satellite data, and specialized computing software including geographic information systems, image processing, modeling, and statistics. Together these provide the basis from which to efficiently tackle analysis of regional to global environmental issues.

All of the problems mentioned above, and in particular that related to global climate change, require large-scale knowledge of vegetation: the distribution of vegetation and landscape units, the amount or biomass of vegetation, and the amount of carbon (C) stored in terrestrial vegetation and its fluxes. Remote sensing is seen as the key to providing this information up to a global scale. Development and demonstration of a methodology to to

1

derive such vegetation information using synthetic aperture radar (SAR) remotely sensed imagery is currently being tested at the NASA Michigan Forests Test Site (MFTS), and this is the focus of this dissertation.

Why use SAR? Synthetic aperture radars do not record reflected or emitted solar radiation as do optical sensors (such as Landsat), but are active sensors which transmit their own energy and then record its reflectance back to the sensor. SARs use the microwave portion of the electromagnetic spectrum, and have wavelengths ranging from 1 cm to 60 cm. In forests, optical sensors in the short wavelength visible and near-infrared are responding to internal leaf structural and pigment characteristics. At its longer wavelengths, the magnitude of SAR reflectance is dependent on larger structural characteristics (tree architecture) and moisture content. With such longer wavelengths SAR may also effectively penetrate the forest canopy to provide information on tree bole biomass, tree moisture, soil moisture, and surface topography. Because it is independent of solar illumination, and precipitation and clouds are invisible to SAR's longer wavelengths, this sensor is used for diurnal monitoring, and for acquisition of information in frequently cloud-covered boreal or tropical regions. Thus SAR is expected to have advantages in quantifying biophysical parameters (biomass, C storage), and in mapping vegetation, and this provides the foundation for the research goals described below.

1.2   Contributions and Goals of this Dissertation

Several North American study sites located in different biomes have been initiated by NASA as long term research sites for the purpose of Synthetic Aperture Radar (SAR) vegetation ecology studies. These test sites were initiated in particular for the SIR-C/X-SAR program. SIR-C/X-SAR is a multi-channel SAR which was flown aboard the space shuttle Endeavor in April 1994, and again in October, 1994. NASA SIR-C/X-SAR test sites whose efforts are directed toward ecological investigation include the Michigan Forests, USA (north temperate-boreal forest transition), Duke Forest, USA (southern pine-hardwoods), Prince Albert and Nelson House, Canada (extreme boreal), Howland Maine, USA (boreal), Manaus, Brazil (upland and plain tropical forests), and Sena Madureira, Brazil (tropical forests) sites (Stofan et al., 1995). These and other affiliated research sites are contributing to analysis of the multi-date SIR-C/X-SAR data set. The MFTS was established in 1990, and the purpose of the research associated with this site is to investigate the use of SAR image data in land-cover classification, biophysical parameters estimation, image calibration, and development of theoretical microwave canopy scattering models. The location of the test site in Michigan and its situtation within the northern hardwood-conifer forest (NHCF) is shown in Figure 1.1.

Since its inception in 1990, the MFTS has been imaged not only by SIR-C/X-SAR, but also by ERS-1/2 and JERS-1, and has received frequent JPL AIRSAR overflights. These SAR sensors are discussed in section 1.3. Analysis of the image data to achieve the goals of
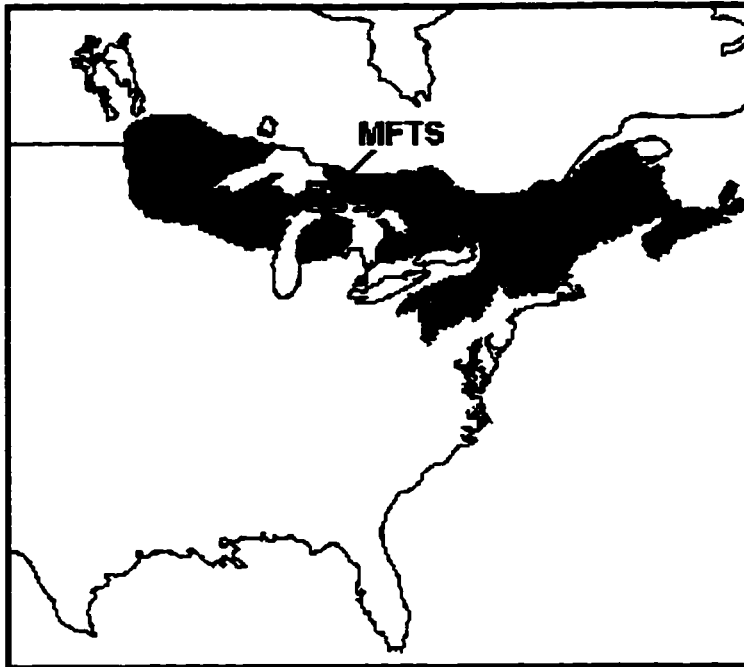
Figure 1.1: Michigan Forests Test Site (MFTS) and northern hardwood and
conifer forest (NHCF) (adapted from Mladenoff and Pastor,
1993, Bormann and Likens 1979).

the test site has proceeded in step with image acquisition. The research goals of this disser-
tation have been central to meeting those for landcover classification and forest biophysical
parameters estimation using SIR-C/X-SAR data. Additionally this dissertation extends
beyond these to estimate C storage and change and recommend methods for incorporating
such information in larger empirical and process models.

The specific contributions of this dissertation are:

1. Development of the test site reference data set, including test stand structure and
biomass,

2. Multi-temporal land-cover classification,

3. Forest biomass estimation, and

4. Quantification of C storage and change.

These are developed and discussed below with emphasis on the purpose of each.

1. Development of the Test Site Data Set:

Most classification procedures, including those developed for the present study, are given
some form of training data from ground surveys which are used to statistically define the
classes that are to be separated. Also, biomass estimation algorithms developed by empir-
ical regression relate biomass of known areas on the ground with image backscatter from

the same areas on the imagery using some combination of channels. Empirical based C estimations such as those for above-ground net primary productivity (ANPP) over a continuous geographic region incorporate allometric equations developed in part from ground measurements.

For these reasons an extensive database of ground reference data was intended to be a major effort of the MFTS from the beginning. Toward this end 70 four-ha permanent test stands representing the distribution of forest cover in the test site were established in the MFTS beginning in 1990. Chapter 2 documents the sampling methodology, statistical analysis, and results for the detailed measurements which were made in each stand to quantify stand community composition, structure, and biomass. This database is central to the SIR-C/X-SAR derived land-cover classification, biomass estimation, and C estimation analysed in this dissertation but will also be used by additional researchers at the University of Michigan Radiation Laboratory and at other institutions.

2. Land-cover Classification:

Land-cover classification at the MFTS is both a goal in itself and is also a prerequisite for boimass and C estimation which use information on forest structural type in their algorithms. Three aspects of SAR-based classification are explored in this dissertation. These are: (1) use of structural attributes for determining classes, (2) the appropriateness of various classification methodologies, and (3) the possible advantages of multi-temporal classifications. Because of its longer wavelengths (1 - 60 cm), SAR response is to larger structural characteristics of vegetation. These structural characteristics vary by species and/or community, and this is the primary physical basis upon which SAR vegetation class discrimination results. To derive classifications, several methodologies may be employed and include Bayesian, knowledge-based, supervised, unsupervised, and other methodological variants. Here a hierarchical classifier is used which combines a knowledge-based technique to deliniate very general land-cover categories, and then a Bayesian algorithm is used to further subdivide these into more detailed classes. Finally, multi-temporal aspects are explored because biophysical systems in temperate regions undergo distinct changes in each annual cycle, and for forested ecosystems this includes moisture and phenological changes. The dual-flight program (April and October) for the SIR-C/X-SAR instrument aboard the shuttle Endeavor was designed expressly to acquire imagery at different stages of such cycles. This provides a new opportunity in terrain classification where phenology and moisture changes may be used as additional information. Methodologies, analyses and results for SIR-C/X-SAR land-cover classifications are presented in chapter 3.

3. Biomass Estimation:

A goal of this dissertation is to map forest biomass in the image domain. Because SAR operates at much longer wavelengths than optical sensors, it can therefore effectively penetrate even a closed forest canopy and provide information on the tree boles, branches, and underlying surface. For this reason, and because there is a quantifiable relationship between

vegetation biomass and SAR backscatter, SAR has been considered to be especially suited to estimating forest biomass. The biomass results in this dissertation follow a methodology previously developed for the MFTS (Dobson et al., 1995). Application of this methodology follows the classification results in chapter 2 because biomass algorithms have been found to be structurally (class) dependent (Dobson et al., 1995). In the biomass estimation methodology functions are developed using least squares regression which predict biomass as a function of selected SAR frequency and polarization. Different functions are developed for each of the forest communities (structural categories) at the site. Resulting algorithms are then applied on a pixel basis to map biomass over the region.

4. Quantification of Carbon Storage and Change:

There are three goals in the present study to demonstrate the application of SAR to estimating C storage and change: (1) estimate C stored in living vegetation at the MFTS (both above- and below-ground), (2) determine C gain from above-ground net primary productivity (ANPP), and (3) measure changes in C balance related to forest disturbance (clearcutting). To estimate C storage and ANPP a method is developed which uses as inputs the classified image, the biomass image, and allometric equations available in the literature which relate below-ground biomass or ANPP to individual stem diameters. New algorithms are developed which relate below-ground biomass to above-ground biomass and ANPP for each structural class at the stand level. Results are mapped in the image domain as above-ground C, below-ground C, total C and ANPP. In addition, a second method is developed to predict C removed by forest harvesting which uses a combination of image differencing and simple decision rules. Results are maps of clearcuts and quantification of C removed. This is the first study to publish results on C parameters derived from SAR imagery.

The remainder of this introduction provides background information on SAR physical fundamentals, a literature review, and the status of research on SAR applications in ecology.

1.3   SAR Fundamentals

Radars are active sensors operating in the microwave portion of the electromagnetic spectrum which effectively ranges from 1 to 60 cm wavelengths. A SAR, or synthetic aperture radar, is a radar in which a very long antenna is artificially synthesized for the purpose of greatly increasing resolution of the instrument while maintaining a relatively compact physical size. The capabilities of each SAR can be characterized by two factors, its frequency(s)/wavelength(s) (wavelength $= \lambda = 30/f(GHz)$) and polarization(s). Those that have the capability to operate in several frequencies/wavelengths and all possible polarizations are called multi-frequency polarimetric SARs. The four predominant frequencies/wavelengths used in available imaging radars are: X-band (10 GHz, 3.0 cm), C-band (5.3 GHz, 5.6 cm), L-band (1.225 GHz, 24.5 cm), and P-band (0.44 GHz, 68 cm).

5

The length of the SAR wavelength determines the extent to which it can penetrate a forest canopy. Different polarizations of the electromagnetic waves can also be transmitted and/or received in any of the above wavelengths (e.g., hh is horizontal receive, horizontal send, hv is horizontal receive, vertical send). Different geometries of earth features affect the polarization of the energy received, and thus polarization signatures can also be a discriminating tool. SARs can be absolutely calibrated so that backscatter values across many different images from different times can be directly compared.

For forest applications of SAR it is important to understand the causes of backscatter. With optical sensors operating in the visible portion of the spectrum, response is primarily from pigments at the cellular level in canopy leaves. In the near-infrared portion (0.7-1.2), the response has been determined to be from internal leaf structure - cell wall/air interface, and in the remainder of the infrared mainly from moisture content (Rhode and Olson, 1971; Willstater and Stoll, 1918). The longer wavelengths used with SAR respond primarily to two properties: structure/geometry and electrical properties/moisture. Structural characteristics which radar return is dependent upon include shape, size, and orientation of individual scatterers (such as leaves and small branches at X or C bands, and entire trees at L or P bands) plus structure of the entire community (density, height, row spacing and orientation). The electrical properties of a feature may be measured by its complex dielectric constant. Pure water has a dielectric constant of about 80, dry natural materials (including tree bark and heartwood, and dead trees) have a dielectric constant in the range of three to eight, and the vascular cambium of healthy forest trees in the summer condition ranges from approximately 15-30, differentiating to some extent by species (Ulaby et al., 1981; Bergen et al., 1994; Bergen et al., 1995b). Trees (unless seedlings), with their relatively large surface areas and high moisture contents, are particularly good reflectors of radar energy and can produce very high (bright on the imagery) backscatter amplitudes.

The earliest spaceborne imaging radar was Seasat-1, an L-band, hh SAR. It failed 99 days after launch, but provided intriguing images indicating potential applications for geology, land cover mapping, water resources, and agriculture in addition to the ocean features and processes for which it was designed. Thus NASA adopted a program to launch three imaging SARS onboard space shuttle missions over the next fifteen years. The first of these was SIR-A, also an L-band, hh polarized SAR. The SIR-A mission was a success, and one of the interesting discoveries made with SIR-A was its capabilities to image subsurface (buried) river channels and archeological features in arid areas. SIR-B was launched in 1984 with an L-band, hh polarized SAR which had a tilt feature that could be activiated to look at the earth from varying look angles. SIR-B data was used extensively in early vegetation studies, both agricultural and forest.

After a delay in the shuttle schedule, the third SAR, SIR-C, was finally launched in April 1994 onboard the space shuttle Endeavor. It was flown a second time in September/October 1994 for the purposes of providing data from two seasons. SIR-C is a L and C-band multipolarization SAR and was joined by an X-band vv polarized SAR carried as part of the

6

shuttle payload for the Federal Republic of Germany. SIR-C/X-SAR is the first spaceborne multi-frequency, fully polarimetric SAR. The aim of the SIR-C/X-SAR shuttle missions was to collect imagery for environmental monitoring and global change studies. The MFTS was one of several test sites world-wide to be imaged during this shuttle mission, and in addition to the stand structure and biomass data collected from 1991-1994, extensive time-sensitive ground measurements (especially tree moisture, soil moisture, snowpack and precipitation) were carried out during the shuttle overpasses (Bergen et al., 1994; Bergen et al., 1995b).

Several other space agencies have launched spaceborne orbiting SAR satellites. In 1991, the European Space Agency launched ERS-1, a C-band SAR with a resolution of 30 m. In 1993 the National Space Development Agency of Japan launched JERS-1, an L-band SAR with a resolution of 25 m. ERS-2 was launched in 1995 and has the same parameters as ERS-1 which is still orbiting. RADARSAT is a Canadian C-vv SAR launched in 1996, which is used extensively for ice monitoring.

In addition to spaceborne SARs, several airborne SARs have provided imagery for terrestrial applications. The most widely flown is the NASA/JPL AIRSAR. The AIRSAR is a multi-frequency/multi- polarization SAR (C, L, and P frequencies and hh, vv, and hv polarizations) with a resolution of 7 m.

Early AIRSAR and spaceborne SARs including SEASAT and SIR-A were processed optically and not digitally. The resulting imagery could be optically scanned and digitized into "gray values" between 0-64 or 0-255. The advent of SIR-B, AIRSAR, SIR-C/X-SAR and ERS-1 beginning in the mid-late 1980's provided the first fully digital data where the numbers associated with each pixel are the actual amplitude and phase of the backscattered signal. With this information absolute image calibrations and much more refined data extraction are possible, but this capability is still relatively new. While this dissertation uses SIR-C/X-SAR data, it builds upon methodologies and results from all of the above instruments, especially those developed with AIRSAR and ERS/JERS.

1.4 Background on SAR in Vegetation Ecology

SAR applications in vegetation ecology cover a number of areas including land-cover classification and biophysical parameters estimation. The following sections (1) provide a literature review or background on related research to date, and (2) develop the foundation for the methodologies and results presented in the chapters 3-5 on classification, biomass estimation, and estimation of C storage and change, respectively.

1.4.1 Land-Cover Classification: The Hierarchical Structural Approach

Significant development of the classification conceptual model of SAR response to different earth terrain has come from theoretical results synthesized using MIMICS. MIMICS is a forward scattering model for single-frequency and polarimetric SAR based on radia-

tive transfer theory, and may be employed to predict backscattering response as a function of earth terrain and sensor parameters (Ulaby et al., 1990). MIMICS simulations have confirmed the importance of vegetation structure and dielectric properties in classification efforts, and these have been incorporated into the theory underlying the classifier design used in this project.

SAR response at a given wavelength (λ) and polarization is known to be determined by (1) structural or geometric properties and (2) dielectric properties. The contributing structural properties of vegetation are (1) size distribution of vegetation components (for trees main stem, branches, and foliage), (2) orientation of scatterers, and (3) densities of structural elements. Dielectric properties may be defined in terms of discontinuities at boundaries determined largely by volumetric water content, the phase of water (liquid or frozen), and specific dry density of the scatterers. To date a solution for separating the effects of structure and moisture has not been achieved by the SAR research community. However, the moisture contribution to the signal in general is small in the MFTS SIR-C/X-SAR images analyzed compared to that of structure. In the case of multi-temporal classification moisture differences are not noise, but are useful information which can be used to discriminate forest classes or to infer changes in canopy and soil moisture status.

Structural categories or growth forms relevant to SAR are presented in Figure 1.2 (Dobson et al., 1993). A more in-depth discussion of the conceptual model for structural classification of vegetation is developed in Dobson et al. (1996), where the structural classes are compared with MIMICS simulations of each of the classes over a range of size or "age" distributions at C-vv and L-hh. Results of this show that backscatter is sensitive to both the structure and the quantity of structure (vegetation biomass). To separate different vegetation types on these bases, the backscattering coefficient (σ°) must be separable in the spectral, spatial, or temporal domains. In Dobson et al. (1996) only the spectral domain is used but with two frequency/polarization combinations (C-vv, L-hh) whose spectral gradient $\sigma_{L}^{\circ}/\sigma_{C}^{\circ}$ is significantly different to allow successful separation of gross structural classes (e.g., grass, excurrent trees, decurrent trees).

In addition to scattering models such as MIMICS, there is a growing body of research using existing SAR datasets which also present strong evidence for the structural control component of the relationship between terrain and backscatter. Several knowledge-based approaches in this category have been investigated. An unsupervised knowledge-based technique has been developed and used by Van Zyl (1989), and later by Moghaddam and Freeman (1993), where polarimetric data is used in identifying dominant scattering mechanisms from the average Mueller matrix. This is followed by application of a set of hierarchical decision rules to classify very general landcover categories. An approach developed at the University of Michigan (Pierce et al., 1994a) on AIRSAR and SIR-C imagery uses simple knowledge-based rules and is discussed below. Additional work at the University of Michigan used an explicit knowledge-based structural classifier to discriminate very general land-cover and a Bayesian methodology for further subdivision of these classes. (Pierce et

Examples	Foilage	Small Stems	Main Stem
surface	None	None	None
gramineous	blade or needle	none	none
stalk dominated grasses (corn, cat tails)	blade-like	none	erectophile
shrubs	broadleaf	present	none
pine, spruce, fir	needle-leaf	present	erectophile/ excurrent
deciduous broad leaf	broadleaf	present	non-erectophile decurrent
palms	fronds	none	erectophile/ columnor

Figure 1.2: Description of simple structural classes of vegetation.

9

al., 1995).

The JPL AIRSAR is a fully polarimetric airborne SAR operating at P (0.4 GHz), L (1.25 GHz), and C (5.3 GHz) bands. Beginning in 1990, use of JPL AIRSAR at L- and C-bands as a SIR-C testbed for terrain classification was explored in an ecoregion similar to the MFTS at the University of Michigan Biological Station (UMBS) at Douglas Lake near Pellston, Michigan. This work led to the formalization of structural, knowledge-based, and hierarchical land-cover classification concepts (Pierce et al., 1994). Two structural classification levels are defined. General landcover, or Level I categories, are surfaces (water, airports, highways), short vegetation (agricultural, marsh, other herbaceous and short shrubs), and tall vegetation (forest trees, forested wetlands). A Level II classification retains the surfaces and short vegetation categories but further delineates the tall vegetation into categories based on growth-form. Here vegetation is differentiated by gross architecture such as shrub, excurrent, decurrent, and columnar, plus smaller branching and foliage characteristics such as branch size and orientation, leaf type, and/or needle length. The basis for these structural categories is recognizable in Figure 2. A Level I single date knowledge-based classification yielded accuracies greater than 97% based on spatially independent training and testing populations. Extension of this to a Level II classification for tall vegetation using a Bayesian classifier resulted in discrimination of several different forest communities each with classifiation accuracy of better than 96% (Pierce et al., 1994b).

In July of 1991, the ERS-1 SAR was launched into orbit. Its C-vv polarization (5.36 GHz) and inclination angle of 23° has made it optimal for discrimination of earth processes including ice and agricultural crop canopy studies. A second orbiting SAR, JERS-1, was launched in April of 1992, operating at L-band HH polarization (1.25 GHz). For the largely forested MFTS, a single ERS-1 image produced accuracies of 74.9 and 63.5% for Level I and Level II classifications, respectively. In the same study, an analysis using JERS-1 produced overall classifiation accuracies of 97.7 and 65.9% for Level I and Level II, respectively (Dobson et al., 1996). Thus, when used alone, especially at Level II, both ERS-1 and JERS-1 have been found to yield sub-optimal results for land-cover classification. However, when the two sensors are used synergistically, allowing the difference in wavelengths to be exploited to differentiate structural properties of surfaces and vegetation, generalized use for land-cover classification is vastly improved, and this has been demonstrated in a Level II classification. When used in combination by a hierarchical knowledge-based classifier, the structural information content provided by the two SARs with different wavelengths, polarizations and angles of incidence significantly improved the classification results at Level II to 94% accuracy (Dobson et al., 1996).

The general advantage of a structural and knowledge-based decision approach is centered on the fact that it does not rely upon *a priori* knowledge of a local area or region, is not image-specific, and thus is much more likely to be transportable. To date, this technique is operational for Level I JERS/ERS, AIRSAR, and SIR-C/X-SAR data, and has been demonstrated at Level II for JERS/ERS. The advantages of this transportable structural

classifier for world-wide land-use mapping is discussed in depth by Dobson et al. (1996). For example, a long-term goal of the classification efforts for the MFTS is to eventually determine a way to have a fixed set of rules with constants that are adaptable to each image for at least Level I. In this way the same algorithm can be used, while allowing the same discrimination procedure to adapt to the local conditions. The combination of additional structural categories at Level II and a fully polarimetric SAR such as AIRSAR and SIR-C/X-SAR result in a classification problem which is much more complex in a multivariate sense. Here the power of Bayesian techniques in dealing with multivariate datasets are advantageous.

These results from AIRSAR and ERS/JERS raise expectations for a single instrument such as SIR-C/X-SAR with its total of seven power polarization-frequency channel combinations plus four additional polarization phase-difference channels. It is expected that when the additional dimension of multi-temporal data is added that there is the potential for even greater discriminating power. A brief discussion of multi-temporal SAR efforts is given below.

1.4.2 The Multi-Temporal Approach

Theoretical and experimental work has also been done which demonstrates that the use of multi-date imagery should provide additional, useful information for classification. Temporal change observed by AIRSAR, and as quantified in backscatter, has been related to surface and canopy properties of northern hardwoods forests in the MFTS (Dobson et al., 1991). Investigations have been carried out to quantify and explain multi-temporal backscatter for ecoregions other than north-temperate forests, including a semi-arid region in California (McDonald et al., 1990). Both of these explore multi-date imagery within the same season but provide confirmation of temporal change contributions to the SAR signal. In their research on northern forest classification using temporal multifrequency and multipolarimetric SAR (airborne) images, Ranson and Sun (1994) found that use of a temporal data set improved classification accuracy when compared to single date.

Multi-date techniques have been fairly widely applied using optical imagery. A layered multi-temporal approach was investigated for classifying Landsat MSS (Lozano-Garcia and Hoffer, 1985). In a study to map forest cover types in New Hampshire using multi-temporal Landsat Thematic Mapper imagery, researchers concluded that multi-temporal classifications achieved improved accuracy over those from a single date (Schriever and Congalton, 1993). Indices have been constructed from Landsat data to characterize temporal patterns of spectral response of vegetation (Samson, 1993). NDVI is extracted from multi-date AVHRR to monitor seasonal trends such as "green-up" on a regional to global basis.

Recently, researchers in Wisconsin demonstrated the use of phenological variation to arrive at improved forest classifications (Wolter et al., 1995). In their stepwise approach, phenological change (particularly leaf flush and leaf senescence) of a particular species/community

occurring between two time periods is analyzed to separate species/communities which are then masked from the imagery. Further classification then proceeds in a continuing step-wise fashion on the remaining portions of the imagery. In this study which attempted to classify to the species level, an overall classification accuracy of 83.2% was reached. When categories were aggregated to forest communities, accuracy was improved to 93.6%. The authors conclude that a multitemporal approach is an advantageous method in ecoregions where phenological changes occur consistently over large areas.

Both the successes and challenges acknowledged in the above discussions of classification methodologies and multi-temporal classifications suggest that SIR-C/X-SAR may combine the advantages of several former or current sensors in efforts towards improved land-cover classifications. The challenge in the present project is to marry the advantages of the multi-temporal dataset for this fully polarimetric, high resolution SAR with robust hierarchical structural-based classification methodologies; both of which have shown independent successes. The results should be SAR-derived terrain classifications which may serve a variety of purposes. These include improved land-cover maps, inputs to empirical and process-based ecosystem models, and the dataset prerequisites to class-specific inversions from which quantitative estimates of biophysical parameters may be extracted.

1.4.3 Biomass Estimation

The premise that SAR imagery may be used to estimate forest biomass is supported by research to date. In the past five years, a number of exploratory studies have demonstrated the relationship between above-ground standing forest biomass and SAR backscatter at several wavelengths (Dobson et al., 1992; Kasischke, 1992; Kasischke et al., 1994; Le Toan et al., 1992, Rignot et al., 1993, Dobson et al., 1995, and others). Several of these studies have sought to assess the relative usefulness of the several SAR standard frequencies and polarizations in biomass estimation. Dobson et al. (1992) examined the dependence of radar backscatter on aboveground biomass of mono-species loblolly pine *(Pinus taeda)* and maritime pine *(Pinus pinaster)* plantations using P (0.44 GHz), L (1.225 GHz), and C (5.3 GHz) polarimetric (hh, hv, vv) airborne SAR data. They found that radar backscatter increased linearly with increasing conifer biomass until reaching a saturation level which was higher at the lower frequencies (L and P). They found the biomass saturation level to be approximately 200 t/ha at P-band and 100 t/ha at L-band. At C-band, biomass saturated at a much lower level and was also more weakly correlated to above-ground biomass. The coefficient of determination (r^2) between backscatter and biomass for P and L bands, each at three polarizations, varied from 0.894 to 0.957. At C-band r^2 varied from 0.511 to 0.749. The relatively better success at the longer wavelengths is because the shorter wavelength is primarily back-scattered from the canopy leaves and twigs and thus provides no information on the trunk component which may contain over 60% of the above-ground biomass.

Le Toan et al. (1992) demonstrated the possibilities of using multi-frequency/multi-

polarization JPL AIRSAR (P,L,C; hh,vv,hv) to estimate forest biomass. Their test site in SW France was composed almost entirely of plantations of maritime pine *(Pinus pinaster)* ranging in age from 8 to 46 yrs. They found that the dynamic range of the SAR backscatter, and thus the potential for retrieving the most significant information, was highest in P-band and decreased with increasing frequencies. They also determined that cross-polarized backscatter (hv) was the most sensitive to forest biomass variation. The best coefficient of determination was obtained between P-hv and trunk biomass ($r^2 = 0.95$). They looked at a variety of variables and found that there was a strong positive relationship between radar backscatter and height, biomass, dbh, basal area, and age in decreasing order. No significant correlation was found with tree density. They suggest that their experimental results show potential usefulness especially for P-band SAR to estimate forest biomass. They suggest that "cross comparison with observations on other forest sites and validation of observations by physical modeling are a requisite to the development of application programs (Le Toan et al., 1992)."

Kasischke et al. (1994) studied ERS-1 C-vv single polarization SAR to determine its possibilities for estimation of forest biomass in young loblolly pine forests in North Carolina. The authors hoped to show that while C-band SAR has been found to be less useful in older and mature closed-canopy stands, it still may be useful in estimating biomass for young open canopied stands. They found correlation coefficients between 0.87 and .93 for the young stands and concluded that the C-vv ERS-1 SAR has potential for monitoring biomass changes during early successional stages of north-temperate conifers.

Other studies have concentrated on assessing or refining methodologies for deriving biomass information from SAR imagery. In his dissertation, Kasischke (1992) described his analysis for the estimation of biomass from AIRSAR imagery with in-depth attention to tree biomass components for well-studied plantations of loblolly pine. His dissertation is part of an on-going study to develop a better model of the cause-effect relationship between the structure of Loblolly pines (branching sizes, angles; needle sizes, angles, etc.) and the SAR backscatter coefficient. He found significant correlations, and concluded that using regression approaches to do this was useful in the exploratory stage and for effiecient estimates, and that theoretical scattering models which incorporate these findings and make it possible to apply the inverse process using backscatter to predict biomass should be investigated further.

Dobson et al. (1995a) published the results of a first analysis to extract biophysical quantities from SIR-C/X-SAR data. This study demonstrated that forest structure must be taken into account prior to developing retrieval algorithms. Thus the process involved first classifying the imagery and then developing the empirical relationships between the imagery and biophysical parameters of interest for each structural category. To account for this, SAR data is used to estimate the fundamental biomass components of height, basal area (BA), and crown biomass. The trunk biomass (the highest proportion) is then estimated from estimates of BA and height combined with *a priori* knowledge of structural class taper

factors. Lastly crown biomass and trunk biomass are combined to arrive at total biomass. Results showed that biophysical characteristics were estimated with relatively small rms errors. Total aboveground biomass (0-25 kg/m^2) was estimated with an rms error of 1.4 kg/m^2. The rms error is the root mean square error as given by:

$$rms = \sqrt{\frac{\Sigma(x - \bar{x})^2}{n}} \qquad (1.1)$$

where where $\bar{x}$ is the arithmetic mean, $(x - \bar{x})^2$ is the squared deviation of an individual observation from the arithmetic mean, and n is number of samples.

1.4.4 Interfacing SAR and Carbon Cycle Modeling

This section introduces the rationale for interest in deriving C estimates from remotely sensed data and discusses the potentials for SAR-derived quantifications in particular. The terrestrial component of the C (C) cycle has been and continues to be extensively studied at the level of internal organism and local ecosystem processes. Of more recent emphasis is the regional to global scale quantification and modeling of these processes prompted to a large degree by the centrality of CO_2 to the issues of global warming. With CO_2 as the primary greenhouse gas after water vapor, the C cycle holds a key position in any potential climate change. Due to a number of reasons, including uncertainties in projected C balances between global sources and sinks (Tans et al., 1990), there is great interest in studying the role of the terrestrial biosphere in the C cycle. This is the impetus for the work done in the present study to demonstrate that a SAR-based methodology may be developed to model forest C storage, annual growth, and forest disturbance, and which will enhance or complement other efforts to refine our understanding of terrestrial C storage and flux.

The C cycle is a fundamental terrestrial biosphere flux and functions as the major integrator of other fluxes such as N, P, S, water, and energy in land biogeochemical cycling. Terrestrial vegetation and soils contain a significant portion of global C – approximately three times as much C as does the atmosphere (Clark, 1982). Because of their large perennial woody structure which requires the products of photosynthesis for maintenance and continued growth, forests worldwide have stored a comparatively larger quantity of C than other vegetation types. The forest storage compartment, however, has undergone rapid change in the past two centuries and continues to do so as a result of human modification of the landscape, particularly forest clearing. Since 1860 there has been a large global flux of C from the land towards the atmosphere. About 1980 a new landmark was reached when C released from terrestrial ecosystems was surpassed by that from the combustion of fossil fuels (Alban and Perala, 1992).

Scientists are currently attempting to balance the global C budget as measurements and analyses indicate that the sum of presently understood global C sources and sinks is out of balance. Despite the increased release of C by harvesting and burning, it is suspected that

the terrestrial biosphere may be a large *net* C sink, and further, that this sink may reside primarily in north temperate (Tans et al., 1990) or boreal forests (Bonan, 1991).

Table 1.1 shows the estimations from anthropogenic sources, and the remainder indicates a terrestrial sink of 0.2 Gt ($\pm$ 0.8 uncertainty). This ignores the sources due to land use change and inclusion of this (largely net deforestation, estimated as 1.6 Gt) gives (from Schimel, 1995):

$$\text{land use net emission}(1.6) + \text{calculated imbalance}(0.2) = \text{terrestrial sink}(1.8) \qquad (1.2)$$

Other researchers have suggested a greater net C sink in the northern hemisphere of 2.0 - 3.4 Gt/C/yr (Tans et al., 1990; Ciais et al., 1995; Dai and Fung, 1993; Friedlingstein et al., 1995; Denning et al., 1995).

In deriving quantifications of C, storage is only one key variable. Net primary production (NPP) is of equal importance, and has been described by Field et al. (1995) as the central C-related variable summarizing the interface between plant and other processes. It involves the removal of C from the atmosphere and assimilation by primary producers after gross photosynthesis and leaf and maintenance respiration have occurred. What remains is used for NPP, which is equivalent to plant growth, or the amount of structural material (leaves, wood, roots, etc.) produced (Aber and Melillo, 1991). There are two ways of defining NPP, one based on biomass and the other on gas exchange. The biomass NPP is defined as:

$$\text{NPP} = b_{t+1} - b_t + L_{t+1} \qquad (1.3)$$

where b_t and b_{t+1} are the plant biomass at the beginning and end of the time interval respectively, and L_{t+1} is the new litter produced during the interval. The gas-exchange NPP is defined as:

$$\text{NPP} = GPP + R_a \qquad (1.4)$$

where GPP is gross primary production, or C fixed during photosynthesis, and R_a is autotrophic respiration which includes both maintenance and construction respiration (Field et al., 1995).

Interest in more accurate quantification of terrestrial biosphere C storage and NPP stems not solely from the desire to balance the numbers. The numbers provide insight

Fossil fuel, flaring, cement	+5.4 Gt
Atmospheric accumulation	-3.2 Gt
Ocean uptake	-2.0 Gt
Calculated imbalance	-0.2 Gt

adapted from Schimel (1995).

Table 1.1: Components of the global C cycle.

into the effects of human-induced change and clues to potential management mitigations of problems. The figures above show that human use of forest resources has had, and continues to have, a significant impact on this balance. As a source, harvesting of tropical forest biomass (especially burning) is the largest component of the C flux into the atmosphere from terrestrial ecosystems. Studies in the Pacific Northwest of North America have shown a large net release of CO_2 when old-growth forests are harvested, and a lag of at least 200 years before C storage approaches pre-harvest levels. Despite such deforestation, the suggestion that there is potentially a large sink for C in terrestrial ecosystems in the northern hemisphere has heightened interest in quantifying the role of terrestrial plant communities in the global C cycle in northern and boreal biomes (Tans et al., 1990). In North America, the NHCF was heavily logged between 1800 and 1940, and as these forests regrow, this may contribute to a sink in this region of possibly as much as 0.5 - 1.0 Gt/yr (Sedjo, 1992). Because second-growth forests follow a logistic growth curve where growth rates decrease as storage and age increase, this may be a temporary phenomenon, ceasing as these forests reach maturity (Schimel, 1994). Management can mimic this, however, and Alban and Perala (1992) found that the more short-lived aspen in the lake states (Michigan, Minnesota, Wisconsin) grown on planned 40-year rotations will sequester several times as much C per year as old-growth forests. Theoretically, on a global scale, establishing new forest in non- or de-forested areas could temporarily sequester all of the potential annual buildup of atmospheric CO_2. Approximately 465×10^6 ha of forest (about 10% of current forest worldwide) would postpone potential increases of atmospheric CO_2 by several decades (Vitousek, 1991). Such potential mitigation through terrestrial ecosystem management could have significant impact, but in addition to issues of balancing the numbers at the global scale, there remains a lack of precise data providing a vehicle for agreement on the amount of C storage and flux at management scales worldwide.

Challenges to Quantifying Carbon

To further understand and quantify how the terrestrial biosphere functions in the C cycle, whether for management or global modeling, regional to global measurement technologies are crucial. A most basic input to almost all methodologies is a spatial database of land cover. At global scales, this data may be pieced together from maps and government geographic information system (GIS) databases, and more recently, from remotely sensed data such as AVHRR (Advanced Very-High Resolution Radiometer) to assemble a representation of landcover at a very coarse spatial resolution (USGS, 1993).

Each of these has limitations. Published landcover maps are typically based on Holdridge and Köppen bioclimatic analyses which use temperature and precipitation to infer potential vegetation. These generally provide only the geographic distributions of potential natural vegetation that does not account for agricultural or urban conversion; yet approximately 10 - 20% of earth land surface has been entirely converted from its original vegetation state,

additional percentages have been altered, and this figure continues to increase (Townshend et al., 1991). Further, potential vegetation assumes mature states only, where the actual fact is that even those areas still in "natural" vegetation are found at various stages of succession and thus functioning at varying rates of growth. Because global maps are too general, continental scale published maps or GIS databases are often used and between them they are lacking in consistency and inclusiveness of all vegetation types. Several researchers have predicted C flux based on such vegetation databases, for example, Melillo et al. (1993). Recently AVHRR has been classified for various regions including the United States. This dataset represents an improvement over potential vegetation maps on a broad scale, although investigations for local to regional use have found some significant misclassifications (Dobson et al., 1996).

The second issue is that a clearly defined set of vegetation classes is yet to be widely adopted. Given the desire to model on a global scale it is likely that remotely sensed data will be increasingly used and the choice of classification scheme will result from a marriage of the physical response of sensors to vegetation characteristics rather than traditional botanical schemes. Such classes will be based on the use of simple observable plant structural or physiognomic characteristics. Vegetation classes may only be needed for several broad structural categories at the top of a hierarchical scheme, and at very specific levels, local interpretation can be made based on knowledge of local floristics when desired. Recently the U.S. Federal Geographic Data Committee in conjunction with other government (e.g., Department of Interior, Environmental Protection Agency, NASA) and private sector organizations (Nature Conservancy, Ecological Society of America) has proposed a vegetation classification and information standard based primarily on such plant physiognomic characteristics.

The spatial distribution of other C-related vegetation attributes such as NPP are even more inconclusively mapped, although good attempts to quantify NPP world-wide have been made (Leith, 1972; Melillo et al., 1993) over the past several decades. NPP has been measured or modeled by both empirical and process-based methods. Empirical regression-based relationships are typically developed and used in local settings such as applied forestry where they may be highly accurate, but measurements are limited to these local areas by the intensiveness of the method. These observations have been extended in a generalized way to global scales using an assemblage of regression-based measured data from test sites in each biome, multiplying these by biome area (based on maps of potential vegetation) and then summing these results across biomes (Whittaker and Likens, 1975). Process-based models vary in their inclusiveness, but generally seek to model inputs and outputs from a systems approach. The useful characteristic of process-based models is that by varying inputs they may model how variables such as NPP may change due to climatic forcings. Both of these modeling methodologies could benefit from input datasets which would incorporate not only improved land cover, but also the quantity of forest biomass or forest age.

Potential Role of SAR in C Modeling

Consequently, among the research community interested in terrestrial biogeochemical cycling, there is acknowledged lack of consistency, coverage, and accurate representation of key inputs to understanding the global C cycle. In a summary of the issues and initiatives identified by the International Satellite Land Surface Climatology Project (ISLSCP) Workshop, June, 1992, Sellers et al. (1993) state that the only realistic way to produce the products to alleviate this lack is through the analysis of satellite data. Satellite data can provide a significantly improved measure of actual land-cover and eliminate the ambiguities currently extant in global vegetation maps derived from varying methodologies and definitions. It provides an updatable dataset and is the ideal tool for monitoring change. These elements in turn should increase the reliability of C quantification whether based on empirical or process methods. In addition to initialization and monitoring, use of satellite data will be directed towards evaluation of regional to global processes modeling.

A number of sensors are currently operational and each should be exploited to its unique advantages in providing information relevant to quantifying and modeling terrestrial biosphere dynamics. For vegetation data sets, AVHRR has demonstrated potential to provide maps of vegetation classes, FPAR (fraction of PAR (photosynthetically active radiation) absorbed by the green canopy), LAI (leaf-area index), and a very coarse approximation of above-ground biomass on a repeatable basis (Sellers et al., 1995). With AVHRR (and likewise Landsat MSS and TM), discrimination between different vegetation types (e.g., deciduous tree and shrub) is frequently confounded by their similar spectral reflectance properties at these optical wavelengths. To date synthetic aperture radar (SAR) has had the most success in discriminating in such cases due to its sensitivity to larger structural characteristics. SAR response to dielectric properties gives the sensor additionally enhanced discriminating power between fairly similar forest types (e.g., conifers) on a moisture gradient. Not only is it possible to distinguish between the different types, but it is possible to determine the magnitude of the difference in terms of mass as SAR has also been shown to be highly sensitive to above ground biomass on fine scales. Both orbiting SARS (ERS-1, ERS-2, JERS-1, Radarsat) and the SIR-C/X-SAR instrument recently carried onboard the space shuttle Endeavor in 1994 have relatively fine spatial resolution comparative to other sensors generally considered for estimation of land cover and biophysical parameters.

Recently, success in deriving biophysical parameters, including biomass, from SIR-C/X-SAR imagery has been demonstrated through analysis of image data from the NASA Michigan Forests test site (MFTS), and previous publications have discussed SAR's particular capabilities and advantages as a remote sensor in such efforts (Dobson et al., 1995a; Way et al., 1994). Land-cover classification work at this test site is based on the use of a hierarchical classifier emphasizing plant structural characteristics. The present project builds on previous advances in both classification and estimation of biophysical parameters to study key components of C dynamics. We explore the use of SIR-C/X-SAR imagery to directly

18

estimate C storage and flux associated with living woody vegetation on the timescale of an annual growing season. This methodology using SAR allows for a convenient way to move directly to estimation of the C parameters of above- and below-ground C and ANPP in order to provide a better approximation of these components at a fine measurement scale. Because of excellent discrimination between large structures (forests) and absence of such structure (clear-cuts or agricultural and urban conversion), SIR-C/X-SAR data has good potential for monitoring C removal in the form of land-use change. This human-mitigated dimension must be accounted for to fully characterize major components of C flux in the region of this study due to an active forest clearcutting program. All of these can be considered end results, used as inputs to models, and employed as reliable evaluation datasets for comparison with process-based models.

SAR has potential to play two large-scale roles in the types of C cycle modeling being discussed. A solely SAR-based method can use SAR-derived land-cover classifications, biomass estimations, and allometric equations to achieve a much more robust and accurate empirical model of C flux including C storage and NPP. Secondly, an expanded SAR-derived dataset of land-cover classes and biomass would form a greatly enhanced input dataset for process-based models due to its incorporation of the actual *quantity and functional state* of each vegetation type, as opposed to simply type, of terrestrial vegetation. This study demonstrates the first SAR-based effort, and further research will incorporate the second. Typical of many remote sensing efforts the present project concentrates on demonstrating the methodology in a particular biome. The methodology could be applied in test sites in other biomes to piece together a more regional or global database.

Figure 1.3 summarizes the general process model for extracting ecological information from SAR. During the pre-processing stage SAR data, in this case SIR-C/X-SAR, is calibrated, and then features (or image channels) are extracted. Terrain classifications including land-cover classifications have been developed using prototype data from AIRSAR and hand-held radars (scatterometers). Using knowledge gained from these, classifications are developed and used on SIR-C/X-SAR. Resulting structural categories are used in class-specific inversions to derive biophysical parameters such as biomass and C.

```
              ┌─────────────────────────┐
              │   SAR Data Acquisition   │
              └─────────────────────────┘
                          ▼
                  ┌───────────────┐
                  │   Calibration  │
                  └───────────────┘
                          ▼
              ┌─────────────────────────┐
              │     Extract Features     │
              └─────────────────────────┘
┌─────────────────────────┐         ▼
│ Classifiers Developed from│   ┌─────────────────────────┐
│    Theoretical Models     │──▶│   Terrain Classification  │
│    Scatterometer Data     │   └─────────────────────────┘
│  Trained on AirSAR Data   │
└─────────────────────────┘     .   .    .    .
              ┌─────────────────────────┐
              │ Class Specific Inversions│
              └─────────────────────────┘
                          .
              ┌─────────────────────────┐
              │ Quantitative Estimates of│
              │  Biophysical Parameters  │
              │  (e.g., biomass & carbon,│
              │  basal area. height, density,│
              │  LAI)                    │
              └─────────────────────────┘
```
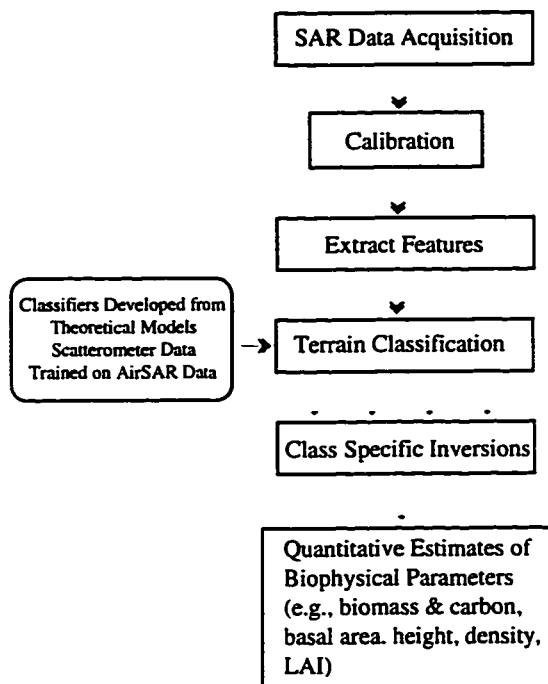
Figure 1.3: General process model for SAR classification and extraction of biogeophysical parameters

20

CHAPTER 2

MFTS REFERENCE DATA AND ANALYSIS

2.1 Biometric Survey Objectives

Research using a new remote sensor often involves sampling of both image data of a geographic study area and "reference" data from those same areas on the ground. This allows the analyst to study and quantify the relationships between earth terrain features and image reflectance (or backscatter in the case of SAR). For land-cover classification work, reference data is used in supervised classifications. In biophysical parameters estimation including biomass, reference data is used in developing empirical functions or physical models which may (1) explain the form of the relationship between what is on the ground and the backscatter from some combination of channels of the imagery, or (2) given image backscatter, predict what is on the ground. To both train and validate models directed towards land-cover classification and biomass/carbon estimation using new image data from the SIR-C/X-SAR mission it was necessary to collect sufficient reference data. Therefore, central to the overall research plan for the MFTS has been the establishment of a number of forest test stands on the ground which would meet the requirements of rigorous quantitative and statistical analysis.

To achieve this goal, 70 four-hectare forest test stands were established in the MFTS. These stands are representative of the range of north-temperate and boreal forest communities found at the test site. They are also distributed over the range of ages and densities found in the region. Each stand has been intensively sampled according to a defined sampling scheme to arrive at a statistical interpretation of stand structure, species composition, and above-ground biomass. An explanation of the sampling methodology, data analysis, and presentation of results for the reference data sampling (biometric survey) of the forest test stands is the purpose of this chapter. Table 2.1 presents the overall objectives of the MFTS biometric survey discussed in this chapter.

This chapter contains (1) an introduction to the physical characteristics and forest composition of the site, (2) a discussion of the sampling design and techniques, and (3) a description of the data processing and statistical analyses. Included in these sections are

Objectives
1.Estimation of stand structure by stand, stratum, and species for variables: species composition, diameter, height, crown depth, basal area, and density
2.Development of species height prediction equations and estimation of heights
3. Estimation of biomass by stand stratum and species for: foliage, bole, branches
4. Construction of a GIS database with the layers: Land cover, hydrology, and transportation (MIRIS) Topography (USGS) Test Stands (GPS survey)

Table 2.1: MFTS biometric survey objectives.

relevant maps, diagrams, and tables. Results and more detailed information are presented in serveral appendices.

2.2 Site Physical Characteristics and Forest Composition

2.2.1 Physical Characteristics

The MFTS, centered on 46.39° N. Latitude and 84.88° W. Longitude, is located in Chippewa County in the eastern part of Michigan's Upper Peninsula. The greater study area encompassing the entire ascending and descending SIR-C/X-SAR swaths is approximately 60 km E-W and 50 km N-S. Jurisdictionally, much of the study site, and all of the forest test stands are within the boundaries of the Eastern Division of the Hiawatha National Forest. Figure 1.1 shows the location of the test site in Michigan.

The MFTS was chosen as a long-term study site for several reasons. Most importantly is its geographic situation along the ecotone or transition zone between the north-temperate and boreal forest biomes. Because of this, the site contains significant diversity of forest communities, and thus results should be extensible to both the north and south. Further, the presence of relatively homogenous communities of varying ages and densities and of large geographical extent was an important criteria. Relatively level topography was also a factor. Local incidence angle, which is a function of local topography or slope, can be a confounding influence in the strength of SAR backscatter and would present unwanted complications in an initial study concentrating on effects of vegetation type. Figure 2.1 presents the general land cover for the region.

The site contains several distinct physiographic regions which support a diversity of forest communities. The several physiogrphic regions are indicated on Figure 2.2 by letter designation. They include a large area of excessively drained glacial outwash sands (the Raco Plains) (A) which dominate the center of the image and support red and jack pine upland conifer. The near northeast contains upland aspen and northern hardwood and

	Upland Conifer		Agriculture
	Lowland Conifer		Wetland
	Northern Hardwoods		Water / Airport
	Aspen / Birch		Urban
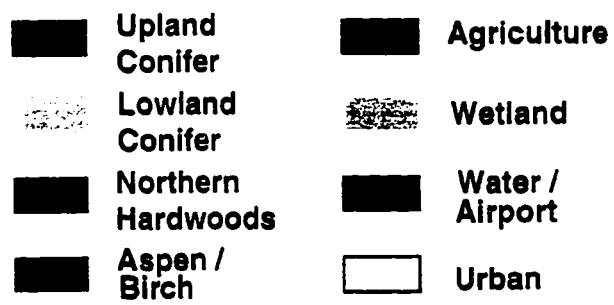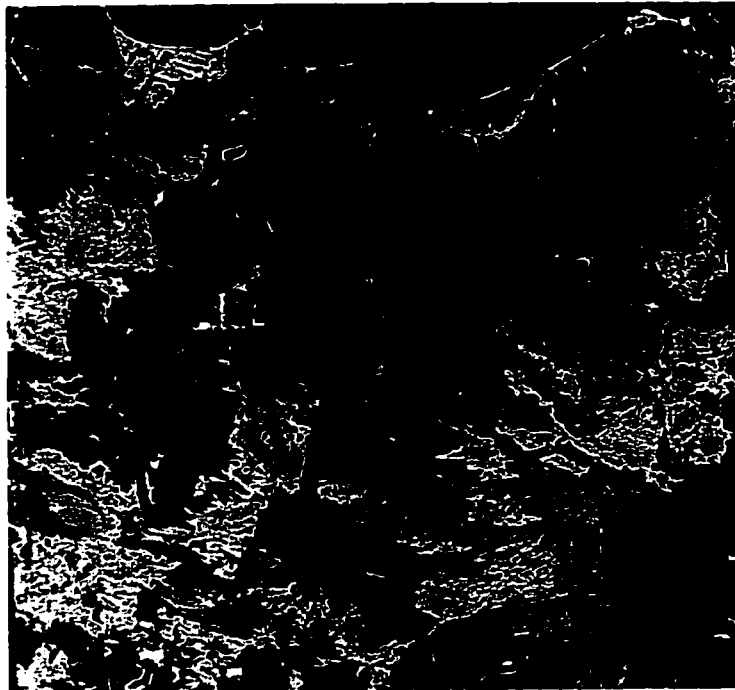
Figure 2.1: Regional land cover (source: MI Dept. of Natural Resources MIRIS).
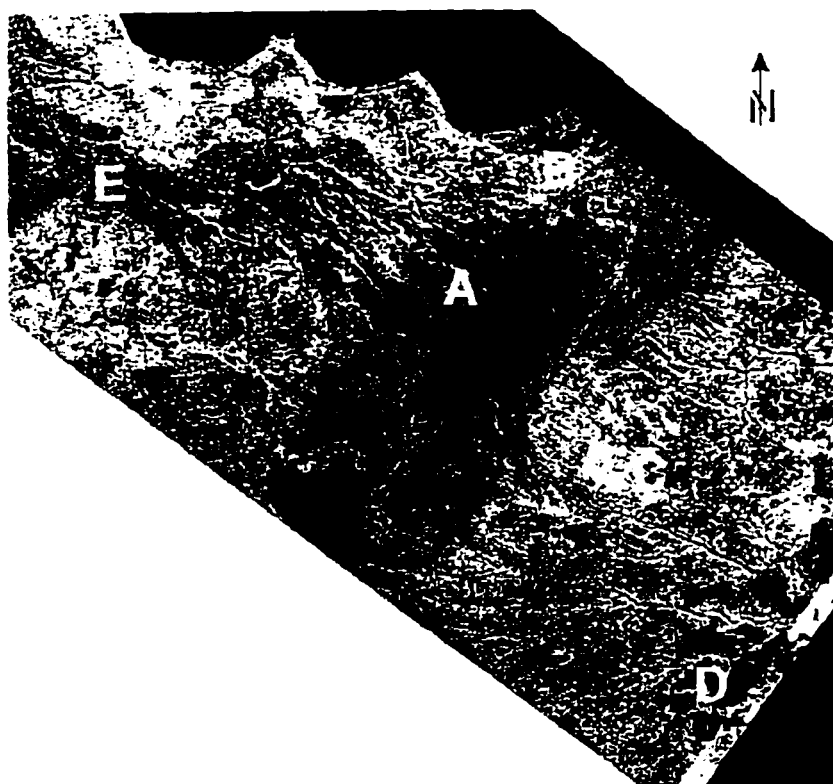
Figure 2.2: Composite SIR-C/X-SAR image. Data-take 22.2, SRL-2, October 1, 1994. Incidence angle = 22.2°. Red = L-hv, Green = C-hv, Blue = X-vv.

lowland mixed conifer/hardwood (B). The Delirium Wilderness wetlands of lowland conifer and lowland mixed conifer/hardwood are found in the south and southeast (C). In the extreme southeast is a large area of agriculture on lake plain (D). Moderately well drained morainal features supporting aspen and northern hardwood interspersed with low-lying somewhat poorly drained areas of lowland conifer and mixed conifer/hardwood comprise the western half (E). The far northern edge of the site borders Lake Superior and consists of poorly drained substrate supporting lowland conifer and lowland mixed conifer/hardwoods (F).

Regional climate of the MFTS is characterized by a mean annual temperature of 5° C, July average temperature of 24.5° C, January average temperature of −14° C, growing season of approximately 130 days, and mean annual precipitation of 79 cm (Barnes, 1981).

2.2.2 Forest Composition

The broader ecological setting of this study, and of the MFTS, is the northern hardwood and conifer forest (NHCF). The NHCF is a transitional forest, occupying the ecotone between the boreal forest to the north and the north-temperate or central hardwoods to the south. As a transition zone it has its unique species, but to a large degree contains those of both the boreal and north-temperate forest biomes. Its geographic area extends from Minnesota in the west through the Great Lakes to New England and the Canadian maritime provinces in the east, and in higher elevations, south to central New York and Pennsylvania. Unique transitional tree species of the NHCF include eastern white pine, red pine, hemlock, and yellow birch. Major species of the boreal forest found in the NHCF are trembling aspen, balsam fir, jack pine, and white/black/red spruce; those of the central hardwoods include sugar maple, beech, and basswood. The region is shown in Figure 1.1.

As the name suggests, there is both a deciduous and coniferous component in the NHCF. The deciduous component is comprised of several overlapping communities. These contiguous communities share many floristic and structural characteristics, and delineation into discrete forest types is somewhat arbitrary. Overlaps occur in two ways - along a phsiographic/moisture gradient, and along a successional sequence. In the deciduous component along a moisture gradient, aspen/birch/mixed conifer occupy lower, hydric sites, and aspen/northern hardwoods occupy higher, mesic sites. Succession in the deciduous component can best be thought of as a continuum of decreasing aspen and increasing maple dominated types. Coniferous forests show a similar overlap phenomenon. Along a moisture gradient, lowland conifer composed of black spruce and larch or northern white-cedar occupy the wetter sites, and white pine, red pine,and jack pine occupy increasingly drier sites in that order. While mesic site red and white pine often eventually succeed to northern hardwoods, this is rarely allowed to occur due to frequent harvesting rotation. Conifers occupying the extreme sites (lowland conifers and jack pine) maintain essentially the same community composition as they age. Given the diversity of physiography in the MFTS, all of these

25

gradients and their associated vegetation are present.

Table 2.2 lists forest communities and dominant species which have been studied throughout the duration of the SIR-C/X-SAR project at the MFTS. A comprehensive list of the species found in the forest test stands and encountered during the biometric survey is provided in Table 2.3. This table gives the species common name, the binomial Latin name (genus, species), and the six letter code used to designate the species during field recording.

Upland Conifer	
Jack Pine	(*Pinus banksiana*)
Red Pine	(*Pinus resinosa*)
White Pine	(*Pinus strobus*)
Lowland Conifer	
Black Spruce	(*Picea mariana*)
White Spruce	(*Picea glauca*)
Northern White-Cedar	(*Thuja occidentalis*)
Balsam Fir	(*Abies balsemea*)
Larch	(*Larix laricina*)
Northern Hardwoods (upland)	
early successional species:	
Trembling Aspen	(*Populus tremuloides*)
Bigtooth Aspen	(*Populus grandidentata*)
Pin Cherry	(*Prunus pensylvanica*)
Paper Birch	(*Betula papyrifera*)
late successional species:	
Sugar Maple	(*Acer saccharum*)
Red Maple	(*Acer rubrum*)
Beech	(*Fagus grandifolia*)
Yellow Birch	(*Betula alleghaniensis*)
Hemlock	(*Tsuga canadensis*)
Lowland Mixed	
Paper Birch	(*Betula papyrifera*)
Trembling Aspen	(*Populus tremuloides*)
Black Spruce	(*Picea mariana*)
Balsam Fir	(*Abies balsemea*)
Larch	(*Larix laricina*)

Table 2.2: Forest communities and dominant species studied at the MFTS during the SIR-C/X-SAR project.

Acronym	Latin name	Common name
ABIBAL	Abies balsamea (L.) Mill.	Balsam Fir
ACEPEN	Acer pensylvanicum L.	Striped Maple
ACERUB	Acer rubrum L.	Red Maple
ACESAC	Acer saccharum Marsh.	Sugar Maple
ACESPI	Acer spicatum Lam.	Mountain Maple
AROMEL	Aronia melanocarpa (Michx.) Ell.	Chokeberry
ALNRUG	Alnus rugosa (Du Roi) Spreng.	Speckled Alder
AMESPP	Amelanchier Medic.	Serviceberry
BETALL	Betula alleghaniensis Britton	Yellow Birch
BETPAP	Betula papyrifera Marsh.	Paper Birch
CHACAL	Chamaedaphne calyculata (L.)	Leather-leaf
CORALT	Cornus alternifolia L. f.	Alternate-leaf Dogwood
CORCOR	Corylus cornuta Marsh.	Beaked Hazel
CRASPP	Crataegus L.	Hawthorn
FAGGRA	Fagus grandifolia Ehrh.	American Beech
FRAAME	Fraxinus americana L.	White Ash
FRANIG	Fraxinus nigra Marsh.	Black Ash
ILEVER	Ilex verticillata (L.) A. Gray	Winterberry
LARLAR	Larix laricina (Du Roi) K. Koch.	Tamarack
LEDGRO	Ledum groenlandicum Oeder	Labrador-tea
LONCAN	Lonicera canadensis Marshall	Fly-honeysuckle
NEMMUC	Nemopanthus mucronata Raf.	Mountain-holly
OSTVIR	Ostrya virginiana (Mill.) K. Koch	Eastern Hop-hornbeam
PICGLA	Picea glauca (Moench) Voss	White Spruce
PICMAR	Picea mariana (Mill.) B.S.P.	Black Spruce
PINBAN	Pinus banksiana Lamb.	Jack Pine
PINRES	Pinus resinosa Ait.	Red Pine
PINSTR	Pinus strobus L.	Eastern White Pine
POPGRA	Populus grandidentata Michx.	Bigtooth Aspen
POPTRE	Populus tremuloides Michx.	Trembling Aspen
PRUPEN	Prunus pensylvanica L. f.	Pin Cherry
PRUSER	Prunus serotina Ehrh.	Black Cherry
PRUVIR	Prunus virginiana L.	Chokecherry
QUEELL	Quercus ellipsoidalis E. J. Hill	Northern Pin Oak
QUERUB	Quercus rubra L.	Northern Red Oak
SALSPP	Salix L.	Willow
SAMRAC	Sambucus racemosa L.	Red-berried Elder
SORAME	Sorbus americana Marsh.	Mountain-ash
THUOCC	Thuja occidentalis L.	Northern White-cedar
TILAME	Tilia americana L.	American Basswood
TSUCAN	Tsuga canadensis (L.) Carr	Eastern Hemlock
ULMAME	Ulmus americana L.	American Elm
VIBACE	Viburnum acerifolium L.	Arrowwood
VIBCAS	Viburnum cassinoides L.	Withe-rod

Table 2.3: Comprehensive list of species at the MFTS.

2.3 Sampling Design and Techniques

2.3.1 Stand Selection and Planning

The first task was to identify and establish the forest test stands which would be used for the biometric survey. The criteria used were those presented in the Table 2.4. Identification of potential stands was done by consulting the U.S. Forest Service Compartment and Stand Maps for the Hiawatha National Forest in conjunction with the above criteria. All potential stands were visited in the field to assure that they did in fact meet the criteria before making the final selection. As a result, 70 four-hectare stands were established and 66 were measured at the MFTS, beginning in 1991. Each of the stands is designated by a number, and using these numbers, the stands may be located on the overview map MFTS Forest Test Stands in Figure 2.3. For each species or community, stand selection was done to fill in a roughly uniform distribution of size and density classes. Table 2.5 gives the percent of forest test stands represented in each of the forest communities under study. This is displayed graphically in the pie charts in Figure 2.4. Table 2.6 lists stands organized by community and age group. Table 2.7 is organized by stand and then gives the species and size class of each. Some stands also have a letter designation in addition to their number, and these are provided in Tables 2.6 and 2.7, and on Figure 2.3.

Criteria
1) Stands selected should fill the distribution of forest communities present at the site
2) Stands selected should fill the distribution of ages and densities present at the site within each forest community
3) An individual stand selected should be uniform in regard to its community (species composition), age, and density
4) Stands should be > than 4 ha in size with a minimum dimension of > than 100 m
5) Stands selected should be on level, or nearly level, terrain
6) Stands selected should be jurisdictionally within the bounds of the Hiawatha National Forest and accessible by automobile

Table 2.4: Criteria for selection of forest test stands.

Community	Percent of stands
Aspen	11%
Northern hardwoods	17%
Red pine	29%
Jack pine	30%
White pine	3%
Lowland conifer	10%

Table 2.5: Percent of stands in each forest community.

28

Community/age group	Stand number	N of stands
Aspen, upland		
pole	84	1
sapling	33(S), 45(EE), 49(JJ), 69, 70	5
Aspen, lowland		
pole	47(HH), 87	2
Northern hardwoods		
mature	28(N), 29(0), 34(T), 46(GG), 48, 53, 57	7
pole	31(Q), 76, 85, 86, 91	5
Red pine		
mature	23(G), 25(K), 43(CC), 50(KK), 52	5
pole	68, 71, 72, 73	4
sapling	22(D), 51(LL),77, 81, 82, 83	6
seedling	40(Z), 41(AA), 78, 79, 80	5
Jack pine		
mature	24(I), 27(M), 35(U), 61, 67	5
pole	56, 60, 62, 63, 64, 65	6
sapling	36(V), 38(X), 42(BB), 54, 55, 58, 59	7
seedling	37(W). 39(X), 66	3
White pine		
mature	74, 75, (also 23(G), 25(K))	2
Black spruce		
mature	26(L), 44(DD)	2
N. white cedar		
mature	32(R)	1
Hemlock		
mature	90	1
Lowland mixed conifer		
mature	30(P), 88, 89	3

Table 2.6: Forest test stands by community type and age group.

In actual practice, identification and measurement of the forest test stands occurred over a time frame of several years. The first year of measurement at the Raco Supersite occurred in 1991, when 13 stands were identified and measured. In 1992 an additional 15 stands were identified and measured. During the summer 1993, the remaining 42 stands were identified and 38 were measured. Because forest trees, especially younger trees, exhibit significant growth over a span of several years, 24 stands were remeasured in 1994 to arrive at current measurements and to assess growth rate. The stands remeasured included young sapling jack pine, red pine, and aspen stands. Older stands continue to grow as well, but the percent change is small because growth is much less significant than in younger stands. The remeasure of younger stands was especially important in using the data with SIR-C/X-SAR imagery because it was acquired in 1994. The remeasure was also used for validation of above-ground net primary production (chapter 5). Table 2.7 also provides the year the stand was measured and remeasured.

2.3.2 Sampling Design

Before any measurements were made in a test stand the dimensions of the stand were established by laying out a baseline and transects. Most stands were 200 by 200 m. Some stands were laid out slightly differently, e.g., longer baselines and shorter transects, when the stand configuration or landscape made this necessary. The following description is for a typical 200 x 200 m stand. A 200 m baseline was established in each stand at a minimum distance from the forest edge of twice the height of the tallest trees. The left end of the baseline when facing into the stand was designated the meter mark 0.0 and the right end the meter mark 200.0. The baseline was divided into five equal (40 m) segments. Starting at 0.0 m, a meter mark was randomly chosen in the first segment as the point of departure of the first transect, typically running orthogonal to the baseline. Four additional transects were established at 40 m intervals. Eight points were located along each transect at 25 m intervals, the first point being randomly chosen as a meter mark between 1 and 25. The 40 sample points thus generated served as the basis for a 10% sample of the upper stratum (trees $\geq$ 5 m in height). The ends of the baseline were marked by metal rods in the ground and flagging overhead. The transect starting points and upper stratum sample points were marked with labeled wire flags.

A nested set of circular plots of area 100, 16 and 1 m^2 was permanently established at each sample point to characterize the upper stratum (trees >5 m in height), middle stratum (trees 1-5 m in height) and lower stratum (trees <1 m in height), respectively. The radii of circular plots for the upper and middle strata were 5.64 and 2.26 m, respectively. A 1 x 1 m portable sampling frame was used to sample the lower stratum. Two middle stratum plots and three lower stratum plots were located within each 100 m^2 upper stratum plot. The axis of the plot centers was orthogonal to the transect. The centers of the middle stratum plots were at the centers of the two radii of the upper stratum plot, i.e., 2.82 m on either

Stand number	Community	Age group	Year measured	Year re-measured
22 (D)	red pine	sapling	1991	1994
23 (G)	red & white pine	mature	1991	
24 (I)	jack pine	mature	1991	
25 (K)	red & white pine	mature	1991	
26 (L)	black spruce, lowland	mature	1991	
27 (M)	jack pine	mature	1991	
28 (N)	northern hardwoods	mature	1991	
29 (O)	northern hardwoods	mature	1991	
30 (P)	mixed conifer, lowland	mature	1992	
31 (Q)	northern hardwoods	pole	1991	
32 (R)	cedar, lowland	mature	1991	
33 (S)	aspen, upland	sapling	1991	1994
34 (T)	northern hardwoods	mature	1991	
35 (U)	jack pine	mature	1991	
36 (V)	jack pine	sapling	1992	1994
37 (W)	jack pine	seedling	1992	1994
38 (X)	jack pine	sapling	1992	1994
39 (Y)	jack pine	seedling	1992	1994
40 (Z)	red pine	sapling	1992	1994
41 (AA)	red pine	sapling	1992	1994
42 (BB)	jack pine	sapling	1992	1994
43 (CC)	red pine	mature	1992	
44 (DD)	black spruce, lowland	mature	1992	
45 (EE)	aspen, upland	sapling	1992	1994
46 (GG)	northern hardwoods	mature	1993	
47 (HH)	aspen, lowland	pole	1992	
48 (II)	northern hardwoods	mature	1992	
49 (JJ)	aspen, upland	sapling	1992	1994
50 (KK)	red pine	mature	1992	
51 (LL)	red pine	sapling	1992	1994
52	red pine	mature	1993	
53	northern hardwoods	mature	1993	
54	jack pine	sapling	1993	1994
55	jack pine	sapling	1993	1994
56	jack pine	pole	1993	
57	northern hardwoods	mature	1993	
58	jack pine	sapling	1993	1994
59	jack pine	sapling	1993	1994
60	jack pine	pole	1993	
61	jack pine	mature	1993	
62	jack pine	pole	1993	
63	jack pine	pole	1993	

Table 2.7: Forest test stands year measured.

Stand Number	Community	Age group	Year measured	Year remeasured
64	jack pine	pole	1993	
65	jack pine	pole	1993	
66	jack pine	seedling	1993	1994
67	jack pine	mature	1993	
68	red pine	pole	1993	
69	aspen, upland	sapling	1993	
70	aspen, upland	sapling	1993	
71	red pine	pole	1993	
72	red pine	pole	1993	
73	red pine	pole	1993	
74	white pine	mature	1993	
75	white pine	mature	1993	
76	sugar maple	pole	1993	
77	red pine	sapling	1993	1994
78	red pine	seedling	1993	1994
79	red pine	seedling	1993	1994
80	red pine	seedling	1993	1994
81	red pine	sapling	1993	1994
82	red pine	sapling	1993	1994
83	red pine	sapling	1993	1994
84 **	aspen, upland	pole		
85	northern hardwoods	pole	1993	
86	northern hardwoods	pole	1993	
87	aspen, lowland	pole	1993	
88	mixed conifer, lowland	mature	1993	
89 **	mixed conifer, lowland	mature		
90 **	hemlock, lowland	mature		
91	northern hardwoods	pole	1993	

Table 2.7 cont'd.

* Measured only by point sampling

* Established, but not yet measured
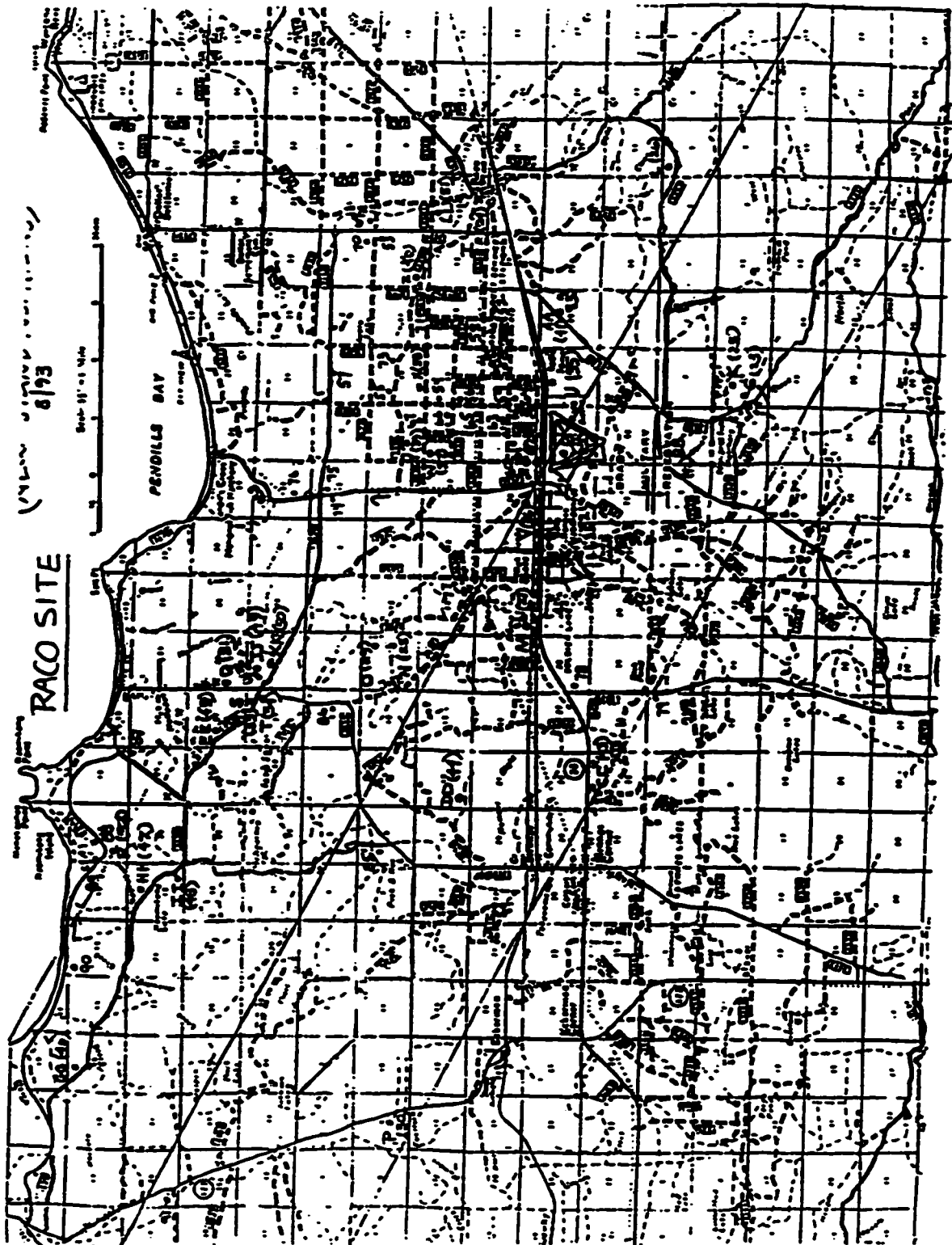
Figure 2.3: MFTS forest test stands.

33

Community Representation

61%
10%
17%
11%

■ northern hardwoods

■ aspen

▩ upland conifer
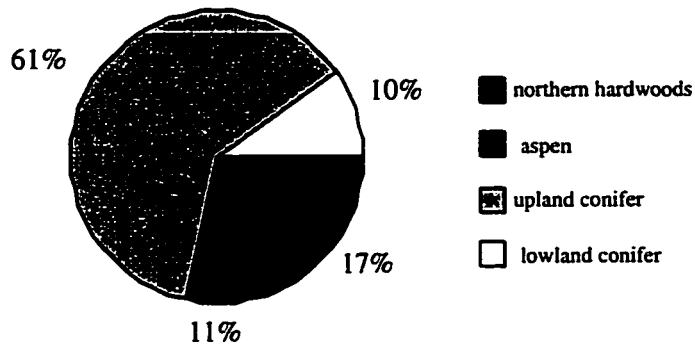
☐ lowland conifer

Upland conifer by age group

30%
19%
23%
28%

■ mature

■ pole

▩ sapling

☐ seedling

Deciduous by age group

25%
40%
35%

■ mature

■ pole

▩ sapling

Red pine by age group

30%
25%
20%
25%

■ mature

■ pole

▩ sapling

☐ seedling

Jack pine by age group

33%
14%
29%
24%

■ mature

■ pole

▩ sapling

☐ seedling
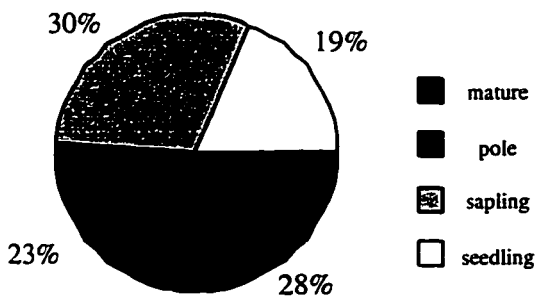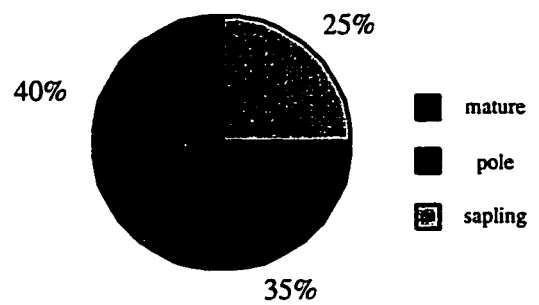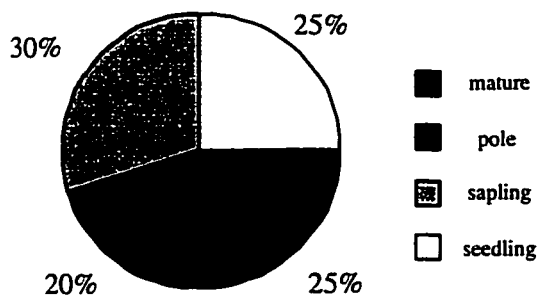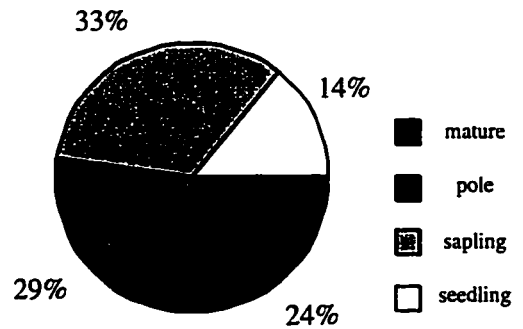
Figure 2.4: Stand distributions by community and age group.

side from the center of the upper stratum plot. The centers of the lower stratum plots were at the centers of the upper stratum and two middle stratum plots. A red or orange flag was used to mark the center of the upper stratum plot. The other points were marked by yellow flags. Flags were identified according to a three-digit description. The first digit corresponded to the transect number, the second to the sample plot, and the third to the subplot. Subplots were sequentially numbered from left to right when facing away from the baseline. Figure 2.5 depicts the layout of a typical 200 x 200 m test stand. Figure 2.6 shows the arrangement of an individual plot on a transect containing sampling sub-plots for all three strata.

2.3.3 Sampling Methodology

Measurements were to be used to (1) estimate stand structure in terms of species composition, height, diameter, crown depth, basal area (BA) and density, and (2) estimate biomass. Therefore, measurements which would either provide direct estimates of these parameters, or could be used in regression equations to estimate the above parameters were identified. These were (1) species, (2) diameter, (3) total height, and (4) clear bole height. Note that species and diameter measurements followed the same protocol for each measurement year. Heights, however, were sampled more intensively in the first two seasons than the last two. Diameter and species are quick and easy measurements to make. Height, on the other hand, is more time intensive. Therefore, only a subsample of heights were taken in all years, and these were then used in development of species-specific diameter-to -height equations from which to estimate the remaining heights. More specific measurement methodology follows.

For the upper stratum, the diameter at breast height (dbh) and species of all living and dead stems in the upper stratum plot originating at or below 1.37 m above ground level (thus each stem in a multiple-stemmed tree is measured) was recorded (to 0.1 cm) using a diameter tape or calipers. Species were recorded using the six letter code given in Table 2.5 which consisted of the first three letters each of the genus and species (e.g., PINRES for red pine). If a stem was dead, an "X" was added to the end of the code (e.g., PINRESX). For the first 28 stands (1991 and 1992), five trees in each 5-cm diameter class for each species in a stand were measured by clinometer for total height and clear bole height (to 0.5 m). Clear bole height is defined as the distance from the base of the stem to the base of the lowest live branch. A random direction from which to commence measuring heights was chosen at each plot. Sampling continued until all diameter classes were completely represented, or until all plots had been inventoried. The total height of all dead individuals was recorded. For the other 38 stands measured in 1993 and 1994, total height and clear bole height of the nearest living individual to the plot center was measured, resulting in 40 stratum one measured heights per stand. Basal stem diameter (15 cm above the ground) was measured (to 0.1 cm) for each individual in the middle stratum by species using vernier calipers. Total
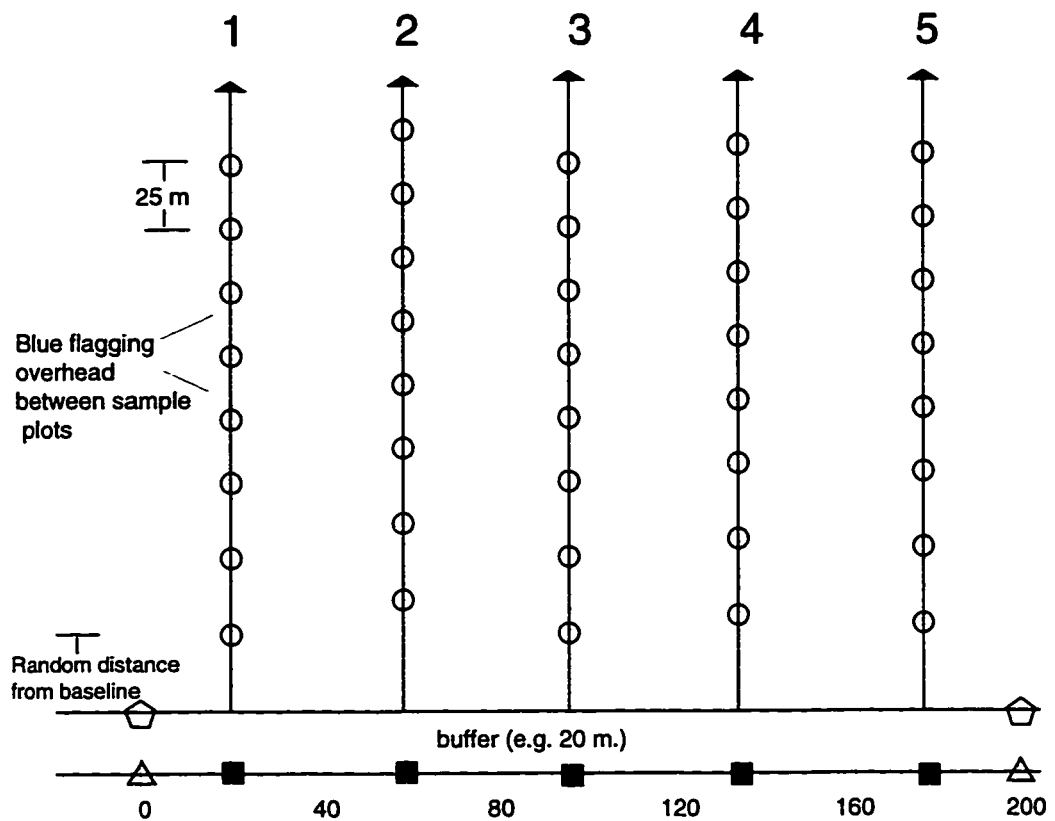
Figure 2.5: Diagram of stand layout.

Figure 3: Diagram of Plot layout
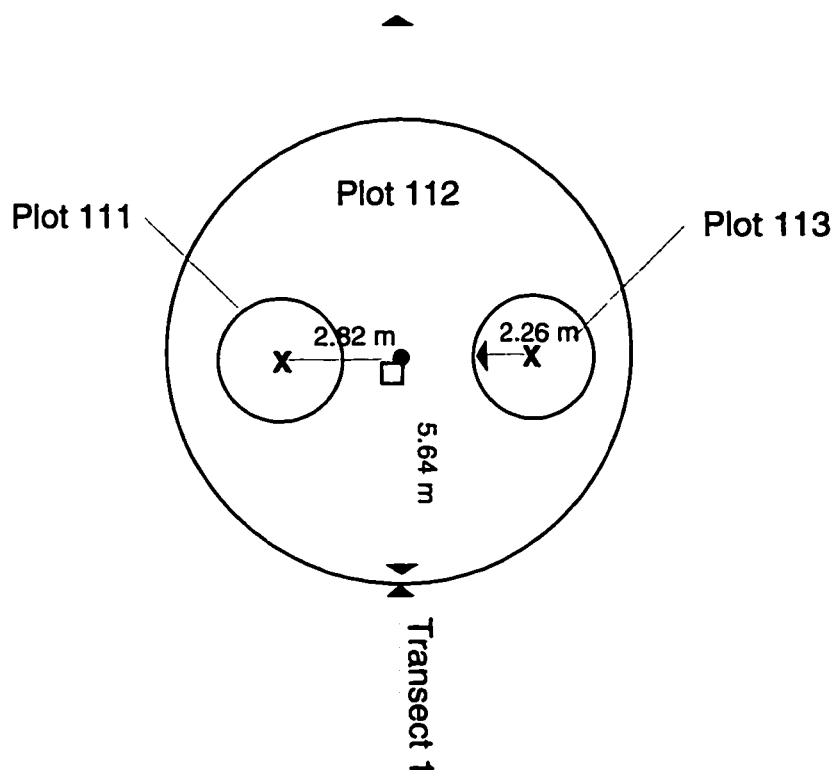
Plots Key	Symbol Key
Permanent: 112 Upper stratum 111,113 Middle stratum **Temporary:** Lower statum plots, $1m^2$ around center of each permanent plot	X = yellow flag ● = red flag ⟶ = transect azimuth

Figure 2.6: Diagram of plot layout.

height (to 0.1 m) of all individuals was measured using a height pole for the first 28 stands to develop diameter-height regressions for the middle story. For the remaining 38 stands measured in 1993 and 1994, only the nearest individual to the middle stratum plot centers were measured resulting in 80 stratum two measured heights per stand. Percent cover of the lower stratum was derived from ocular estimates using a 1 m x 1 m square portable frame which was placed at the centers of the upper and middle stratum plots. In stands containing stratum 2 and/or stratum 1 individuals, percent cover only was recorded. In seedling stands, both percent cover and number of seedling stems by species were recorded.

2.4 Data Processing and Analysis

Over 64,000 trees (stems) were measured during the four measurement seasons. Thus the task of data processing and analysis was a large one consisting of several steps as listed in the table below.

| 1. Data recording and preparation |
| 2. Stand structure analysis |
| 3. Calculated Heights Analysis |
| 4. Stand biomass analysis |

Table 2.8: Data processing and analysis steps.

Most of the desired statistics had been identified early on in the project, and drove the sampling methodology. However, the data processing was designed so that additional, yet-undefined, statistics could be generated from the sample data in the future (one example of this might be within-stand spatial analysis). Assuring that the data were error-free and ready for analysis was a most time-consuming part of the analysis. Efficiency and consistency was achieved by using software (EXCEL and SAS) that was appropriate for the task at a particular stage, and by writing SAS programs that would act on all the data and output multiple statistics at once. These steps are documented in the following sections

2.4.1 Data Recording and Preparation

Data recording and preparation consisted of five general steps summarized in the following table. These steps are further elaborated below.

| 1. Data recording |
| 2. Data input from paper or transfer from dataloggers |
| 3. Creation of EXCEL stand data files |
| 4. Error checking and correction |
| 5. Transfer of files from EXCEL to SAS |

Table 2.9: Data recording and preparation steps.

Data Recording

Data were recorded in the field by either of two methods. The first method involved writing measurements on paper data sheets. In the second method, operators used hand-held dataloggers to record data in an electronic spreadsheet, analogous to the paper data sheets. In both cases, a defined set of data were always recorded. Header information was entered once at the top of each data sheet (or data file) and included the number of the stand, the date, and the measurement crew. Stratum 1 and stratum 2 were recorded on the same data sheets/file. Stratum 3 (ground cover) was recorded separately and will be discussed separately in section 2.4.6. A sample data sheet for the stratum 1 and 2 measurements is shown in Figure 2.7. For each stem measured in stratum 1 and stratum 2, the following were recorded:

1. Location: location had to account for which transect, plot, and sub-plot a tree was in, and therefore a three-character code was used. For example, 322 denotes transect 3, plot 2, subplot 2 (upper stratum plot).

2. Stratum: coded 1 for upper stratum or 2 for middle stratum.

3. Species: the six-letter coded listed in table 3 was used, e.g., PINRES for red pine (PINRESX if dead).

4. Diameter: dbh (1.37 m) for stratum one trees, and basal diameter (15 cm) for stratum 2 trees (to 0.1 cm)

5. Total Height: for selected trees according to the sampling methodology as stated in section 1.3.4

6. Clear Bole Height: measured to lowest live branch and for same trees as Total Height

Data Input or Transfer and Creation of EXCEL Stand Data Files

In the case of data collected on paper, data needed to be input at the computer upon return from the field. The data were entered into EXCEL spreadsheets, one stand per spreadsheet. Each of the above 1-6 fields became an EXCEL column, and all data were then entered in their appropriate cells. Data collected on dataloggers was exported in its native LOTUS format and simply read into EXCEL. Files were stripped of their headers. Files were then named for the number of the stand and the year they were measured, e.g., the filename for stand 22 remeasured in 1994 is R22.94 (R for Raco Site). At the same time, three more columns in addition to 1-6 above were added which would make future data processing more convenient. EXCEL functions were used to automatically create columns to code:

1. Stand number: This number was filled in on each line so that each measured tree was associated with a stand number .

STAND ID.: (1, 2) #61   DATE: 6-11-93
OBSERVERS: AO +DC   PAGE 3 OF 5

PLOT	STRATUM	SPECIES	DIAMETER	TOTALHT	BOLEHT
S-S-1	2	no stems			
S-S-2	1	PINBAN	11.6	9.5	5.5
S-S-3	2	no stems			
S-8-2	1	PINBAN	38.0		
S-8-2	1	PINBAN	14.7	.	
S-8-2	1	PINBAN	22.2		
2-1-1	2	no stems			
2-1-2	1	PINBAN	10.5	15	11
2-1-3	2	no stems			
2-1-2	1	PINBAND	11.3		
2-1-2	1	PINBAN	12.7	.	
2-1-2	1	PINBANX	11.0		
2-1-2	1	PINBAN	17.7		
2-1-2	1	PINBAN	15.2		
2-1-2	1	PINBANX	9.9		
2-1-2	1	PINBAN	13.5		
2-1-2	1	PINBAN	16.5		
2-1-2	1	PINBAN	11.4		
2-1-2	1	PINBAN	13.8	.	
2-1-2	1	PINBAND	8.3		
2-1-2	1	PINBANX	9.0		.
2-1-2	1	PINBAN	10.7		
2-1-2	1	PINBAN	13.9		
2-1-2	1	PINBAN	15.5		.
2-1-2	1	PINBAN	11.9		
2-1-2	1	PINBANA	9.6		
2-1-2	1	PINBANX	7.5		
2-1-2	1	PINBAN	16.1		
2-1-2	1	PINBAN Y	8.2	.	
2-1-2	1	PINBAN X	7.7		
2-1-2	1	PINBAN	17.2		
2-1-2	1	PINBAN	12.0		.
2-2-1	2	no stems			
2-2-2	1	PINBAN	11.3	10	5
2-2-3	2	no stems			
2-2-2	1	PINBAN	9.3		
2-2-2	1	PINBAND	5.3		
2-2-2	1	PINBAN	13.9		
2-2-2	1	PINBAN	3.8		
2-2-2	1	PINBAN	11.7		
2-2-2	1	PINBAN	19.9		
2-3-1	2	no stems			
2-3-2	1	PINBAN	9.8	9	4.5
2-3-3	2	no stems			
2-3-2	1	PINBAN	12.2		
2-3-2	1	PINBAN	14.5		
2-3-2	1	PINRES	39.0		

Figure 2.7: Sample data sheet for stratum 1.

2. Year: Year the tree was measured

3. Type: being either conifer (coded 1) or deciduous (coded 2). This was determined from the species name.

4. Status: being either dead (0), living (1), or diseased (2). This was determined from the species name where a name code such as PINRESX denoted dead, and PINBAND denoted diseased (Diseased was coded for jack pine only and only in 1993. This information has not been used to date and diseased trees have always been considered live in all analyses).

Error Checking and Correction

After all data were assembled into EXCEL files by stand, error checking was begun. This was done in two stages. First a manual check was done by proofreading the file against the paper data sheet if that were the original recording medium or by visually checking the output of the datalogger file which had been converted into EXCEL. Experience with these procedures had shown that this was unlikely to clear up all errors. Therefore a logical error-checker was written as an EXCEL program and run on each file. This error checker looked for logical errors such as heights which were outside of a recorded stratum class, plot numbers which did not correspond to stratum numbers, or diameters which were too large or small to be logical, etc. The logical error-checker proved to be extremely useful and located many errors understandably not found by visual proofreading. Lastly a spelling dictionary was constructed consisting of all possible species codes and each file was checked against this. In all cases where errors were found they could be corrected either on sight by the author, or by consulting original paper data sheets.

Transfer of Files from EXCEL to SAS

After files were considered "clean" they were sorted to be in plot number order, stripped of their column headers, and exported as plain comma-delimited ASCII text files (csv format). Each case (tree) had the following variables and variable names:

stand (2-digit stand number)

year (2-digit year)

plot (3-digit plotnumber)

stratum (coded 1 or 2)

species (6 or 7 letter code)

diam (diameter in cm)

mht (measured total height in cm)

bht (measured bole height in cm)

status (coded 0=dead, 1=live, 2=diseased)

type (coded 1=conifer, 2=deciduous)

The files were then transferred to the UNIX environment where several new variables were added to the stand text files. These variables were to be used specifically for the calculated heights estimation and were derived from preliminary analysis of the stand data:

tba (total basal area of stand in m^2)

uba (upper stratum basal area of stand in m^2)

mba (middle stratum basal area of stand in m^2)

td (density [stems/ha] of stand)

ud (density of upper stratum)

md (density of middle stratum)

nplots (number of plots sampled for the stand)

All of these numbers were repeated for each tree, or each line, of a stand file. Preliminary estimates for BA and density were included so that, for example, total basal area of a stand could be used in addition to diameter or diameter squared to predict the height of an individual tree (they were later recalculated). Next the stand files were concatenated into one file of 64,433 cases by 17 variables. This file was sorted by stand number and year. It was then imported into SAS and became the master file from which any number of SAS analyses could be generated and additional variables created. Because all analyses acted the same on the entire file, consistency was assured over all stands. At the same time that the existing 17 variables were read into SAS using a **Proc Data** procedure, a number of new variables were also created that would be needed for structural, height, and/or biomass analysis. New variables created were:

logdiam (natural log of the diameter)

logdiam2 (natural log of the diameter squared)

logmht (natural log of the measured height)

diam2 (diameter **2)

invdiam (1/diam)

invba (1/BA)

tba2 (stand total basal area**2)

diamtba (diameter * stand total basal area)

logtba (natural log of stand total basal area)

ba (basal area of an individual tree = 0.00007854*diam2)

mba1 (conversion of the BA of a stratum 2 stem to what it represents per ha)

uba1 (conversion of the BA of a stratum 1 stem to what it represents per ha)

crat (crown ratio = (mht-bht)/mht)

cdep (crown depth = mht-bht)

stem2 (conversion of a stratum 2 stem to what it represents per ha)

stem1 (conversion of a stratum 1 stem to what it represents per ha)

The resulting master file contains data for 40 variables by 64,433 cases (trees), the total of all stems measured from 1991 through 1994 (57,040 live and 7,394 dead).

2.4.2 Stand Structure Analysis

The most basic statistics describing stand structure were generated at three levels: 1) stand, 2) stratum by stand, and 3) species by stand and stratum. The statistics generated at each of these levels include those listed in Table 2.10. Note that some statistics were only generated for stratum one. This was because measurements for these variables were taken for stratum one only.

1. Diameter (mean and std. deviation)
2. Total measured height (mean and std. deviation)
3. Crown depth (mean and std. deviation, stratum 1 only)
4. Basal area (totals)
5. Density (stems/ha - totals)

Table 2.10: Basic stand structure statistics.

Before analyzing the data, plots were made to get an idea of what the distributions looked like. Final versions of these plots were created by a SAS **Proc Gchart** procedure and the results are available in Appendices H and I in Bergen et al. (1995a). Appendix H contains diameter and height histograms by species across all stands. Appendix I contains diameter and height histograms by stand across all species in the stand.

43

Results of stand structure statistical analyses are available in this dissertation and in Bergen et al. (1995a). In the dissertation, stand level means and/or totals for the above variables are included as part of Appendix A: Stand Summary Statistics. Statistics for BA and density are further broken down in this table into statistics giving information on status or type such as total live stems/ha, BA conifer percent, etc. Means and totals of the above variables by stand, stratum, and further by individual species for live trees only, were created by the SAS **Proc Tabulate** procedure and are presented in Bergen et al. (1995a) in Appendix E: Stand Structure by Stratum and Species.

2.4.3 Calculated Heights Analysis

Because derivation of the biophysical parameter height is a MFTS image analysis goal, reliable estimates of tree heights was a biometric survey objective. Height is also an important variable because height and diameter are the two most important predictor variables for biomass, another image analysis goal and one studied in this dissertation. Most allometric biomass equations used some combination of these two variables. While diameter was measured for all trees, height was only measured on a subset of those because it is more time-consuming to measure. Because there is a strong positive relationship between diameter and height, equations could be built using the subset of trees for which both variables were measured, and these equations could then be used to predict the height of the remaining trees. As mentioned, some form of diameter is the most common predictor of height, and if species height equations were being built for each species in each stand separately, likely some form of diameter could be the sole predictor variable. However, in this analysis, it was desired to develop one set of species height equations which would work across all test stands. This introduces the problem of between-stand variability in the relationship between diameter and height for any given species. To address this issue, it was necessary to introduce a variable(s) into the predicted height equations which would account for this variability between stands. The variables used were chosen on the hypothesis that two biological reasons for a varying relationship between diameter and height are site index and stem crowding or density. For example, in general it would be expected that given two red pine plantations with trees with approximately equal mean diameters, but one had a higher BA, that the stand with the higher BA would likely have taller trees. This is likely due to a higher site quality for the taller trees plus a taller, less branchy form for closely grown trees. For this reason, the following additional variables were used in developing species height equations: (1) stand total BA (tba), (2) stand total BA^2 (tba2), and (3) stand total BA * diameter (diamtba). Similar variables based on stand density were also created. The density variables proved less useful in most cases early in the development of the species height equations and so were dropped.

An additional concern was the number of cases used to build each height predictor equation. Many species were represented by a large number of measurements, and thus

separate equations could be developed for each of these. Because the forest communities studied in this project have significantly different diameter to height relationships, species-specific equations are desirable (e.g., sapling pines or n. white-cedar are thicker than sapling hardwoods or black spruce of equivalent height). However, a number of species occurred very infrequently in the dataset and too infrequently to construct a valid height prediction equation for that species. Therefore, the infrequently occurring species were temporarily recoded to the most similar frequently occurring species. For example *Fraxinus nigra* was recoded to be the same as *Fraxinus americana* for the purposes of height predictor equation development only.

Histograms were plotted for all of the species/species groups to assess their height and diameter distributions. Because of the sampling protocol, most were skewed to the left (many smaller stems and then a normal distribution of larger trees). Scatterplots of height vs. diameter were done; most had a strong positive fairly linear or slightly curvilinear relationship. Having prepared and examined the data, the next step was to hypothesize the most likely variables predictor equations. As mentioned these included diameter and BA of the stand (to account for density influence on the height-diameter relationship) plus their squares and products. After several "dry runs" of creating different variable combinations, it appeared that the two most consistently best forms of equations were either a log-log type or a polynomial type. These in fact are two of the most widely applied forms for the diameter-height relationship:

Log-log (natural log): $log(Height) = a + b\,log(Diameter)$ (2.1)

Polynomial: $Height = a + b(Diameter) + c(Diameter^2)$ (2.2)

Following the above investigations of the dataset, the SAS program **Proc Reg** was used in a stepwise regression mode to suggest the best predictor equation by species for both types of equations. In both cases the appropriate (either untransformed or log-transformed) diam, diam2, tba, tba2, and diamtba were given as possible variables, and then the best set of variables at the 0.05 level of significance was chosen for each species for each of the two types. The initial output results from this procedure suggested that in some cases the polynomial form was better and in other cases the log form was better, based on the R^2 and the MSE. However, after transforming the resultant log heights (antilog procedure)and regressing the predicted measured heights on the known measured heights, for all species the log model results had R^2 and MSE's which were equivalent or worse than the polynomial model. Therefore, a polynomial regression was used to develop equations for all species. The resultant final equations are given in Table 2.11.

Species	Model		R²	N of trees
abibal			.8878	991
	INTERCEP	-0.312317		
	DIAM	0.810917		
	DIAM2	-0.008355		
	DIAMTBA	0.002640		
acerub			.9206	2829
acespi	INTERCEP	-0.053945		
tilame	DIAM	0.985245		
	DIAM2	-0.019003		
	TBA	0.006302		
	DIAMTBA	0.009784		
acesac			.9420	1324
	INTERCEP	-0.472167		
	DIAM	1.177551		
	DIAM2	-0.025605		
	TBA	0.065797		
	TBA2	-0.001620		
	DIAMTBA	0.009196		
alnrug			.8189	131
	INTERCEP	0.377733		
	DIAM	1.102191		
	DIAMTBA	-0.004568		
amespp			.7938	809
ostvir	INTERCEP	0.852765		
	DIAM	0.296181		
	DIAM2	0.015870		
	TBA2	-0.000566		
	DIAMTBA	0.031192		
aromel			.7296	36
	INTERCEP	1.196736		
	DIAM2	0.437723		
betall			.8609	171
	INTERCEP	0.656460		
	DIAM	0.947649		
	DIAM2	-0.009799		
betpap			.9450	219
	INTERCEP	0.548349		
	DIAM	0.859468		
	DIAM2	-0.010753		
	DIAMTBA	0.007314		

Table 2.11: Height prediction equations.

Species	Model		R^2	N of trees
corcor			.3372	324
coralt	INTERCEP	0.649879		
corsto	DIAM	0.684856		
	TBA	0.005883		
faggra			.9410	1637
	INTERCEP	0.176495		
	DIAM	0.974520		
	DIAM2	-0.011538		
	DIAMTBA	0.002528		
fraame			.9279	50
franig	INTERCEP	-0.149437		
	DIAM	2.155701		
	DIAM2	-0.044145		
	DIAMTBA	-0.009090		
larlar			.9765	21
	INTERCEP	-0.930448		
	DIAM	1.337746		
	DIAM2	-0.020541		
	TBA2	0.001539		
	DIAMTBA	-0.004876		
picgla			.9378	113
	INTERCEP	-2.014485		
	DIAM	0.965499		
	DIAM2	-0.011677		
	TBA2	0.001340		
picmar			.9183	165
	INTERCEP	-4.212692		
	DIAM	1.245605		
	DIAM2	-0.019224		
	TBA	0.150598		
	TBA2	-0.001285		
pinban			.8568	2532
	INTERCEP	0.152655		
	DIAM	0.532980		
	DIAM2	-0.009915		
	DIAMTBA	0.017242		
pinres			.9184	1099
	INTERCEP	-0.657224		
	DIAM	0.669415		
	DIAM2	-0.004735		
	TBA	-0.126088		
	TBA2	0.008188		

Table 2.11 cont'd.

Species	Model		R²	N of trees
pinstr			.9098	226
pinsyl	INTERCEP	-7.116103		
	DIAM	0.931696		
	DIAM2	-0.008313		
	TBA	0.415283		
	TBA2	-0.005499		
popgra			.9006	1152
popbal	INTERCEP	0.038512		
popdel	DIAM	0.914963		
	DIAM2	-0.022723		
	DIAMTBA	0.016074		
poptre			.9366	1909
	INTERCEP	-0.868723		
	DIAM	1.284616		
	DIAM2	-0.017115		
	TBA	0.069598		
	TBA2	-0.000564		
	DIAMTBA	-0.001625		
prupen			.8914	1297
pruser	INTERCEP	0.075151		
pruvir	DIAM	0.441082		
pruspp	DIAM2	-0.044792		
	TBA	0.081080		
	TBA2	-0.003192		
	DIAMTBA	0.047054		
querub			.9684	103
queell	INTERCEP	0.476589		
	DIAM	0.397380		
	DIAM2	-0.005962		
	TBA2	0.000371		
	DIAMTBA	0.012646		
salspp			.4787	324
	INTERCEP	0.336147		
	DIAM	0.800008		
	DIAM2	-0.075952		
	TBA	0.034101		
	TBA2	-0.000737		
	DIAMTBA	0.006947		

Table 2.11 cont'd.

Species	Model		R²	N of trees
ilever			.3549	247
ledgro	INTERCEP	0.973919		
loncan	DIAM	0.344983		
lonspp				
nemmuc				
samcan				
sampub				
sorame				
thuocc			.8730	161
	INTERCEP	0.013757		
	DIAM	0.831188		
	DIAM2	-0.010600		
tsucan			.8958	41
	INTERCEP	0.507701		
	DIAM2	-0.007108		
	DIAMTBA	0.017833		
vibcas			.4921	134
vibspp	INTERCEP	0.779214		
	DIAM	0.597172		

Table 2.11 cont'd.

This procedure resulted in a calculated height for every live tree in the SAS datafile. However, in a number of cases, true measured heights existed. Therefore a step was taken to create a new, final, height variable called bioht which was the measured height for a tree if it existed, else it was the calculated height. This height (bioht) was subsequently used for producing tables of height statistics and in the biomass equations. Appendix F: Heights, in Bergen et al. (1995a) provides detailed height data including bioht means and standard deviations by stand, year, stratum, and species.

One additional summary height variable was created which would be preferred for use with SAR image processing. A basal area weighted average height was calculated for each stand. This was done to counteract the effect that a significant number of smaller subdominant trees could have in lowering the apparent mean height of the stand, including the dominant overstory trees. The calculation was as follows:

$$\frac{\sum_{i,j} (d_i^2 \frac{\pi}{4}) (h_j)}{\sum n_i * d_i^2 * \frac{\pi}{4}}$$ (2.3)

Where n_{ij} = the number of stems/ha of diam i and ht j , d = diameter (in m), and h = height (in m). This statistic, as well as those in Table 2.10 are summarized by stand in Appendix A: Stand Summary Statistics.

49

2.4.4 Stand Biomass Analysis

Once heights were calculated for all files, all variables needed for the biomass estimation were available. The following table lists the general steps necessary in producing valid results for a number of biomass statistics.

1. Locate potential allometric biomass component equations for all species
2. Determine "best" biomass component equations for each species
3. Write SAS biomass estimation program to estimate biomass for each component of each individual tree
4. Write SAS programs to produce summary statistics by stand, stratum, and species, for each component and to produce stand totals such as summer total, winter total, conifer total etc.

Table 2.12: Biomass analysis steps.

Potential stratum 1 (trees > 5 m) allometric biomass equations were assembled from those used in a preliminary analysis done at Michigan Technological University plus additional references located from the literature. Additionally, potential stratum 2 (1 m $\leq$ trees < 5 m) equations were gathered from any of the above equations which might also be suitable for (e.g., were developed on) trees of the size found in our stratum 2 and from a recent publication (Perala and Alban, 1994) which reported biomass equations specifically developed for shrub and sapling trees.

Curves for all of these species specific equations were plotted using a distribution of diameters from 0 to 50 cm and heights predicted from our height equation for that species. With this, any regression equations which were clearly "unusual" were found and dropped from further consideration. For stratum 1 some biomass equations used in the preliminary analysis were retained and others were adopted from Perala and Alban. This process also confirmed that for stratum 2, the regression equations developed by Perala and Alban performed the best for all species. Biomass equations and their sources in the literature are given in Table 2.13

A SAS program was written to calculate dry biomass in kg by biomass component (stem, branch, and foliage) for each tree in the SAS data file. Futher, the program calculates all the variables needed for additional programs to produce summary statistics by stand, including summer total, winter total, summer crown, and winter crown. Finally, the program also converts all of these to a per hectare basis.

Species	Biomass component equation	R^2
ABIBAL	STRATUM 1 (Perala and Alban, 1994)	
	Bole $y=0.005751 * (d^{2.082}) * (h^{0.3834}) * 1.331 + 0.02348 * (d^{1.926}) * (h^{0.76}) * 1.097$	.98
	Branches $y=0.02403 * (d^{3.501}) * (h^{-1.2}) * 0.7111 + 0.001216 * (d^{2.306}) * 6.059$	.90
	Foliage $y=0.03583 * (d^{3.12}) * (h^{-1.099}) * 0.6333$	.89
	STRATUM 2 (Perala and Alban, 1994)	
	Bole $y=0.08088 * ((10 * sd)^{2.662})/1000$	.96
	Foliage $y=0.1193 * ((10 * sd)^{2.23})/1000$	.88
ACERUB	STRATUM 1 (Perala and Alban, 1994)	
ACESAC	Bole $y=0.02102 * (d^{2.191}) * 1.461 + 0.02347 * (d^{1.888}) * (h^{0.9912})$	.99
ACEPEN	Branches $y=0.1072 * (d^{2.841}) * (h^{-1.04}) + 0.0038 * (d^{2.337})$	.92
ACESPI	Foliage $y=0.01913 * (d^{1.867}) * 0.4962$	.82
TILAME	STRATUM 2 (Perala and Alban, 1994)	
	Bole $y=0.06242 * ((10 * sd)^{2.486}) * (5^{0.3991})/1000$	.95
	Foliage $y=0.09901 * ((10 * sd)^{2.113})/1000$	.91
ALNRUG	STRATUM 1 (Perala and Alban, 1994)	
	Bole $y=0.02025 * (d^{2.246}) * 1.271 + 0.02198 * (d^{1.865}) * (h^{1.046})$	.91
	Branches $y=0.08248 * (d^{3.753}) * (h^{-1.847}) + 0.0009194 * (d^{2.487}) * 0.1909$	.89
	Foliage $y=0.07611 * (d^{2.763}) * (h^{-1.483})$	.85
	STRATUM 2 (Perala and Alban, 1994)	
	Bole $y=0.0298 * ((10 * sd)^{2.666}) * (5^{0.4243})/1000$	.96
	Foliage $y=0.08227 * ((10 * sd)^{2.058})/1000$	.88
AMESPP	STRATUM 1 (Crow and Erdmann, 1983)	
AROMEL	Bole $y=EXP(-2.943 + 0.878 * LN((d^2) * h))$	.99
OSTVIR	Branches $y=EXP(-6.128 + 1.087 * LN((d^2) * h))$	.56
SORAME	Foliage $y=EXP(-3.648 + 0.556 * LN((d^2) * h))$	.57
	STRATUM 2 (Perala and Alban, 1994)	
	Bole $y=0.163 * ((10 * sd)^{2.494})/1000$	.95
	Foliage $y=0.107 * ((10 * sd)^{1.925})/1000$	.87
BETALL	STRATUM 1 (Perala and Alban, 1994)	
	Bole $y=0.01445 * (d^{2.451}) + 0.05481 * (d^{2.619})$	.99
	Branches $y=0.01748 * (d^{2.55}) + 0.0009194 * (d^{2.487})$	.93
	Foliage $y=0.00696 * (d^{2.003})$	.72
	STRATUM 2 (Perala and Alban, 1994)	
	Bole $y=0.0298 * ((10 * sd)^{2.666}) * (5^{0.4243})/1000$	.96
	Foliage $y=0.08227 * ((10 * sd)^{2.058})/1000$	.88
BETPAP	STRATUM 1 (Perala and Alban, 1994)	
	Bole $y=0.02198 * (d^{2.215}) * 1.265 + 0.02214 * (d^{1.857}) * (h^{1.048})$	.99
	Branches $y=0.08908 * (d^{3.772}) * (h^{-1.893}) + 0.0008746 * (d^{2.496}) * 0.1971$	.98
	Foliage $y=0.0852 * (d^{2.744}) * (h^{-1.51})$	.89
	STRATUM 2 (Perala and Alban, 1994)	
	Bole $y=0.02373 * ((10 * sd)^{2.687}) * (5^{0.4838})/1000$	.96
	Foliage $y=0.06132 * ((10 * sd)^{2.174})/1000$	.88

Table 2.13: Biomass equations.

Species	Biomass component equation	R^2
CORCOR	STRATUM 1 (Ker, 1980)	
	Bole $y=EXP(-3.0782 + 1.8482 * LN(d) + 0.8715 * LN(h))$	.99
	Branches $y=EXP(-2.0235 + 3.4366 * LN(d) - 1.643 * LN(h))$	.91
	Foliage $y=EXP(-4.1049 + 1.7241 * LN(d))$	.93
	STRATUM 2 (Perala and Alban, 1994)	
	Bole $y=0.04544 * ((10 * sd)^{2.848}) * (5^{0.1594})/1000$	.90
	Foliage $y=0.07188 * ((10 * sd)^{2.244})/1000$	.72
CORSTO	STRATUM 2 (Perala and Alban, 1994)	
CORALT	Bole $y=0.05237 * ((10 * sd)^{2.663}) * (5^{0.2258})/1000$	.91
ILEVER	Foliage $y=0.1615 * ((10 * sd)^{1.985}) * (5^{-0.1682})/1000$	.83
NEMMUC		
FAGGRA	STRATUM 1 (Ker, 1980)	
	Bole $y=EXP(-2.9936 + 1.8565 * LN(d) + 0.8336 * LN(h))$	.99
	Branches $y=EXP(-3.5982 + 2.3708 * LN(d))$	.89
	Foliage $y=EXP(-3.7607 + 1.6303 * LN(d))$	.86
	STRATUM 2 (Perala and Alban, 1994)	
	Bole $y=0.05237 * ((10 * sd)^{2.663}) * (5^{0.2258})/1000$	.91
	Foliage $y=0.1615 * ((10 * sd)^{1.985}) * (5^{-0.1682})/1000$	.83
FRAAME	STRATUM 1 (Ker, 1980)	
FRANIG	Bole $y=EXP(-2.75 + 2.0199 * LN(d) + 0.5412 * LN(h))$	.99
	Branches $y=EXP(-1.3458 + 3.4031 * LN(d) - 1.9487 * LN(h))$	.95
	Foliage $y=EXP(-3.043 + 2.3071 * LN(d) - 0.9888 * LN(h))$	.94
	STRATUM 2 (Perala and Alban, 1994)	
	Bole $y=0.05041 * ((10 * sd)^{2.545}) * (5^{0.34})/1000$	.95
	Foliage $y=0.07334 * ((10 * sd)^{2.088})/1000$	.91
LONSPP	STRATUM 2 (Perala and Alban, 1994)	
LONCAN	Bole $y=0.115 * (sd^{2.749})$	.90
LEDGRO	Foliage $y=0.1176 * (sd^{1.891})$	.85
SAMCAN		
SAMPUB		
VIBCAS		
VIBSPP		
PICGLA	STRATUM 1 (Perala and Alban, 1994)	
	Bole $y=0.01014 * (d^{1.509}) * (h^{0.783}) * 1.177 + 0.03123 * (d^{1.783}) * (h^{0.926}) * 0.8345$	.99
	Branches $y=.07316 * (d^{3.53}) * (h^{-1.784}) * 0.6615 + 0.03095 * (d^{1.002}) * (h^{1.103}) * 0.6338$	.92
	Foliage $y=0.03064 * (d^{2.787}) * (h^{-0.7147})$	.91
	STRATUM 2 (Perala and Alban, 1994)	
	ABIBAL equations used	
PICMAR	STRATUM 1 (Grigal and Kernick, 1984)	
LARLAR	Bole $y=0.1183 * (d^{2.26})$	.98
	Branches $y=(0.0251 * (d^2)) + (0.0004 * (d^{3.324}))$	.91
	Foliage $y=0.061 * (d^{1.411})$	.77
	STRATUM 2 (Perala and Alban, 1994)	
	ABIBAL equations used	

Table 2.13 cont'd.

Species	Biomass component equation	R^2
PINBAN	STRATUM 1 (Perala and Alban, 1994)	
	Bole $y=0.0157 * (d^{1.775}) * (h^{0.3952}) * 1.294 + 0.01395 * (d^{1.709}) * (h^{1.327})$	.98
	Branches $y=0.002956 * (d^{2.83}) + 0.2391 * (d^{2.943}) * (h^{-1.769}) * 0.3556$	.94
	Foliage $y=0.0008988 * (d^{2.903}) * 1.569$	.82
	STRATUM 2 (Perala and Alban, 1994)	
	ABIBAL equations used	
PINRES	STRATUM 1 (Perala and Alban, 1994)	
	Bole $y=0.01408 * (d^{2.09}) + 0.02137 * (d^{1.809}) * (h^{1.037}) * 0.8823$	.90
	Branches $y=0.03118 * (d^{4.098}) * (h^{-2.271}) * 0.6497 + 0.0005819 * (d^{2.714}) * 4.199$	.95
	Foliage $y=0.0006622 * (d^{3.122}) * 1.313$	.89
	STRATUM 2 (Perala and Alban, 1994)	
	ABIBAL equations used	
PINSTR	STRATUM 1 (Ker, 1980)	
	Bole $y=EXP(-3.202 + 1.899 * LN(d) + 0.724 * LN(h))$	.98
	Branches $y=EXP(-2.6466 + 1.7086 * LN(d))$	.73
	Foliage $y=EXP(-2.6925 + 1.4653 * LN(d))$	.78
	STRATUM 2 (Perala and Alban, 1994)	
	ABIBAL equations used	
POPGRA	STRATUM 1 (Koerper and Richardson, 1980)	
	Bole $y=0.001 * (EXP(3.5894 + 2.6544 * (LN(d))) + EXP(3.4255 + 2.2034 * (LN(d))))$	.98
	Branches $y=0.001 * (EXP(0.5799 + 2.9459 * (LN(d))) + EXP(-0.4643 + 2.938 * (LN(d))))$	.95
	Foliage $y=0.001 * (EXP(1.2846 + 2.1483 * (LN(d))) + EXP(-1.6095 + 2.3834 * (LN(d))))$	.88
	STRATUM 2 (Perala and Alban, 1994)	
	Bole $y=0.1671 * ((10 * sd)^{2.329})/1000$	.97
	Foliage $y=0.2266 * ((10 * sd)^{2.068}) * (3^{-0.5506})/1000$	.91
POPTRE	STRATUM 1 (Koerper and Richardson, 1980)	
	Bole $y=0.001 * (EXP(3.5894 + 2.6544 * (LN(d))) + EXP(3.4255 + 2.2034 * (LN(d))))$	.98
	Branches $y=0.001 * (EXP(0.5799 + 2.9459 * (LN(d))) + EXP(-0.4643 + 2.938 * (LN(d))))$	.95
	Foliage $y=0.001 * (EXP(1.2846 + 2.1483 * (LN(d))) + EXP(-1.6095 + 2.3834 * (LN(d))))$	.88
	STRATUM 2 (Perala and Alban, 1994)	
	Bole $y=0.07789 * ((10 * sd)^{2.563}) * (3^{0.1107})/1000$	.94
	Foliage $y=0.08338 * ((10 * sd)^{2.248}) * (3^{-0.4375})/1000$	.82
PRUSER	STRATUM 1 (Crow and Erdman, 1983)	
PRUPEN	Bole $y=EXP(-2.943 + 0.878 * LN((d^2) * h))$	.99
PRUVIR	Branches $y=EXP(-6.128 + 1.087 * LN((d^2) * h))$	.56
PRUSPP	Foliage $y=EXP(-3.648 + 0.556 * LN((d^2) * h))$	.57
	STRATUM 2 (Perala and Alban, 1994)	
	Bole $y=0.1263 * ((10 * sd)^{2.496})/1000$	.94
	Foliage $y=0.03475 * ((10 * sd)^{2.512})/1000$	.99

Table 2.13 cont'd.

53

Species	Biomass component equation	R^2
QUERUB QUEELL	STRATUM 1 (Perala and Alban, 1994)	
	Bole $y=0.004408 \cdot (d^{2.047}) \cdot (h^{0.8264}) + 0.02635 \cdot (d^{1.88}) \cdot (h^{0.979})$	.99
	Branches $y=0.01684 \cdot (d^{2.514}) + 0.000478 \cdot (d^{3.125})$	.90
	Foliage $y=0.04801 \cdot (d^{1.455})$	.81
	STRATUM 2 (Perala and Alban, 1994)	
	Bole $y=0.06487 \cdot ((10 \cdot sd)^{2.836})/1000$	.97
	Foliage $y=0.1018 \cdot ((10 \cdot sd)^{2.152})/1000$	.94
SALSPP	STRATUM 1 (Koerper and Richardson, 1980)	
	Bole $y=0.001 \cdot (EXP(3.5894 + 2.6544 \cdot (LN(d))) + EXP(3.4255 + 2.2034 \cdot (LN(d))))$	.98
	Branches $y=0.001 \cdot (EXP(0.5799 + 2.9459 \cdot (LN(d))) + EXP(-0.4643 + 2.938 \cdot (LN(d))))$	.95
	Foliage $y=0.001 \cdot (EXP(1.2846 + 2.1483 \cdot (LN(d))) + EXP(-1.6095 + 2.3834 \cdot (LN(d))))$	.88
	STRATUM 2 (Perala and Alban, 1994)	
	Bole $y=0.04262 \cdot ((10 \cdot sd)^{2.705}) \cdot (5^{0.2872})/1000$	.94
	Foliage $y=0.07912 \cdot ((10 \cdot sd)^{2.14})/1000$	.84
THUOCC	STRATUM 1 (Perala and Alban, 1994)	
	Bole $y=0.009025 \cdot (d^{1.896}) \cdot (h^{0.39}) + 0.04475 \cdot (d^{1.851}) \cdot (h^{0.5099})$	.99
	Branches $y=0.006964 \cdot (d^{2.599}) + 0.03812 \cdot (d^{1.472})$	.94
	Foliage $y=0.01001 \cdot (d^{2.303})$	.94
	STRATUM 2 (Perala and Alban, 1994)	
	ABIBAL equations used	
TSUCAN	STRATUM 1 (Ker, 1980)	
	Bole $y=EXP(-3.0535 + 1.8174 \cdot LN(d) + 0.7576 \cdot LN(h))$	.99
	Branches $y=EXP(-2.1353 + 2.9165 \cdot LN(d) - 1.4459 \cdot LN(h))$	.94
	Foliage $y=EXP(-2.5014 + 2.5251 \cdot LN(d) - 1.2168 + LN(h))$	.94
	STRATUM 2 (Perala and Alban, 1994)	
	ABIBAL equations used	

Table 2.13 cont'd.

In the above equations, y is defined as biomass on a dry-weight basis (kg), d is diameter at breast height (cm), sd is diameter at 15 cm. (cm), h is total height (m).

In the cases where several species are listed beside one biomass equation, it can be assumed that the equation was developed for the first species listed. The same equation was used to estimate biomass for other species which follow because no published equations were available.

2.4.5 Remeasure

As was discussed in section 2.3.1, some test stands were remeasured. This was done for two reasons: (1) to estimate growth, and (2) to update 1991-1993 stand structure and biomass estimates for use with 1994 image data. For the remeasure, stands were sampled at a lower intensity as determined by an analysis of error rates (sampling error as % of the mean) achieved for the original measurement. Table 2.14 shows the number of sample plots needed to achieve desired error rates of 15-20% or better (calculated for diameter measurements). The desire to sample fewer plots was driven by time and funding

Stand	Community	N of plots needed	
		15% error	20% error
22	red pine - sapling	20	11
33	aspen - sapling	13	7
35	jack pine - sapling	50	28
36	jack pine - sapling	40	22
38	jack pine - sapling	16	9
41	red pine - sapling	32	18
49	aspen - sapling	39	22

Table 2.14: N of plots for desired error rate

constraints. The figures given in Table X suggested that the sampling intensity could be lowered for the remeasure and still achieve approximately a 20% error rate.

2.4.6 Ground-Cover Analysis

As mentioned in sections in 1.3, ground-cover analysis proceded differently from the stratum 1 and 2 analysis. The main objective for the ground-cover measurement was to quantify the percent of substrate which was covered with living, green vegetation for each stand. This statistic was easily arrived at by calculating an average and standard deviation of ground-cover percent based on the 120 measurements per stand. Gound-cover percent by stand is given in Appendix A: Stand Summary Statistics.

2.5 GIS and Other Ancillary Data

In 1990, compilation of a multi-layer geographic information system to be used by for this dissertation research and for all researchers working in the test site was begun. It was planned to cover not just the area of the Northern Michigan site test stands, but all of Chippewa county (59 townships). The completed GIS is compiled on two different scales, one with a 12.5 m pixel size for use with spaceborne SAR data, including the SIR-C/X-SAR data used in this dissertation, and one with 4 meter pixel resolution for use with JPL AIRSAR data. All data were obtained (and retained) in the NAD27 datum, and all processed files were output to the UTM coordinate system. The GIS has the following layers:

1. Topography,

2. Transportation including state and federal highways, county roads, two-track roads, and residential streets transportation,

3. Hydrology,

4. Land cover, and

5. Test stands.

Topography, hydrology, and transportation are primarily useful for image warping and orthorectification. Land-cover is also useful for warping and used as a visual reference and validation source. Following is a fuller description of the source and composition of each layer.

2.5.1 GIS Data Layers

Transportation

The source of the transportation GIS layer was Michigan DNR MIRIS data for Chippewa county which had been digitized over several years from 1:24,000 USGS quadrangle maps as a major DNR project. The county-level level data was acquired in Integraph SIF format (vector). It was converted from SIF to ERDAS .dig format using the C-Map Program. The .dig vector files files were converted to raster format in ERDAS at the desired 4 and 12.5 meter pixel resolutions. They were then exported from ERDAS format to PCI, the package used for image processing.

Hydrology

Hydrology also was derived from Michigan DNR MIRIS data, and the same procedures were followed as for the transportation layer. The hydrology layer includes rivers, streams and lakes.

Topography

The source for topography was USGS digital elevation models (DEM) at the scale of 1:250,000. DEMs at the scale of 1:24,000 are available for a few selected quadrangles, but not covering our entire area. DEMs were read into ERDAS and converted to the UTM datum and required pixel resolutions using several ERDAS programs designed to do this. Again, they were exported from ERDAS to PCI format.

Land Cover

The source of the land-cover GIS layer was Michigan DNR MIRIS data for Chippewa county. This data set was compiled by the DNR for the entire state on a township by township basis using 1979 aerial photographs and field checks. It is classified to level III of the USGS/Michigan land use classification scheme (Anderson et al., 1976). For example, 411 is forest - upland hardwood - beech/sugar maple. The same procedures used for other MIRIS data were needed for the land-cover data (format changes and rasterizing), and in addition it was necessary to recode the data to fit into an 8-bit format (e.g., 411 became 20). Error checking against DNR paper maps was needed on the land-cover data as MIRIS data obtained directly from MI DNR has not been cleaned and built and a number of polygons were either coded incorrectly or had no numbers associated with them. GIS data were

converted to ERDAS format and then to PCI for use with image processing.

Test Stands Source

Because a highly accurate GIS layer of the test stands (within 10 m) was needed, I planned and carried out a global positioning system GPS survey of the stands and processed the data to create a GIS layer containing geo-referenced polygons representing the forest test stands. Trimble Pathfinder GPS units which were compatible with the base station installed at the Escanaba office of the Hiawatha National Forest were secured. The first 28 stands were surveyed in August 1992, and the remaining 38 in November of 1993. GPS coordinates were taken at two points in each stand: meter 0.0 and meter 200.0 on the baseline. Coordinates were taken in the WGS-94 datum and were output as Universal Transverse Mercator (UTM) coordinates based on the NAD-27 datum to correspond to the other layers of the GIS which were always NAD-27. At least 180 sample coordinates were taken at each point. Coordinates were differentially post- processed against reference data supplied by the U.S. Forest Service GPS base station in Escanaba, MI, and then averaged for each point, to yield the most accurate position possible (approximately 5 m in the open, and 10-15 m under closed tree canopies). The two differentially processed and averaged coordinates for each stand were combined with other stand information including n of transects, n of plots per transect, all offsets, and azimuths, in a program which output stand polygons, both regular-shaped and irregular shaped in individual GIS format (ERDAS .dig) files. These were then reformatted into a single layer containing all the stands in PCI. When overlaid on the SAR imagery and other GIS layers, the stand layer showed the desired degree of positional accuracy (better then +/- 15 m). GPS coordinates inUTM of the lower left and upper right corners of each stand are provided in Appendix A: Stand Summary Statistics following measurement data in the table.

CHAPTER 3

MULTI-TEMPORAL CLASSIFICATION OF SIR-C/X-SAR

3.1 Introduction

The SIR-C/X-SAR instrument is the first to acquire simultaneous multi-frequency SAR imagery from space. It has fully polarimetric capabilities at L- and C-band and a single polarization (vv) at X-band. The April and October dual-flight program of the 1994 SIR-C/X-SAR missions was designed expressly to capture a data set of earth terrain features and processes at two different times of the year. The scientific basis for this design is the fact that the majority of biophysical systems worldwide undergo distinct changes throughout each annual cycle. The acquisition of imagery at two stages in this cycle is especially critical to the goals of SIR-C/X-SAR supersites investigating ecology, oceanography, and hydrology components of earth system sciences whose particular and shared patterns and processes are generally in flux. In ecology specifically, this flux is characteristically expressed in time-cyclic vegetation phenology, in vegetation and substrate moisture conditions, and in gas-exchange cycles. The SIR-C/X-SAR mission plan, having coupled imaging over a daily time frame, repeated at two distinct times during the annual cycle, provides a dataset offering great potential in efforts important to ecology such as land-cover classification and estimation of biophysical parameters.

The first mission took place during the period April 9–19, and the second September 30–October 10. Imagery taken in these two distinct seasons is a synoptic data set documenting two very different stages in annual processes related to ecology. In northern hemisphere temperate regions the April imagery provides spring information and the October imagery provides information for late summer/early fall. The changing seasonal patterns and processes of ecology which may be observed and quantified by SAR in general are related to vegetation foliation (phenology), and moisture status of the vegetation and substrate. At the MFTS (Figure 1.1) the April mission occurred at the beginning of the spring thaw before deciduous leaf-out, and the October mission occurred in the season of late summer/early fall just prior to and during the fall color change of forest deciduous vegetation.

Additionally, because both of these times were periods of rapid change specific to their

time of year, daily imaging within each of the 11 day missions provides a record of seasonal transition. Thus, in addition to the large between season differences, there are also smaller within season moisture trends (e.g., thawing). Superimposed on top of these seasonal differences or trends are less predictable moisture fluctuations (e.g., precipitiation). Thus the dataset may be said to contain two types of temporal information about earth terrain and processes: (1) seasonal moisture and phenology trends and (2) moisture events, particularly precipitation.

Each of the two types of data can and should be exploited for their particular and different scientific purpose. The large-scale seasonal differences and trends may be employed as additional information in classifier development and this is the focus of the multi-temporal research described in this chapter. This is based on the hypothesis that it is possible to use imagery taken at distinctly different moisture and phenology states to enhance land-cover classification results due to increased capability for separation of vegetation types. This will be the case if in fact the environmental and phenologic conditions which change with time on the ground do so in a fashion consistent with what is found on the imagery. Using the SIR-C/X-SAR dataset, classifications may be developed capitalizing on these phenologic and moisture differences while holding incidence angle and azimuth as constant as the dataset can allow. Table 3.1 lists the available SIR-C/X-SAR scenes and their attributes for the MFTS and highlights the portion of the dataset used to study multi-temporal classifier development. The sensitivity of SIR-C/X-SAR image backscatter to finer daily perturbations due to precipitation will be the focus of future work. The work presented in this chapter builds on: (1) prior work in SAR-based classification methodologies, and (2) multi-date classification explored with other sensor systems.

3.1.1 Objectives

The objectives of this study are:

1) To demonstrate the appropriateness of hierarchical and structural-based land-cover classification methodologies developed with other sensors (ERS-1/JERS-1 and AIRSAR) for use with the SIR-C/X-SAR sensor and to use these to discriminate terrain cover at increasing levels of specificity.

2) To study the multi-temporal properties of the SIR-C/X-SAR dataset by comparing the success of classifications optimized for a single date, multi-date pooled classifications, and multi-temporal classifications.

3) To better understand the relationship between large seasonal changes in terrain as they are related to backscatter as a function of SIR-C/X-SAR sensor parameters of frequency and polarization.

Date	Orbit	Incidence Angle (scene center)	Azimuth	Vegetation			Ground		
				Spring	Fall		State (F/T)*	Snow (Y/N)	State (W/D)**
					Early	Late			
SRL-1									
4/9	**6.1**	**31.4**	**SW**	*			**F**	**Y**	
4/10	22.22	20.1	SW	▪			F?	Y	
4/13	66.2	22.7	SE	▪			?	Y	
4/14	82.2	30.8	SE	▪			T?	Y	W?
4/14	86.4	24.5	NE	▪			T?	Y	W?
4/15	98.12	36.8	SE	▪			T?	Y	W?
4/15	**102.41**	**31.7**	**NE**	*			**T?**	**Y**	**W?**
4/16	114.1	41.8	SE	▪			T	Y	W
4/16	118.6	37.3	NE	▪			T	Y	W
4/17	134.3	41.3	NE	▪			T	Y	W
4/18	150.2	44.3	NE	▪			T	Y	W
4/19	162	44.7	SE	▪			T	Y	W
SRL-2									
9/30	**6.2**	**31.8**	**SW**		*		**T**	**N**	**D**
10/1	22.2	21.1	SW		▪		T	N	D
10/4	66.2	22.0	SE		▪		T	N	D
10/5	82.2	31.0	SE		▪		T	N	D
10/5	86.4	25.4	NE		▪		T	N	D
10/6	98.2	38.1	SE		▪		T	N	D
10/6	**102.41**	**33.8**	**NE**			*	**T**	**N**	**D**
10/7	114.1	43.7	SE			▪	T	N	M
10/7	118.6	41.2	NE			▪	T	N	M
10/8	134.3	41.2	NE			▪	T	N	W
10/9	150.31	41.2	NE			▪	T	N	W
10/10	166.3	41.2	NE			▪	T	N	M

*F = frozen, T = thawed
*W = wet, D = dry

Table 3.1: MFTS SIR-C/X-SAR scenes and attributes.

Chapter 1 included an introduction to the backgrounds and conceptual models for hierarchical, structural, and multi-temporal classifications. In this chapter the following are discussed: Section 3.2 explains the imagery preprocessing techniques; Section 3.3 interprets the ecology of the test site and the multi-date SIR-C/X-SAR image scenes analyzed; Section 3.4 provides a more in-depth examination of the classification methodologies; Section 3.5 presents results and discussions for each of the three types of classifications listed in Objective 2; and section 3.6 provides conclusions.

```
┌─────────────────────────────┐
│      Scene selection from SLC  │
│      calibrated data set        │
└─────────────────────────────┘
              ▼
┌─────────────────────────────┐
│  Extraction of header information │
│  and image data for desired features │
└─────────────────────────────┘
              ▼
┌─────────────────────────────┐
│         GCP selection           │
└─────────────────────────────┘
              ▼
┌─────────────────────────────┐
│      Orthorectification         │
│      Radiometric calibration    │
│         output to UTM           │
└─────────────────────────────┘
              ▼
┌─────────────────────────────┐
│      Automated co-registration  │
└─────────────────────────────┘
              ▼
┌─────────────────────────────┐
│      Radiometric upgrading      │
│      (speckle noise reduction)  │
└─────────────────────────────┘
              ▼
┌─────────────────────────────┐
│       Feature training and      │
│      testing data extraction    │
└─────────────────────────────┘
```
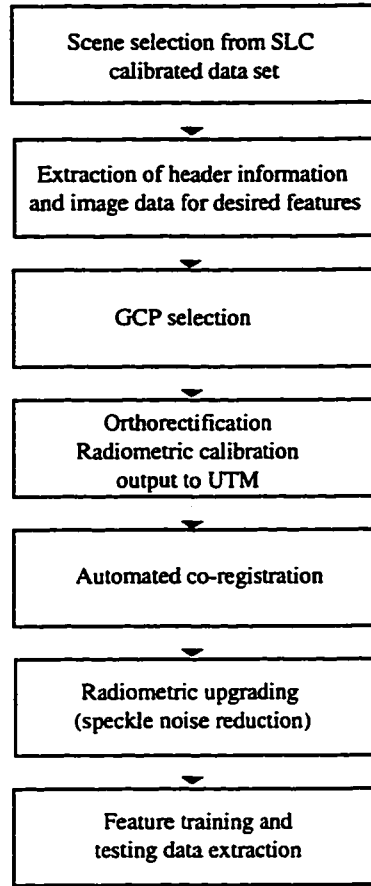
Figure 3.1: Image preprocessing sequence.

3.2 Imagery Preprocessing

3.2.1 Imagery Analyzed

A sequence of processing steps beginning with scene selection and concluding with the extraction of desired features from absolutely calibrated, orthorectified, and radiometrically upgraded imagery was planned and implemented. This is shown in the diagram Figure 3.1.

Detailed information for each scene chosen, plus preprocessing parameters is provided in Table 3.2. The four scenes analyzed for this study were selected to meet three conditions: (1) the scenes should represent the greatest possible range of seasonal environmental conditions, (2) incidence angle should be held as constant as possible, and (3) azimuth look angle should remain constant, or be offset by 180°. The first criteria was accomplished by choosing orbits 6 and 102 on the first and seventh day of each mission, respectively. This gave the largest spread of dates while still meeting criteria two and three.

3.2.2 SIR-C/X-SAR Data

As a NASA supersite, the MFTS received frequent imaging during the 1994 SIR-C/X-SAR dual missions. The site was imaged twelve times between April 9-19 during the SRL-1 mission, and twelve times between September 30 - October 10 during SRL-2. Data were acquired in both ascending and descending modes of the orbit. The ascending path had a track angle of approximately 52 - 53°, for each mission, and the descending path a track angle of 127 -133° for SRL-1, and 127 - 128° for SRL-2. The time of the overflights ranged from 5:25 a.m. local time (EDT) to 2:55 p.m. for SRL-1 and 6:41 a.m. to 3:06 p.m. for SRL-2. Data were taken over a range of planned incidence angles from approximately 20 to 40° (Bergen et al., 1994; Bergen et al., 1995b). The local time for the data-takes used in this study are given in Table 3.2.

The SIR-C data is fully polarimetric at C-band ($\lambda = 1.35$ cm) and L-band ($\lambda = 5.3$ cm). X-SAR data is single polarization X-vv ($\lambda = 3.125$ cm). Nominal pixel resolution of the sensor varies, but averages around 7 m in azimuth and 20 m in range for SIR-C and around 7 m for both range and azimuth for X-SAR. The data were processed by the Jet Propulsion Laboratory (JPL) and the Deutsche Forschungsanstalt for Luft- und Raumfahrt (DLR) to single-look complex values in slant range. Calibration values for antenna pattern correction and amplitude and phase correction are those provided by JPL and DLR. No further calibration is applied to these standard SAR image products. A comparison of the standard JPL calibration factors with those derived from local point and distributed targets is discussed in another paper (Sarabandi et al., 1995). Further processing of the data at The University of Michigan included orthorectification and filtering. Data were orthorectified to a digital elevation model (DEM) interpolated from 1:100,000 DLG hypsography using a program developed jointly by VEXCEL Corporation and The University of Michigan Microwave Image Processing Laboratory. This was followed by filtering to reduce the effects of fading (speckle).

3.2.3 Orthorectification

As an air or spacecraft carrying a SAR flies along a particular path (azimuth), imagery is acquired in slant range. This means that the radar is pointed at an area of terrain off to the side of the craft rather than directly underneath it, and thus measureable distances on the slant-range imagery vary across the image. Elevation information can be used in an orthorectification process to correct for the pixel displacements in range and azimuth resulting from the underlying geometric properties of SAR data acquisition. It is necessary to orthorectify prior to classification for two reasons. First, pixels can be resampled to a ground-range rectangular spacing at the same time retaining their correct radiometric properties (an area correction for the backscattering coefficient). Second, the process allows imagery to be output on a standard grid and earth ellipsoid, in this case UTM (Universal Transverse Mercator), NAD-27. This further allows for the correct overlay of test site

geographic information system (GIS) layers (including training and testing stands) with the imagery. An orthorectification program was developed by The University of Michigan Microwave Image Processing Laboratory in cooperation with VEXCEL Corp., Boulder, Colorado (Kellndorfer et al., 1996a). The orbit data were retrieved from the SIR-C and X-SAR headers, and corrections were made using ground control points (GCPs). These were collected using USGS Digital Line Graph data (DLG) at 1:100,000 plus global positioning system (GPS) point data taken in situ. Only six GCPs were needed on average to supplement the header information. Accuracy was determined to be ± 50 meters in X and Y.

3.2.4 Co-Registration

After the data were orthorectified as accurately as possible, several co-registrations needed to be done as a final refinement so that the imagery could be overlaid with the highest level of confidence. All SIR-C scenes needed to be co-registered, and one scene was chosen as the master, and the others matched to it. Following this the X-SAR imagery was coregistered to the SIR-C imagery. To accomplish this an automated registration program based on the correlation method (Schowengerdt, 1983) was written at the Microwave Image Processing Laboratory. Final results showed registration errors of no more than ± 1 pixel (50 m).

3.2.5 Filtering

To reduce the effects of fading (speckle) due to the coherent properties of SAR backscatter, it is generally useful to apply filtering techniques. In this case two filters were applied in a sequential fashion which reduced the $\pm 1\sigma$ variance around the mean to 0.1 dB. This filtering also reduces the resolution of the data which is about 150 m after application of both filters (in homogeneous areas).

The "Edge Preserving Optimized Speckle" (EPOS) filter (Hagg and Sties, 1994) is designed to preseve edges while significantly reducing the noise in interior homogenous regions. To further smooth the data a 3 x 3 median filter was applied. After both filters the effective N of looks (N of times the data was averaged) was in all cases > 100, varying to a minor degree between the images. The mean of several homogeneous test regions did not change significantly due to filtering, which was the desired outcome. The median filter can potentially alter the mean of an area, however since it was applied here after the speckle filter the means of homogeneous areas were not affected. A better strategy would be needed to avoid rounding-off any corners.

3.2.6 Feature Extraction

Training and testing site data were then extracted for SIR-C along with X-SAR X-vv. The final features include the average power in dB scaled 0-255 for L-hh, vv, hv, C-hh, vv, hv, and X-vv. Due to a sensor misalignment during the missions, X-band data was not acquired during SRL-1 6.1 and SRL-2 6.2 datatakes, and a significant number of datatakes have low overlap between SIR-C and X-SAR. For example SRL-1 102.41 has only approximately 60% overlap. There is good (95%) overlap for SRL-2 102.41. The following gives a summary of the physical model behind the images and how the features are extracted from image files.

The Physical Model: The physical model of the incident and backscattered electric fields can be stated as:

$$E^{scatt} = \frac{1}{r} S E^{inc} \tag{3.1}$$

where E^{scatt} is the backscattered (to sensor) electric field vector, $\frac{1}{r}$ accounts for propogation loss, E^{inc} is the incident (sensor to target) electric field vector, and S is the scattering matrix.

This equation may be expanded to show the individual scattering matrix elements and polarization vectors (for example, S_{vv}):

$$\begin{bmatrix} E_v^{scatt} \\ E_h^{scatt} \end{bmatrix} = \begin{bmatrix} S_{vv} & S_{vh} \\ S_{hv} & S_{hh} \end{bmatrix} \begin{bmatrix} E_v^{inc} \\ E_h^{inc} \end{bmatrix} \tag{3.2}$$

Image Feature Construction: The SAR backscatter values we work with in SAR image processing are termed σ^0. Using an example at some λ and at S_{vv} polarization:

$$\sigma^0 = \frac{4\pi}{A} |S_{vv}|^2 \tag{3.3}$$

where σ^0 is the backscatter coefficient, A is the ground area of a pixel, and $|S|^2$ is power at a particular λ and vv polarization. Note that A is the ellipsoid ground area and that the process of orthorectification replaces it with the correct A.

When the imagery is received after initial processing by JPL, each frequency (band) is present as a separate file containing 10 8-bit integers for each pixel. The first two integers are scaling factors and the remaining 8 are the real and imaginary parts of the amplitude for each polarization combination (vv,hh,hv,vh), scaled by $\sqrt{\frac{4\pi}{A}}$; for example,

$$a + bi = \sqrt{\frac{4\pi}{A}} S_{vv} \tag{3.4}$$

where S_{vv} is the scattering matrix element at some λ and polarization (here vv polarization), and a is the real and b the imaginary part. This is squared to get σ^0 of equation 3.1:

$$a^2 + b^2 = |S_{vv}|^2 \tag{3.5}$$

The power images (e.g. $|S_{vv}|^2$) are scaled to dB by:

$$|S_{vv}|^2(dB) = 10 \log_{10} |S_{vv}|^2(linear) \hspace{3cm} (3.6)$$

These are then rescaled 0-255 for use in image processing software by:

$$[|S_{vv}|^2(dB) + 40](\frac{255}{40}) \hspace{3cm} (3.7)$$

3.3 The Michigan Forests Test Site

In order to co-register the location of forest test stands with orthorectified SAR data, a GIS layer containing the stands was constructed in the UTM coordinate system using a differential global positioning system (GPS) survey (Bergen et al., 1995a). Accuracy of the GPS coordinates is 5-10 m relative to the WGS-84 ellipsoid.

Detailed measurements were made in each stand to quantify stand composition, structure, and biomass and these have been described in greater detail in chapter 2. These provide a level of information beyond nominal categories by which stands may be subdivided for classification purposes, especially important in developing understanding of structural categories. Of importance to level II classification described in a subsequent section, is the ability to categorize based on growth form and foliage charactersitics (e.g., type, length) or to sub-categorize stand structure within a particular community in terms of its basal area (BA) or its density. This database also provides information against which to check classification accuracy as mixed cover-type classifications within any particular stand may be correctly interpreted. For example the purity of cover type can be explicitly quantified to distinguish between a stand of 70%/30% jack/red pine respectively versus a stand of 99% or almost pure jack pine (Bergen et al., 1995a).

3.3.1 Temporal Conditions: Site and Imagery

Site condition differences between seasons at the MFTS are dominated in general by (1) foliage phenology with no foliation in April and full foliation in October, and (2) soil moisture which is in a saturated state in April and dry to moist in October. Within each mission a gradient of seasonal change is also evident. In April, change over the 11 day mission was primarily related to moisture: melting of the snowpack, thawing of the soil, and rising of sap in woody stems. In October, deciduous leaves were still green at the beginning of the mission, but by the end most had changed color. Overall, there was a general drying of vegetation and substrate. These and other important characteristics of moisture and phenology at the time of the datatakes used for classification are briefly summarized in Table 3.3. Extensive in situ measurements were made of vegetation and soil dielectric and gravimetric/volumetric moisture, and analyses of these can be found in Bergen et al. (1994, 1995b).

A set of four composite images at L-hv, L-hh, and C-hv is shown in Figure 3.2. Several relevent regions characterized by their physiography and forest communities are indicated

65

Constant parameters			
Sensor parameters			
Band	**L**	**C**	**X**
Frequency(GHz) / Wavelength (cm)	1.25/24	5.3/5.66	9.6/3.125
Polarizations	polarimetric	polarimetric	vv
Image parameters			
Product type	single-look, complex, slant range		SSC
Format for classification	orthorectification/ converted to ground range		
Resampled pixel spacing	12.5m		
N of looks (after filters)	> 100		
Features extracted	L-vv, hh, hv ; C-vv, hh, hv		X-vv

Variable parameters			
Mission: SRL-1	**Orbit:6**	**Data-take: 6.1**	
Date: April 10, 1994	Time: 14:32:17(EDT)		
Sensor parameters			
Pulse bandwidth (MHz)	20.03		19
PRF (Hz)	1440		1440
Image parameters			
Image center	46.41°N, 84.83°W		46.48°N, -84.91°W
Incidence angle (image center)	20.42°		18.7°
Pixel spacing (range/azimuth)	6.66m / 5.03m		6.66m / 5.02m
Pixel resolution (range/azimuth)	22.89m / 7.43m		7.33m / 7.2m
Mission: SRL-2	**Orbit:6**	**Data-take: 6.2**	
Date: Sept. 30, 1994	Time: 19:06:21(EDT)		
Sensor parameters			
Pulse bandwidth (MHz)	20.03		19
PRF (Hz)	1448		1440
Image parameters			
Image center	46.34°N, 84.78°W		46.48°N, -84.91°W
Incidence angle (image center)	31.62°		18.7°
Pixel spacing (range/azimuth)	6.66m / 4.87m		6.66m / 5.02m
Pixel resolution (range/azimuth)	15.08m / 6.85m		7.33m / 7.2m
Mission: SRL-1	**Orbit:102**	**Data-take: 102.41**	
Date: April 15, 1994	Time: 13:00:33(EDT)		
Sensor parameters			
Pulse bandwidth (MHz)	20.03		18.99
PRF (Hz)	1620		1620
Image parameters			
Image center	46.37°N, 84.89°W		46.39°N, -84.99°W
Incidence angle (image center)	32.39°		31.43°
Pixel spacing (range/azimuth)	6.66m / 4.48m		6.66m / 4.49m
Pixel resolution (range/azimuth)	14.91m / 6.20m		7.33m / 7.30m
Mission: SRL-2	**Orbit:102**	**Data-take: 102.41**	
Date: Oct. 6, 1994	Time: 17:12:18(EDT)		
Sensor parameters			
Pulse bandwidth (MHz)	20.03		18.99
PRF (Hz)	1488		1488
Image parameters			
Image center	46.25°N, 84.71°W(top), 46.43°N, 84.99°W(bottom)		46.42°N, -84.99°W
Incidence angle (image center)	33.18°		33.10°
Pixel spacing (range/azimuth)	6.66m / 4.88m		6.66m / 4.88m
Pixel resolution (range/azimuth)	14.54m / 6.86m		7.33m / 6.70m

Table 3.2: SAR data parameters.

Vegetation	6.1 April 9	102.41 April 15	6.2 Sept. 3	102.41 Oct. 6
Moisture Status	not stressed	not stressed	not stressed	not stressed
Moisture State	liquid	liquid	liquid	liquid
Precipitation	0	1 cm	0	0
Deciduous Leaves	no	no	yes (green)	yes (dry)
Surfaces				
Lakes	frozen	part frozen	liquid	liquid
Forests	snow	snow	no snow	no snow
Soil Moisture	saturated	staurated	dry to moist	dry to moist
Soil State	frozen	liquid	liquid	liquid

Table 3.3: Site conditions at the MFTS in April and October.

on the upper right image by letter designation. The areas around (F), (B) and (C) contain mixtures of northern white-cedar conifer swamps and lowland mixed (spruce-aspen-birch) communities. Dense, often vary large trees combined with a moist substrate resulted in high returns in all three frequencies with some variation by season. There is a significant increase in L-band backscatter between April 9 and 15, attributable to thawing of the substrate. This caused water to flow into the swamps and standing water to begin to collect. In turn this affects an increased ground-trunk interaction from L-hh backscatter bouncing of the specular surface of the water. Also contributing to the increase in L-hv in particular is stronger water/sap flow in the trees and thus higher return from branches.

At (E) is an area of higher moraine topography which supports northern hardwoods communities. In both seasons, scattering from complex decurrent crown branching structure and/or foliage causes C-hv to dominate. Slightly lower backscatter values remain fairly constant in both April images when sap was rising in the trunks, but smaller branches remained frozen or partly frozen. Also during both April dates there exists a layer of saturated snow and soil beneath the canopy.

At (A) is the large high-elevation area of highly xeric glacial outwash (sand) called the Raco Plains. This region supports low moisture and nutrient adapted jack pine plus red pine, and due to a harvesting schedule, many of the stands are young trees—seedling to sapling stage—and of very low stature and biomass. The generally low backscatter in this region results from both the low biomass and low vegetation and substrate moisture conditions. The area is additionally punctuated by black patches which are clearcuts. Scattered reddish areas are larger red pine plantations whose backscatter is dominated by L-hv. The Raco Plains area shows significant change between the four images. In the spring, between April 9 and 15, the sap begins flowing, needles and branches become moist, and a higher C-band return results and so the vegetated areas, especially jack pine, appear "greenish" on the imagery. In the fall, between Sept. 30 and Oct. 6, the striking decrease in C-band return is
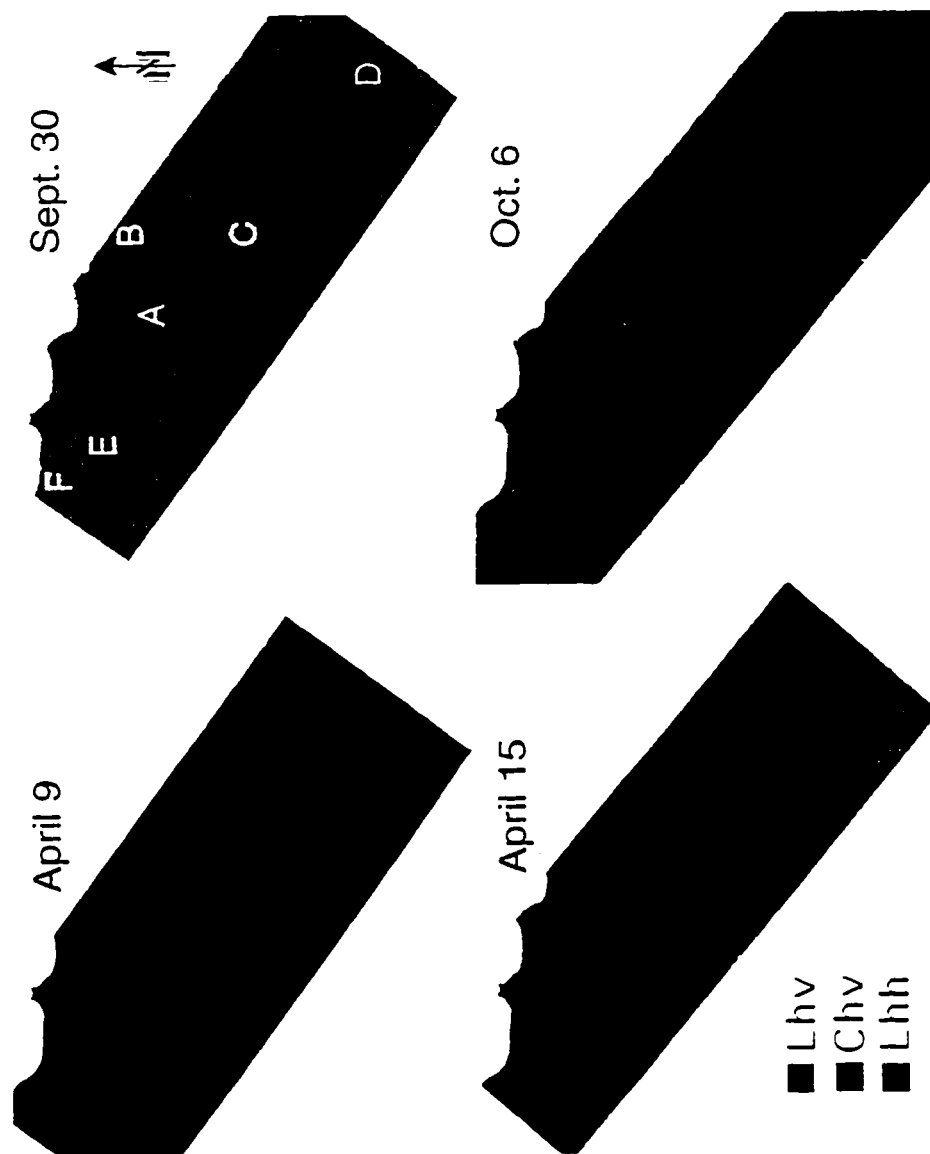
Figure 3.2: SIR-C composites from each date scaled so that color changes relate to temporal changes at the site.

in part attributable to a general drying of the vegetation, resulting in domination of L-band large structural and ground-trunk interaction. Additionally, however, the seasonal drying gradient is steepened by the fact that approximately 1.8 cm of rain fell on Sept. 28, likely having significantly increased backscatter at all frequencies on the Sept. 30 image.

The very southeast portion of the imagery (D) captures the western extent of a large area of agricultural fields (hayfields or pasture) on level lake plain substrate. In April the fields are covered with saturated snow and soil. In the October scene hayfields had dried and much hay had been cut. Major seasonal differences are not highlighted in agricultural portions of the imagery which has been enhanced to emphasize differences in the forest component.

In sum, the very evident patterns on the imagery discussed above are highly correlated to what is known to exist on the ground at the different seasons both in terms of land cover and of biophysical properties. Additionally this imagery shows a high degree of variability between different known cover types and between these cover types at different seasons. These two features - correspondence of the patterns on the imagery to known land-cover conditions and high scene variability - give confidence that this imagery can be used to successfully classify terrain.

3.4 Classification Methodology

An examination of classification processes shows several typcial steps. These include (1) pre-processing (e.g., filtering, feature extraction, training data extraction), (2) classification (e.g., supervised, unsupervised, statistical, non-parametric, knowledge-based), and (3) post-processing (e.g., filters). The pre-processing steps, which were introduced in a previous section, are critical to all classifiers mostly due to the importance of feature extraction which is the process of defining measures of the data that allow good separability of the desired classes. Characteristics of features are discussed further in the following paragraphs.

3.4.1 Features, Classes, and Training and Testing Data

Features can be extracted from the spectral, spatial, or temporal domains. Spectral features use the variability of the radar response as a function of the illumination wavelength, or a combination of wavelength (λ) and polarization, while spatial features use the within-scene variability, and temporal features are the result of using multi-date imagery. This classification study proceeds with seven spectral features (different λ and polarizations) at each of two dates in each of two seasons. Commonly, the temporal aspects of the data are ignored when classification is performed for a single-date observation. Here, temporal features are the focus of the multi-date procedures. No use of the textural feature space (spatial pixel-to-pixel variation) has been made in this study since much of the textural information is destroyed by application of the filtering process. The conceptual model and

experience with airborne SAR (AIRSAR) data, however, shows texture to also be a very powerful discriminant for certain classes (Pierce et al., 1994a).

Given multi-season (April and October) SIR-C/X-SAR imagery for the Michigan Forests site, there are three possible approaches to using features to implement the multi-temporal aspect in classifier development: (1) Ignore the multi-season availability and develop independent classifications for each scene using n features, (2) Develop one classification for a set of x scenes using n features, with x times the number of samples per feature, and (3) Develop a true multi-temporal classification where N of features equals n (number of image λ/polarization combinations plus phase channels) times x (number of scenes).

We hypothesize that the first, which is optimized for each scene separately, could result in a best single classification, but does not result in one which is transportable to other scenes, especially over seasonal change. The second attempts to be applicable over more than one image. Its basis is the assumption that Δt yields negligible $\Delta \sigma^\circ$, hence a singular classifier would be robust in the temporal domain. But if time-dependent changes in phenology/environmental conditions are not negligible, the lumping of samples from different scenes may inflate the variance of the individual features. Thus this is likely a worse classification. The third approach tests the opposite of the second, that is, that Δt yields significant change in $\Delta \sigma^\circ$ for some classes and so uses phenological differences as additional feature information. Hence, multi-temporal classification could improve accuracy over the first approach. However, there is no implication that the specific decision rules will necessarily be "transportable" if the nature of the decision boundaries is in fact time dependent. Each of these methods of combining features (single-date optimized, pooled, and multi-temporal) are explored, their relative viabilities at each classification level are evaluated, and results are compared.

Classes

As mentioned in the discussion of hierarchical-structural classification in section 1.4.1, the level I classes used in this classifier are simple structural classes: urban (if present), tall vegetation (trees), short vegetation (shrub, grass), and surfaces (water, airports). At level II, the next level in the hierarchy, categories for tall vegetation (trees) are made more specific, but equally universal. For example, for tall vegetation, tree architectural forms and foliage type for class names are defined, rather than species. In the MFTS this includes excurrent architecture (upland and lowland conifers) and decurrent architecture (deciduous), broadleaved foliage (deciduous), or needle foliage (upland and lowland conifers). There are also within-form differences (e.g., long vs. short needles on upland conifers), and overall stand structure manifested in age/size/density (Figure 1.2). Contributions of minor structural differences such as needle form and branch angle have been intensively studied and have been verified using the MIMICS theoretical scattering model (Ulaby et al., 1990). For example, in the MFTS the example of varying needle length translates into red pine vs. jack

pine vs. lowland conifer, and illustrates how these simple structural categories can then be matched with local floristic keys. Age and size classes can be defined from the test stands based on known structural measures such as basal area (BA) and density.

Training and Testing Data

Short vegetation training sets consisted of surveyed agricultural fields supplemented with rangeland training sets identified from the SIR-C/X-SAR imagery, AIRSAR imagery, and a GIS land-cover layer. Training sets for the flat category were easily selected on the SIR-C/X-SAR imagery and were primarily from Lake Superior and inland lakes plus an airport. Forest trees are the category of interest for level II classification, as flat and short vegetation categories are considered sufficiently identified at level I. The training sets used at all levels in this study for the tall vegetation category were surveyed forest test stands. In the case of the surveyed stands, the polygons in the stand GIS were shrunk by several pixels on each side by an amount dictated by the size of the averaging filter. Further, each stand was sliced in half, with the top half used for training, and the bottom half used for testing. These steps guaranteed a reasonably accurate and independent sample for each stand. A map of the training and testing regions is given in Figure 3.3. Table 3.4 is a summary of the training and testing data used for this study.

3.4.2   Classification

The classification steps can be very simple or very complex but all classifiers seek to minimize the errors of omission or comission at any step. Statistical (supervised and unsupervised), knowledge-based decision rules, and artificial neural network strategies are some typical examples of types of classifiers. All classifiers must be given a set of values, defined over

the feature space, defining the classes that are to be separated, and then various rules or procedures are invoked to accomplish this task. Often called the "training stage," it is critical that separable classes be used here or a poor classifier will result.

"Supervised" classfiers are given explicitly labelled sets of training data from which to construct the probability density functions (PDFs). Given a supervised procedure, after the training data has been assembled into a set of PDFs, a decision method must be applied to all the pixels in the image to segment the image into the expected classes. A popular statistical classifier uses a Maximum Likelihood Estimate (MLE) of the statistics of known PDFs that describe the data, often assuming Gaussian statistics. Alternatively, a clustering algorithm is often used to select some number of separable classes (clusters) as input to the MLE stage. This is termed "unsupervised" classification and may provide better classification accuracy at the expense of using unlabeled classes. The problem of correctly labelling the classes automatically has yet to be resolved. Alternatively, classifiers which relate backscatter to known physical properties and classify on this basis are called knowledge-based classifiers.

Level I class	Level II class	Level III class	Training		Testing		MIRIS Level II
			N of Areas	N of Pixels	N of Areas	N of Pixels	%
Surfaces			5	5292	5	5292	2.7%
Short Vegetation			27	4395	27	4395	10.9%
Tall Vegetation			28	2790	28	2790	86.4%
Tall vegetation	Upland conifer (excurrent form, large needles)		34	2192	34	2192	38.9%
		jack pine – low BA ($< 14m^2$)	12	879	3	420	
		jack pine – hi BA ($> 14m^2$)	7	479	7	479	
		red pine – low BA ($< 14m^2$)	6	388	6	388	
		red pine – med BA ($14 - 25m^2$)	4	121	4	121	
		red pine – high BA ($> 25m^2$)	5	325	5	325	
	Lowland conifer (excurrent form, small needles)		4	283	4	283	20.3%
		northern white-cedar	2	143	2	143	
		black spruce	2	140	2	140	
	Deciduous (decurrent form, broadleaf)	16		764	16	764	40.7%
		aspen – low BA	4	105	4	105	
		n. hardwoods – med BA ($15 - 25m^2$)	4	126	4	126	
		n. hardwoods – high BA ($> 25m^2$)	8	533	8	533	

Table 3.4: Training and testing data.
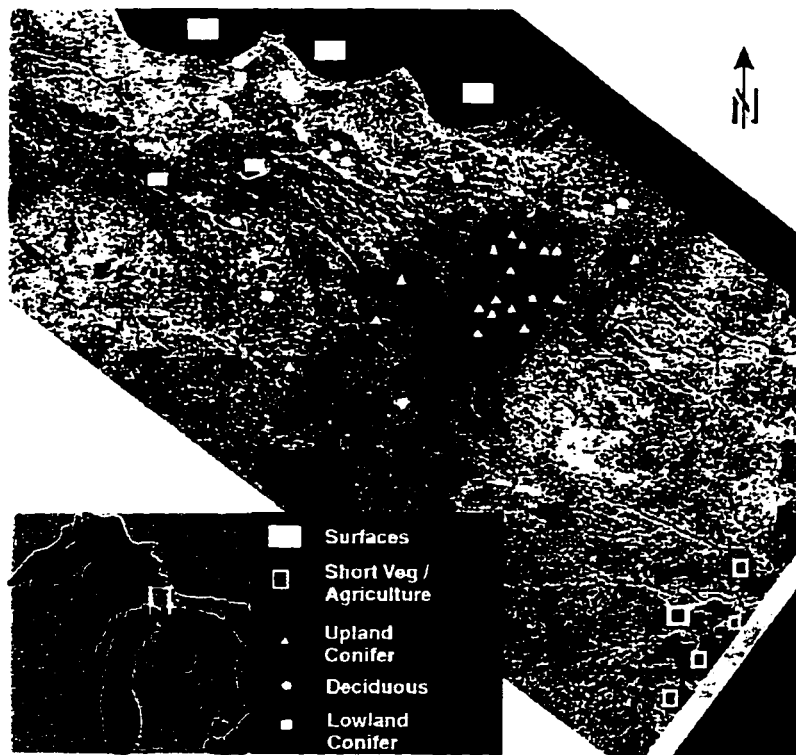
Figure 3.3: Location of MFTS (inset) and of training and testing regions within the site.

We call the classification developed and used for this study a hybrid-hierarchical classification, its procedures being a hybrid of two methodologies. It consists of knowledge-based rules for Level I structural classes, and an unsupervised ISODATA statistical clustering algorithm (Tou and Gonzalez, 1974) for level II. Expert decision rules (the knowledge-base) are used to sequentially classify the image on a per-pixel basis to level I. The ISODATA clustering algorithm is then used to create clusters or signatures for just the forest areas. Because the number of clusters is greater than the number of Level II classes, and in fact may be equivalent to Level III classes (see Table 3.4), the resulting clusters are combined through a process relating them to known Level II structural types based on forest test stands. The outcome is several different types of forest communities within the tree class. The resulting classification may then be applied to the other scenes used for the temporal study using a maximum likelihood (MLE) or minimum distance (MINDIS) algorithm. The classification applied in the image domain is also applied just to a test population from which a general measure of accuracy may be obtained.

We believe this hybrid-hierarchical classifier posesses several advantages over using either statistical or knowledge-based procedures exclusively. A stepwise or hierarchical organization allows the classifier to be divided into steps that are natural, easily created and easily understood. There is also the added advantage that fewer classes are being discriminated at each step than if discriminated all at once, hence improving separability. Prior-probabilities in the ISODATA algorithm may be set equal for all classes which should allow this component to be transportable from scene to scene, both geographically and temporally. The methodology is described in more detail below, and is also given in diagram form in Figure 3.4.

3.4.3   Level I Classifier Methodology

At Level I, knowledge-based classification can easily proceed by a simple algorithm and manual optimization. This method was successful with AIRSAR in previous studies (Pierce et al., 1994). The process of determining algorithm values is the same as with the AIRSAR data: manual optimization for each image until the training stands are classified well, then the test stands are evaluated for their accuracy. When applied to the other image scenes for the temporal study, it was found that the same rules could be used, and thus are the same, for both April and October (a *de facto* multi-time classification). This implies that in fact at Level I, multi-date information may be useful, but is not necessary for achieving an optimum classification which is stable over time. Level I rules of this time independent classification are as follows.

IF (L-hv > (-0.91 · L-hh -33 dB) tall vegetation
    ELSEIF (C-hv > -20 dB) shortveg
    ELSEIF (C-hv ≤ -20 dB and L-hv < -20 dB) surface
    ELSE shortveg
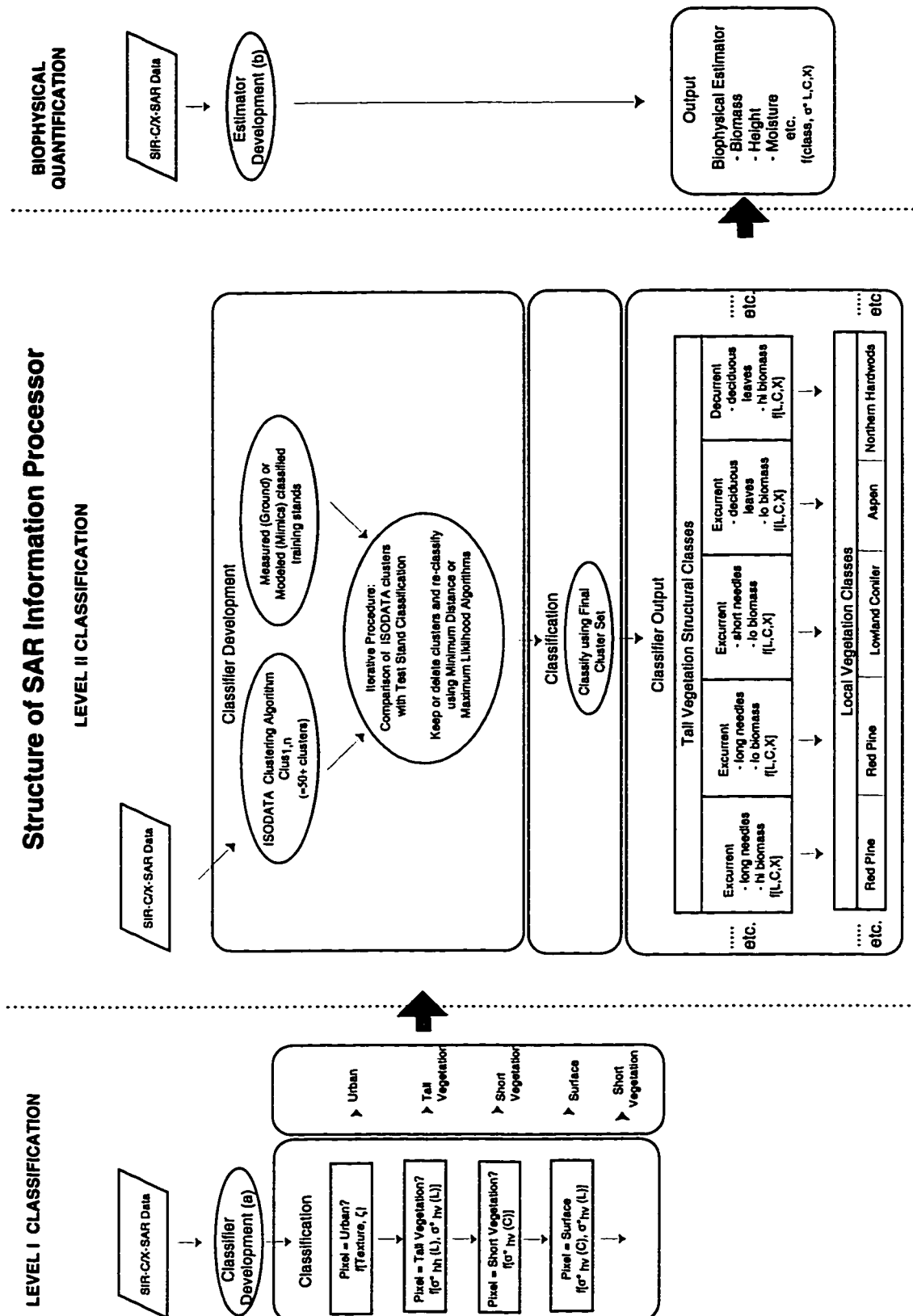
Figure 3.4: Structure of the SAR information processor.

The higher-frequency X-vv data was not used or needed at level I. Its utility comes in discriminating between different kinds of trees in the level II classification process.

3.4.4 Level I Results

Because SAR is a very good discriminator of the the basic level I classes, results at this stage are predictably high: 97% worst case overall for a multi-date classification. Table 3.5 shows the worst-case level I results among the four dates: the early April scene. In all classifications, accuracies are determined using spatially independent samples from the test stands. The small misclassification of short vegetation as surfaces is probably due to the presence of some snow-covered grasses. The slight confusion between short vegetation and trees is due to the snow on the ground beneath the trees acting more as an absorber, causing a decreased ground-trunk interaction, which is the basis for classifying trees. The rough ice in the lakes presented very little trouble for the classifier, with some that was rough and very dirty on the Lake Superior coast occasionally being classified as short vegetation. The Raco airport runways (triangular area in center of image) and parts of an extensive rangeland area just to the west are successfully classified as flat while parts of the plowed fields in the agricultural area (south-east) are also correctly classified as flat. The roads in the test site are usually too thin or overhung with trees to be correctly classified as flat, often appearing as short vegetation. Overall a very encouraging result, with the use of only three power features: L-hh, L-hv, and C-hv.

3.4.5 Level II Classifier Methodology

At this point where an image has been classified to Level I, the next step in the hierarchical procedure is to further classify the forested portion of the image to Level II. A diagram of this methodology is presented in Figure 3.4. At Level II the manual procedure outlined above is not viable; classification is too complex in a multivariate sense, and the rules are no longer related as simply to the physical principles. Hence, adapting the power of a clustering algorithm such as ISODATA is advantageous (Tou and Gonzalez, 1974). The data is appropriate for statistical classification as the power data scaled in dB units presents PDFs that are closer to normal (as is required by the family of Bayesian classifiers)

True class	Classed as		
	Surface	Short veg	Tall veg
Surface	100	0	0
Short veg	4	94	2
Tall veg	0	3	97
Overall: 97%			

Table 3.5: Level I multi-date classification results: testing.

than if they had been scaled linearly. Rather than include differing prior probabilities for each class to improve the results, equal weights are used, since this would be the situation for a global classifier that was not optimized for any geographic region. In some cases all seven power features were used; in others a subset. X-band data was used only from SRL-2 102.41. Feature selection could be determined from the N-dimensional Gaussian fits of the training data.

The ISODATA algorithm as implemented in PCI (PCI inc., 1995) is very flexible and thus requires the choice of a number of input parameters. These include the number of clusters desired (50), the maximum (50) and minimum (20) number of clusters, the maximum number of iterations (20), threshold (0.01)and lumping (1) values, and a seed file which includes the initial cluster centers. The last parameter may be selected by default from the program or may be submitted. In this case the default was not used, and a knowledge-based seed file was submitted which was generated as a random set of backscatter values over the expected ranges for trees. In particular the co-polarized values ranged between 0 and -20 dB, while the cross-polarized value range was between -5 and -25 dB. This improved the number of ISODATA classes that were trees from a few (with no seedfile) to 10 or 20, and was necessary for this procedure to classify trees well. The algorithm uses a subset of the entire image (for images larger than 1024 x 1024) to create the clusters (and signatures if desired) and then applies the classification to the entire image. Included in the statistical algorithm are a number of cluster splitting and lumping rules.

The ISODATA algorithm is run on the entire image and is also evaluated for the training stands to determine if further modification is needed. This procedure using both the ISODATA clusters and knowledge of the test stands is described below. Each test stand was assigned a class based on biomass and dominant vegetation species which resulted in the Level III classes listed in Table 3.4. The ISODATA classification results in a large number of clusters – approximately 20-30 in all cases. The confusion matrix for the ISODATA classification was then compared to this Level III test stands scheme, and the fraction of each Level III class represented in each ISODATA cluster was determined. This is exactly analogous to the confusion matrices used for presenting classifier performance, as in Table 3.7, but with many more "classes." Using this matrix, the Level III class appropriate for each ISODATA cluster is plainly apparent as the class with the maximum representation. For most ISODATA clusters this works well and unequivocally. A few have significant overlap with two or more Level III classes, and in those cases the ISODATA cluster is eliminated (one at a time if there is more than one trouble cluster) and the minimum-distance (MINDIS in PCI) classification performed again on the remaining clusters.

If the resulting classification is better than before it is kept, if not, the eliminated cluster is brought back. This process is repeated until satisfactory results are obtained or until no improvement is made. The choice of which clusters to eliminate, and possibly bring back, has not been automated yet nor has the stopping condition. Every effort was made, however, to continue the process to the best possible outcome in each case. The last step

was re-mapping the Level III clusters to Level II classes and producing the output images.

After the classifications are developed using the above procedure for the single, pooled, and multi-temporal classification types, a minimum distance algorithm is then used to classify all other images desired for the multi-temporal comparison. PCI Maximum-likelihood (MLE) and minimum distance (MINDIS) algorithms were compared and resulted in almost no difference for the dataset, so MINDIS was typically applied due to it significantly shorter computation time.

An example of one of the decision rules which is an outcome of the ISODATA algorithm is shown as part of Figure 3.6 for separation of the three Level II tree classes. The cluster centers for two dimensions are shown with regard to October C-hh and X-vv. The use of the X-band data allows the separation of the Upland Conifer class from the others, while without it the separation is much poorer.

3.4.6 Post-Processing

Filters are often applied to classification results to merge isolated pixels/pixel groups with larger polygons and smooth the appearance of the image. Here, no post-processing of any kind was performed. It was felt that the pre-processing process which produced multi-look images, thus reducing the effects of fading (speckle), was better than the alternative of a single-look classifier followed by some aggregation process. Both seem to perform well, but the former produces a classifier that is more intuitively understandable. The procedure used here would likely perform poorly for a single-look image, due to the effects of coherent fading.

3.5 Results for Level II Temporal Classifications

3.5.1 Optimized for Each Date Separately

The first analytic step in the use of temporal data was to classify each image from each season separately. Classification results for spring images SRL-1 6.1 and SRL-1 102.41 are given in Table 3.6. Those for fall images SRL-2 6.2, and SRl-2 102.41 are given in Table 3.7. The results are presented in confusion matrices with unbiased overall accuracy given at the bottom of each. The latter is calculated as the mean of the diagonal and is not weighted by number of pixels in a class. This is considered unbiased such that a land-cover class with few pixels in it is given equal consideration in the overall accuracy. These results are quite good for September, with the April results slightly worse: April 9 (90%), April 15 (90%), Sept. 30 (95%), and Oct. 6 (98%). Table 3.8 gives results of the SRL-2 102.41 scene when X-vv is not used resulting in a lowering of the unbiased overall accuracy from 98 to 90%.

An examination of the imagery and the classification results suggests that the poorer classification in April, where there is confusion between the upland conifer and deciduous classes, can be attributed to two interacting factors. The first is probably due to the effects

78

of the water-saturated, snow-covered ground combined with leafless deciduous vegetation. C-band scattering is far less - this is apparent on the image composite in Figure 3.2. The stronger surface moisture signal serves to dampen the ability of the classifier to discriminate between certain types of upland conifer and deciduous. In particular the classifier has trouble separating jack pine (shorter needles, more decurrent branching in open-grown stands) and deciduous. The classifier retains its ability to separate red pine (longer needles, retains regular excurrent growth form) from deciduous. The moisture effect is not present in an earlier April image (6.1 SRL-1) where the substrate is still frozen and snow is dry. The other trees are still significantly different: the upland and lowland conifers both retain their green foliage (needles and scales) throughout the year. The second factor is the presence of mixed conifer and deciduous vegetation in forest stands. In this case, the apparent mis-classifications may actually be the artifact of labelled classes which do not adequately account for the variation of natural forest communities, and the power of a sensor with a fine resolution to pick up on within-stand differences on a pixel by pixel basis. The result is an accurate map of stand composition, but one which will have a low accuracy when assigned to a single, dominant, class.

3.5.2 Pooled Classification

In the pooled classification all samples were extracted from the images and the best set of features selected from the four images were merged. Based on this dataset, the pooled classifier was statistically constructed using the ISODATA algorithms and then applied to each scene. While this can restrict the number of features to that of the single-scene method, because it increases the number of samples for each feature, it may significantly inflate the within-feature variance. This can degrade the separability of the clusters or classes.

In fact, because of class confusion due to physical properties of vegetation and substrate, this attempt resulted in all scenes being more poorly classified. A pooled classified image is shown in Figure 3.5. The classification results are shown in Table 3.9.

Surfaces were classified well in both, except much short vegetation (17%) was called surface in April. Deciduous (no leaves) is completely different from lowland (mostly needles) in April, and thus separate fairly well at this time. Both deciduous and upland conifer were strongly confused with lowland mixed in September. This is also seen to a lesser extent in April. Most of this confusion is due to forcing a wide variety of moisture conditions found in the feature space for the lowland mixed in April to coexist in the same class, thus forcing poor choices for class boundaries. In particular lowland in April is overlapping significantly with upland and deciduous in September, greatly lowering the classification accuracy of the latter two classes. A multi-temporal classification, on the other hand, can take advantage of this variability.

(A) SRL-1 6.1 (April 9) (L,C,X) – Testing					
True Class	Classed As				
	surface	short veg	upland conifer	lowland mixed	deciduous
surface	100	0	0	0	0
short veg	6	92	2	0	0
upland conifer	0	12	83	1	4
lowland conifer	0	0	2	85	13
deciduous	0	0	2	6	92
Overall: 90%					

(A) SRL-1 102.41 (April 15) (L,C,X) – Testing					
True Class	Classed As				
	surface	short veg	upland conifer	lowland mixed	deciduous
surface	100	0	0	0	0
short veg	0	97	0	0	3
upland conifer	0	0	86	0	14
lowland conifer	0	0	0	90	10
deciduous	0	1	10	7	76
Overall: 90%					

Table 3.6: Level II single-date classification results: Spring.

(B) SRL-2 6.2 (Sept. 30) (L,C,X) – Testing					
True Class	**Classed As**				
	surface	short veg	upland conifer	lowland mixed	deciduous
surface	100	0	0	0	0
short veg	0	97	3	0	0
upland conifer	0	0	95	0	5
lowland conifer	0	0	0	93	7
deciduous	0	0	8	0	92
Overall: 95%					

(C) SRL-2 102.41 (Oct. 6) (L,C,X) – Testing					
True Class	**Classed As**				
	surface	short veg	upland conifer	lowland mixed	deciduous
surface	100	0	0	0	0
short veg	2	98	0	0	0
upland conifer	0	0	99	0	1
lowland conifer	0	0	0	97	3
deciduous	0	0	4	1	95
Overall: 98%					

Table 3.7: Level II single-date classification results: Fall.

True Class	**Classed As**				
	surface	short veg	upland conifer	lowland mixed	deciduous
surface	100	0	0	0	0
short veg	3	97	0	0	0
upland conifer	0	0	87	6	7
lowland conifer	0	0	0	84	16
deciduous	0	0	17	1	82
Overall: 90%					

Table 3.8: Level II SIR-C alone: SRL-2 102.41 (Oct. 6) (L,C) – testing.

(A) SRL-1 6.1 (April 9) – Testing					
True Class	Classed As				
	surface	short veg	upland conifer	lowland mixed	deciduous
surface	100	0	0	0	0
short veg	17	80	2	0	1
upland conifer	0	7	91	0	2
lowland mixed	0	0	4	91	5
deciduous	0	0	5	3	92
Overall: 90%					

(B) SRL-2 6.2 (Sept. 30) – Testing					
True Class	Classed As				
	surface	short veg	upland conifer	lowland mixed	deciduous
surface	100	0	0	0	0
short veg	0	96	2	0	2
upland conifer	0	0	65	31	4
lowland mixed	0	0	0	93	7
deciduous	0	0	5	65	30
Overall: 77%					

Table 3.9: Level II pooled classification results.
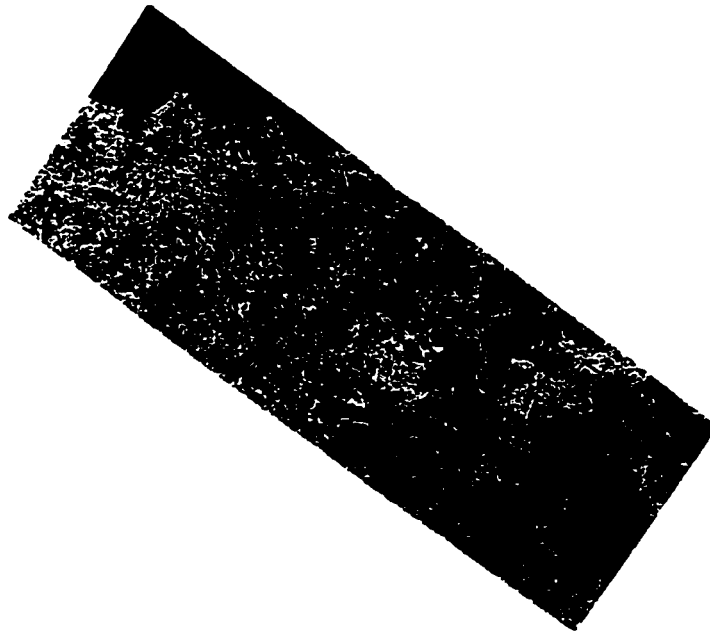
Data:

SRL-1 6.1 (April 9)
(L-hh, L-hv, C-hh, C-hv)

SRL-2 6.2 (Sept. 30)
(L-hh, L-hv, C-hh, C-hv)

SRL-2 102.41 (Oct. 6)
(X-vv)

■	Surfaces
■	Short Vegetation
■	Upland Conifer
▒	Lowland Mixed
■	Deciduous

Figure 3.5: SIR-C pooled Level II classification.

3.5.3 Multi-Temporal Classification

In the multi-temporal classification procedure, the samples extracted from the two images/seasons are kept separate and the feature space is doubled. This doubling risks not meeting the statistical requirements for number of samples per feature; the underlying statistical estimations may be underdetermined if the spectral dimensionality is not kept low. On the other hand, this procedure is advantageous as it keeps the variance within features to the minimum and uses the differences between seasons as additional discriminators. After the multi-temporal classifier is statistically constructed, it is then applied back to each of the images. The classified multi-temporal image is shown in Figure 3.6, and the results in Table 3.10. The multi-temporal classification was significantly more successful than the pooled methodology. It did better overall than all single-date optimized images except for Sept. 30, where it was approximately the same (see Figures 3.7 and 3.10). This means that a multi-temporal approach has the potential to improve classification, especially for a scene from a time of year which is more difficult to classify alone.

True Class	Classed As				
	surface	short veg	upland conifer	lowland mixed	deciduous
surface	100	0	0	0	0
short veg	0	99	1	0	0
upland conifer	0	0	99	0	1
lowland mixed	0	0	0	89	11
deciduous	0	0	0	0	100
Overall: 97%					

Table 3.10: Level II multi-temporal classification results: SRL-1 6.1 (April 9), SRL-2 6.2 (Sept. 30), SRL-2 102.41 (Oct. 6) – testing.

3.5.4 Contribution of X-vv

An interesting side-issue that we explored was the contribution of the X-band data to the classification accuracy. Using the October scene, without X-band, the overall Level-II accuracy was 90% with the tree classes ranging from 82 to 87%. When X-band is included, the overall accuracy is in the high 90's with the tree classes ranging between 95 and 99%: a dramatic improvement. Table 3.8 shows results for the classification of the October 102.41 scene using L and C alone, and these results can be contrasted with those from Table 3.7 where X was added. These results show that X-band can be important for high-accuracy tree classifications.

Cluster Centers

X_{vv} σ^0 (dB) (October)

C_{hh} σ^0 (dB) (October)

Data:

SRL-1 6.1 (April 9)
(L-hh, L-hv, C-hh, C-hv)

SRL-2 6.2 (Sept. 30)
(L-hh, L-hv, C-hh, C-hv)

SRL-2 102.41 (Oct. 6)
(X-vv)

- Surfaces
- Short Vegetation
- Upland Conifer
- Lowland Mixed
- Deciduous
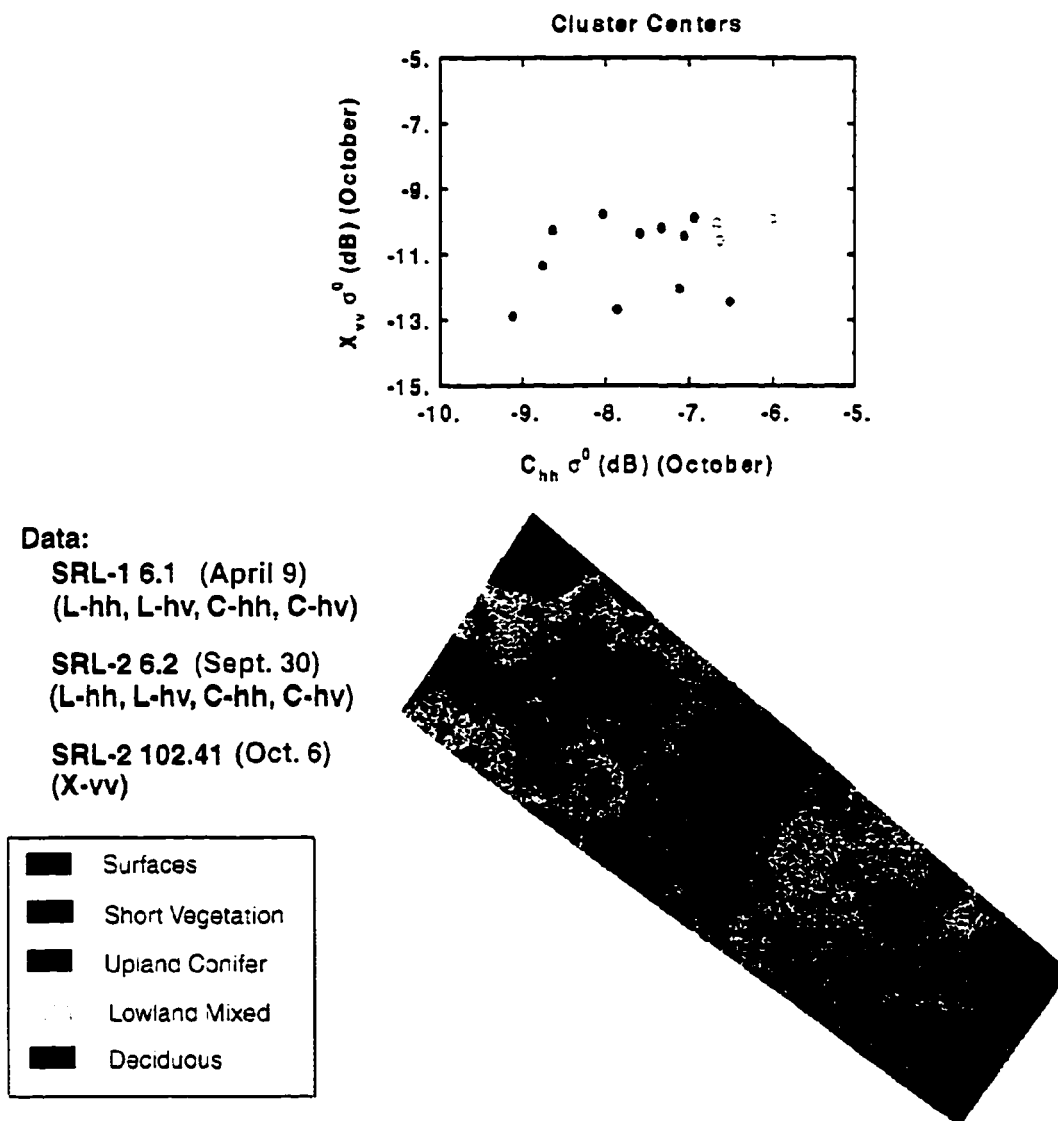
Figure 3.6: SIR-C multi-temporal Level II classification.

Community	σ° C-hv		Winter Crown Biomass %	Winter Crown LAI %
	April 9	Sept. 30	of Summer Crown	of Summer Crown
N. Hardwoods	-12.9	-12.2	94.03	93.89
Aspen	-15.1	-12.4	80.31	42.82

Table 3.11: Comparison of σ° with crown biomass and LAI.

3.6 Temporal Signatures

In a temporal classification the three vectors which are integrated in the SAR backscatter are (1) structure (excurrent/decurrent, etc.), (2) biomass (integrates area, height, and % cover), and (3) moisture. In the final stage of the classification which solves back to these, it is customary to assign names to the combinations which are relatively distinct classes. Our resulting classes are tied to the biomass and structure vectors; the multi-temporal classification, however, relies on all three during the unsupervised portion of the analysis. This provides good reason for adopting the unsupervised approach as part of the methodology; in this case rather than imposing a priori expectations on the dataset, we let the data itself tell us how features separate according to the three vectors.

Analysis of Figure 3.7 confirms that it is evident that classes are exhibiting different backscatter characteristics and are often fairly separable even within a given season. This is the case, for example, for L-hv, Sept. 30, with the exception of northern hardwoods and aspen. The fact that northern hardwoods and aspen are not entirely separable at this single date, however, illustrates the advantages of multi-temporal image classification. The L-hv and C-hv plots especially show that there is a significantly larger diference in backscatter amplitude between the seasons for aspen than northern hardwoods. Because aspens are younger with lower trunk/branch biomass, foliage constitutes a higher proportion of total leaf-on biomass. Thus it is predictable that the aspen would have a higher seasonality effect, particularly in C-hv where the dominant scattering mechanisms at this short wavelength are from leaves and small branches/twigs of the crown. While under full foliation (Sept. 30), the two exibit similar backscatter. When devoid of leaves, the northern hardwoods maintain a high backscatter due to the presence of a perennial complex and high density small branch/twig structure. The aspen have a sparse branch/twig structure and show a significant drop in backscatter compared to the northern hardwoods during the leaf-off season. This difference is exploited in multi-temporal classification to separate out the two classes, which at any given single date and wavelength would potentially have significant overlap. The difference in the seasonality behavior of backscatter between northern hardwoods and aspen can be shown to correspond to the difference in crown biomass and LAI as given in Table 3.11. At the same time, the plots in Figure 3.7 also demonstrate why applying the same rules to fall and spring images do not work. The σ° values are different

across seasons for a given community and thus the classification will be incorrect whether it is applying the same rules to spring and fall or a pooled classification where the samples are lumped across seasons.
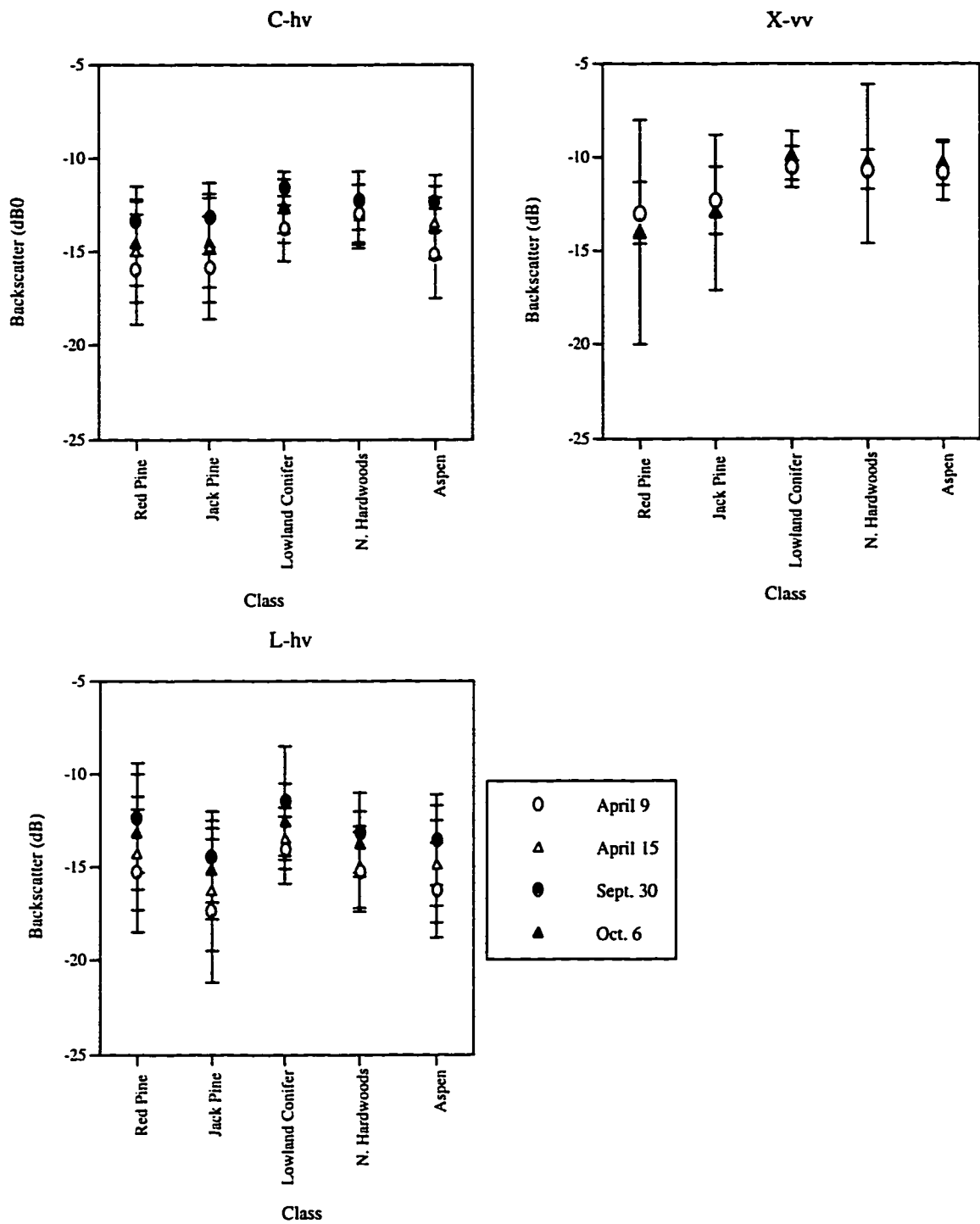
Figure 3.7: Forest temporal backscatter

CHAPTER 4

BIOMASS ESTIMATION

Demonstration that vegetation biomass is retrievable from SIR-C/X-SAR imagery is one of the mission goals for the MFTS. As the first step in meeting this goal, an empirical method for deriving biomass from SAR imagery was developed and an outline of the methodology plus results for one scene (102.41 SRL-1, April 15) are discussed in-depth in Dobson et al. (1995a). The biomass estimation reported in this chapter is done first as a follow-up study to demonstrate the repeatability of the methodology developed by Dobson et al., and second to provide the remaining of the two input images (the other being the classified image) necessary to derive C-related parameters, the focus of the final chapter of this dissertation.

4.1 Physical Model

The physical model for the net backscatter σ° from a forest may be stated as follows (Dobson et al., 1995a):

$$\sigma^\circ = \sigma^\circ_c + \tau^2_c \tau^2_t (\sigma^\circ_t + \sigma^\circ_s + \sigma^\circ_{st})$$ (4.1)

where

σ°_c = backscatter coefficient of the crown layer of smaller woody branches and foliage,

τ_c = transmissivity of the crown layer,

τ_t = transmissivity of the trunk layer,

σ°_t = backscatter coefficient of the trunk layer,

σ°_s = backscatter coefficient of the surface, and

σ°_{st} = backscatter coefficient resulting from interaction of the surface and the trunk layer.

Results published in Dobson et al. (1995a) show that there are two important relationships which must be understood to move correctly from the physical model as shown

above to the empirical retrieval model used to estimate biomass. The first is that there is evidence for a power-law relationship of σ_c^o to biomass. A typical curve of σ^o as a function of biomass will show that σ^o may increase at very low biomass levels due to rough surface scattering (σ_s^o) and surface moisture (M_s) contribution, and always saturates or decreases at high levels due to extinction within the canopy. The second is that species affects the power-law relationship. This occurs because there are different relationships between h (height), d (density), and S (stocking density) for different species. The effect is that the slope of the relationship, especially in the moderate biomass region, is determined by structural attributes of the vegetation (size, density, orientation, number) which vary by species. Thus there is species-related control of the slope. In the plots in Figure 4.1 the test stand total above-ground dry biomass, basal area, and height are plotted against σ^o for each of two polarization combinations at L and C bands using data from the present study (6.2 SRL-2, Sept. 30). It is evident that there is a power law relationship, but that there is much scatter in the data. It is also evident that σ^o saturates or decreases at high levels due to extinction within the canopy.

Thus while it is tempting to attempt to derive a model simply relating biomass to σ^o, it can be seen that the power-law relationship and the structure-controlled slope must be taken into account. Given an understanding of these two relationships, it is possible to account for them in developing a retrieval methodology. Rising backscatter at very low biomass levels means that the sample population is behaving differently – in this case like short vegetation – and the SAR backscatter is a function of different factors than that for forests. These could be analyzed separately; here they have been disregarded as this study concentrates on forests. Scatter in the data resulting from structural control of slope is removed by deriving separate functions for the different structural types (based on an a priori data set such as a classified image). Because σ^o is proportional to Sdh^2 and biomass to Sd^2h, there is one additional factor which can confuse the simple relationship of σ^o to biomass. This factor is between-stand differences in combinations of height, diameter, and density. For example, given two stands, with the same overall biomass, the stand with taller trees and lower density may have a larger σ^o. Accounting for structure takes this into account to some extent. Also in the test stand population stands of varying densities were selected for the sample population.

4.2 Biophysical Model

A biophysical model may be developed which accounts for different wood densities and stand structures. This assumes that wood density and structural type are known. At its simplest the model is:

$$B_d = B_c + B_t \tag{4.2}$$

where

$$B_d = \text{total dry standing biomass(kg/m}^2\text{)},$$
$$B_c = \text{dry biomass of crown(kg/m}^2\text{)}, and$$
$$B_t = \text{dry biomass of trunks(kg/m}^2\text{)}.$$

and

$$B_t \approx \rho_s t_s \bar{h} b_a (\text{ kg/m}^2).$$

where ρ_s = dry density of wood for given structural type, t_s = trunk taper factor for given structural type, and $\bar{h}$ is average tree height.

The polarimetric SAR data is used with multiple linear regression to estimate the three fundamental parameters which separately have a direct relationship between ground and sensor: height, basal area, and crown biomass. The coefficients for the functions are empirically derived for each structural type using measured biometric data. The remaining biomass parameter is the trunk layer biomass which is constructed from estimates of height ($\hat{h}$) and basal area ($\hat{b}_a$) together.

The inversion model is as follows:

$$\hat{B}_{d_i} = \hat{B}_{t_i} + \hat{B}_{c_i}$$

where the parameters of the model are:

$$\hat{b}_{a_i} = f1_i(\sigma^\circ),$$
$$\hat{h}_i = f2_i(\sigma^\circ),$$
$$\hat{B}_{c_i} = f3_i(\sigma^\circ), and$$
$$\hat{B}_{t_i} = f4_i(\hat{b}_{a_i} \hat{h}_i)$$

where $f1$, $f2$, $f3$ and $f4$ are empirically derived and specific to the image analyzed using least-squares regression for each of the i structural types.

4.3 Biophysical Estimation Methods

The following image and statistical analyses were done to construct the functions and then map these into the image domain for scene 102.41 SRL-2, October 6, 1994. This scene is shown in Figure 3.2, lower right.

4.3.1 Features

All potential features were extracted from the SIR-C/X-SAR dataset. These included L-hh,vv,hv,ζ; and C-hh,vv,hv,ζ. Average σ° for each stand was calculated using the PCI STATS program (PCI Remote Sensing Corp, 1995). All SAR data were converted to dB
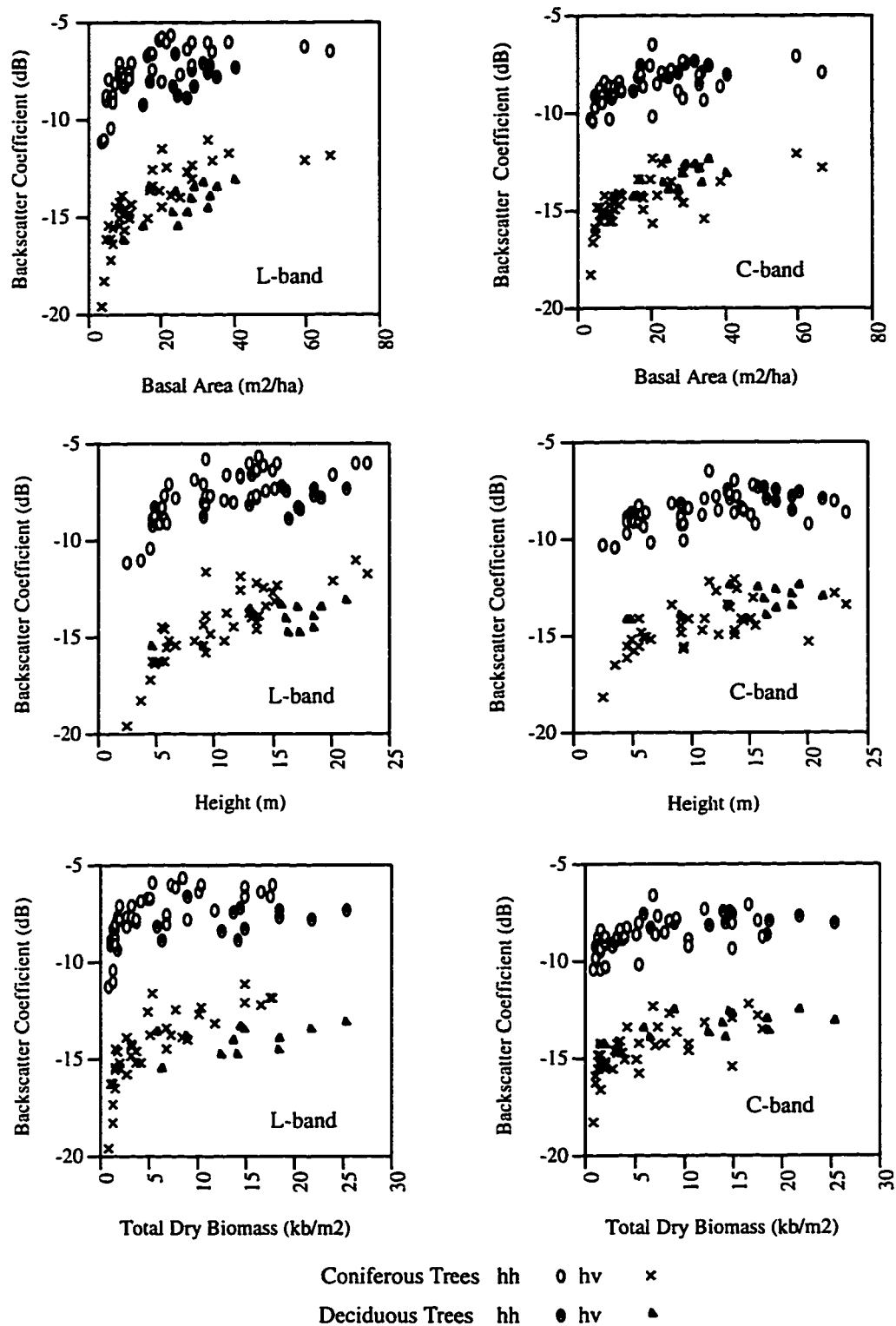
Figure 4.1: SIR-C response to biophysical characteristics.

(logarithmic form). New features in the form of ratio channels were constructed for each combination of band-polarization. Ratio channels, constructed by subtracting dB channels, are important to capture the high biomass portion of the curve which otherwise levels off due to saturation.

4.3.2 Statistical Analysis

The number of cases (stands) used is 53. The stands where $B_d > 2.5$ kg/m^2 were selected to be used in solving for the functions and coefficients presented in Table 4.1. This sets a bound for tall vegetation at ≥ 2.5 kg/m^2, and provides for a consistent relationship between forest trees and $\sigma°$. The low biomass seedling stands were not included as their backscatter is due to different effects, primarily surface roughness and surface moisture. All selected stands were assembled into a SAS formatted file containing Y variables of all extracted and ratio features plus biophysical measured stand data: class (structural type) BA weighted height, BA, crown biomass, trunk biomass, and total biomass.

Based on physical models of SAR interaction with forest trees, some hypotheses could be made regarding the relative importance of the features in the empirical models to be developed. For pole size to mature stands, L-band should be a strong contributor to height and BA components due to its longer λ which penetrates the canopy. Crown functions for all types are likely to be functions of C-band variables as C-band is known to interact with and scatter from leaves and small branches. A possible exception to this is upland conifer where L-band is very dominant even for the crown due to sparse canopies. Smaller (sapling) trees are likely to be strong C-band scatterers in all components due to their smaller structure.

With this knowledge in mind, a stepwise linear regression procedure was done in SAS to build the functions for height, BA, and crown biomass. Trunk biomass is a function of the combined estimates of height and BA, and total biomass is a summation of $\hat{B}_c$ and $\hat{B}_t$ The functions are selected primarily on the basis of the maximum coefficient of determination (r^2) or of multiple determination (R^2). Functions were kept as simple as possible and multiple linear solutions were avoided if possible, that is, if the addition of one or more additional variables resulted in only a small increase in the R^2, they were not added to the function. Table 4.1 lists the retrieval functions by Level II class. The decision to construct functions at this level was based on analyses in Dobson et al. (1995a). This research presented functions at increasing levels of land-cover class specificity, and it was determined that those analogous to Level II resulted in the highest accuracy of the biophysical estimates.

It is important to note that the results for lowland conifer are only based on 4 stands (two white-cedar stands and two spruce stands), and for aspen on 5 stands. The sample sizes for the conifer species make these results significant.

93

Structure		Local Species Name	Biophysical Variate	Units	Equation	N	R^2	RMSE
Group	Sub-Group							
Decurrent	Large	Northern Hardwoods (Maple, Beech)	Height	m	$-1.32\sigma^0_{L,vv} + 3.16(\sigma^0_{L,hv} - \sigma^0_{C,vv}) + 27.38$	9	0.95	0.46
	Branches		Basal Area	m^2/ha	$6.46(\sigma^0_{L,hv} - \sigma^0_{C,vv}) + 74.21$	9	0.80	2.10
			Trunk Biomass	kg/m^2	$0.023 \hat{h b a} + 0.5182$	9	0.98	0.54
			Crown Biomass	kg/m^2	$0.80(\sigma^0_{L,hv} - \sigma^0_{C,vv}) + 0.86(\sigma^0_{C,hh} - \sigma^0_{C,vv}) + 8.73$	9	0.93	0.55
			Total biomass	kg/m^2	$\hat{B}_c + \hat{B}_t$	9	0.98	1.10
Decurrent	Small	Aspens	Height	m	$-5.08(\sigma^0_{L,hh} - \sigma^0_{L,hv}) + 40.49$	5	0.93	0.44
	Branches		Basal Area	m^2/ha	$6.60(\sigma^0_{L,vv} - \sigma^0_{C,hh}) + 30.93$	5	0.80	3.23
			Trunk Biomass	kg/m^2	$0.024 \hat{h b a} - 0.059$	5	0.99	0.16
			Crown Biomass	kg/m^2	$-0.72(\sigma^0_{L,hh} - \sigma^0_{L,vv} + 1.62$	5	0.87	0.14
			Total biomass	kg/m^2	$\hat{B}_c + \hat{B}_t$	5	0.92	0.56
Excurrent	Small	Lowland Conifer	Height	m	$-11.06(\sigma^0_{C,hh} - \sigma^0_{C,hv}) + 74.99$	4	0.96	0.49
	Branches,		Basal Area	m^2/ha	$60.75(\sigma^0_{L,vv} - \sigma^0_{C,vv}) + 102.14$	4	0.99	1.6
			Trunk Biomass	kg/m^2	$0.0078 \hat{h b a} + 4.67$	4	0.74	1.9
			Crown Biomass	kg/m^2	$7.35(\sigma^0_{L,vv} - \sigma^0_{C,vv}) + 11.10$	4	0.99	0.20
			Total biomass	kg/m^2	$\hat{B}_c + \hat{B}_t$	4	0.87	0.71
Excurrent	Small Branches, Medium	Upland Conifer (Jack Pine)	Height	m	$2.50\sigma^0_{L,hv} + 44.65$	18	0.67	3.64
			Basal Area	m^2/ha	$5.16\sigma^0_{L,hv} + 86.18$	18	0.70	3.6
			Trunk Biomass	kg/m^2	$0.019 \hat{h b a} + 0.214$	18	0.99	0.19
	Needles		Crown Biomass	kg/m^2	$0.52\sigma^0_{L,hv} + 8.40$	18	0.70	0.48
			Total Biomass	kg/m^2	$\hat{B}_c + \hat{B}_t$	18	0.97	0.90
Excurrent	Large	Upland Conifer (Red Pine)	Height	m	$4.25\sigma^0_{L,vv} + 4.47\sigma^0_{C,hv} + 107.96$	16	0.78	2.69
	Branches, Long		Basal Area	m^2/ha	$6.77\sigma^0_{L,hv} + 102.90$	16	0.71	5.96
			Trunk Biomass	kg/m^2	$0.015 \hat{h b a} + 0.58$	16	0.99	0.34
	Needles		Crown biomass	kg/m^2	$0.98\sigma^0_{C,hv} + 1.26(\sigma^0_{L,vv} - \sigma^0_{C,hh}) + 16.17$	16	0.81	0.61
			Total Biomass	kg/m^2	$\hat{B}_c + \hat{B}_t$	16	0.96	0.54

Table 4.1: Biomass equations developed on SIR-C data.

4.3.3 Biomass Mapping

Once estimation functions are constructed, it is possible to extend the estimates from the test stands, upon which they were constructed, to the entire image. This process needs as input the estimation functions, the classified image, and the SIR-C/X-SAR image and ratio channels. Height, BA, crown biomass, and trunk biomass were mapped in the image domain on a pixel-by-pixel basis using the above inputs . These can be stated:

$$\hat{b}_{a_i} = f(I_{\lambda,pol} \text{ and } C_i)$$
$$\hat{h}_i = f(I_{\lambda,pol} \text{ and } C_i)$$
$$\hat{B}_{c_i} = f(I_{\lambda,pol} \text{ and } C_i)$$
$$\hat{B}_{t_i} = f(I_{\lambda,pol} \text{ and } C_i)$$

where

$$
\begin{array}{ll}
\hat{b}_{a_i} = & \text{estimated basal area,} \\
\hat{h}_i = & \text{estimated height,} \\
\hat{B}_{c_i} = & \text{estimated crown biomass,} \\
\hat{B}_{t_i} = & \text{estimated trunk biomass,} \\
I_{\lambda,pol} = & \text{image channel(defined by wavelength and polarization),} \\
C = & \text{class, and} \\
i = & \text{ith forest pixel.}
\end{array}
$$

Then, as stated previously (section 4.2):

$$\hat{B}_{d_i} = \hat{B}_{t_i} + \hat{B}_{c_i}$$

The resultant images are shown in Figures 4.2 and 4.3.

4.4 Results

The overall range of biomass values as shown in the images falls in the expected ranges (as captured on the bar scales below the images). See Appendix B for comparison with measured biomass figures. The plots in Figure 4.4 show measured or allometric data versus SAR-derived direct (height, basal area, and crown biomass) estimates at a 0.05 level of significance.
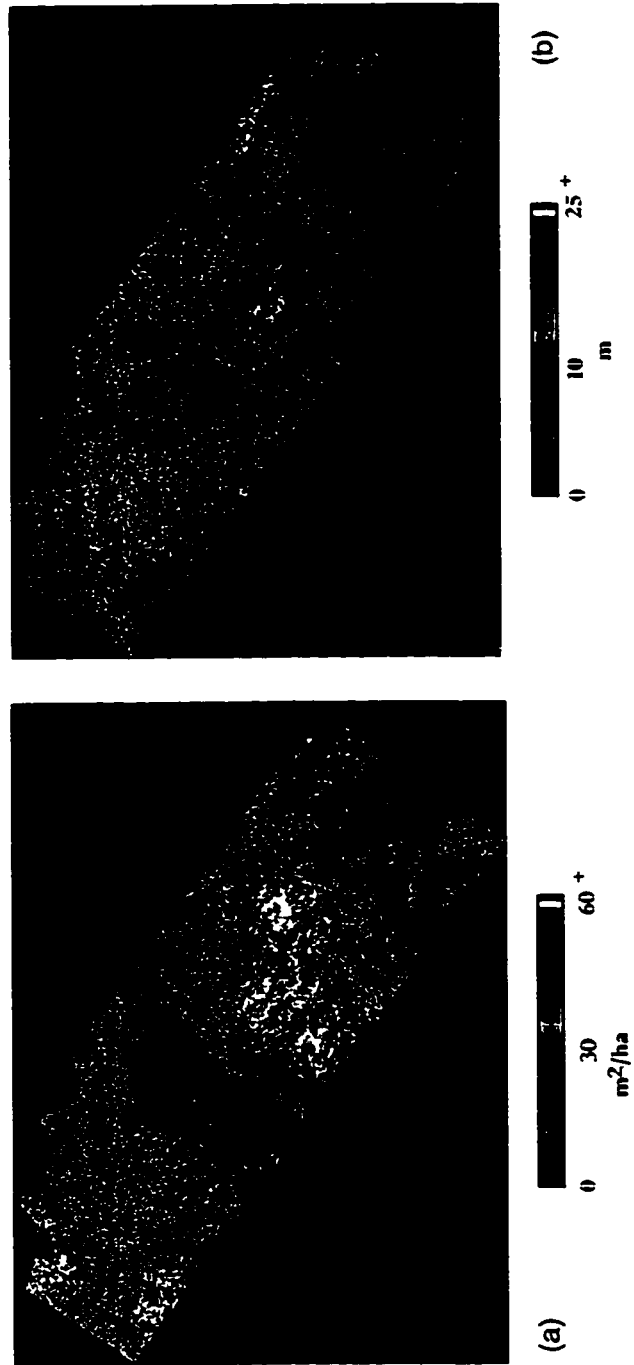
Figure 4.2: Images of SIR-C derived (a) estimates of trunk height, and (b) basal area.
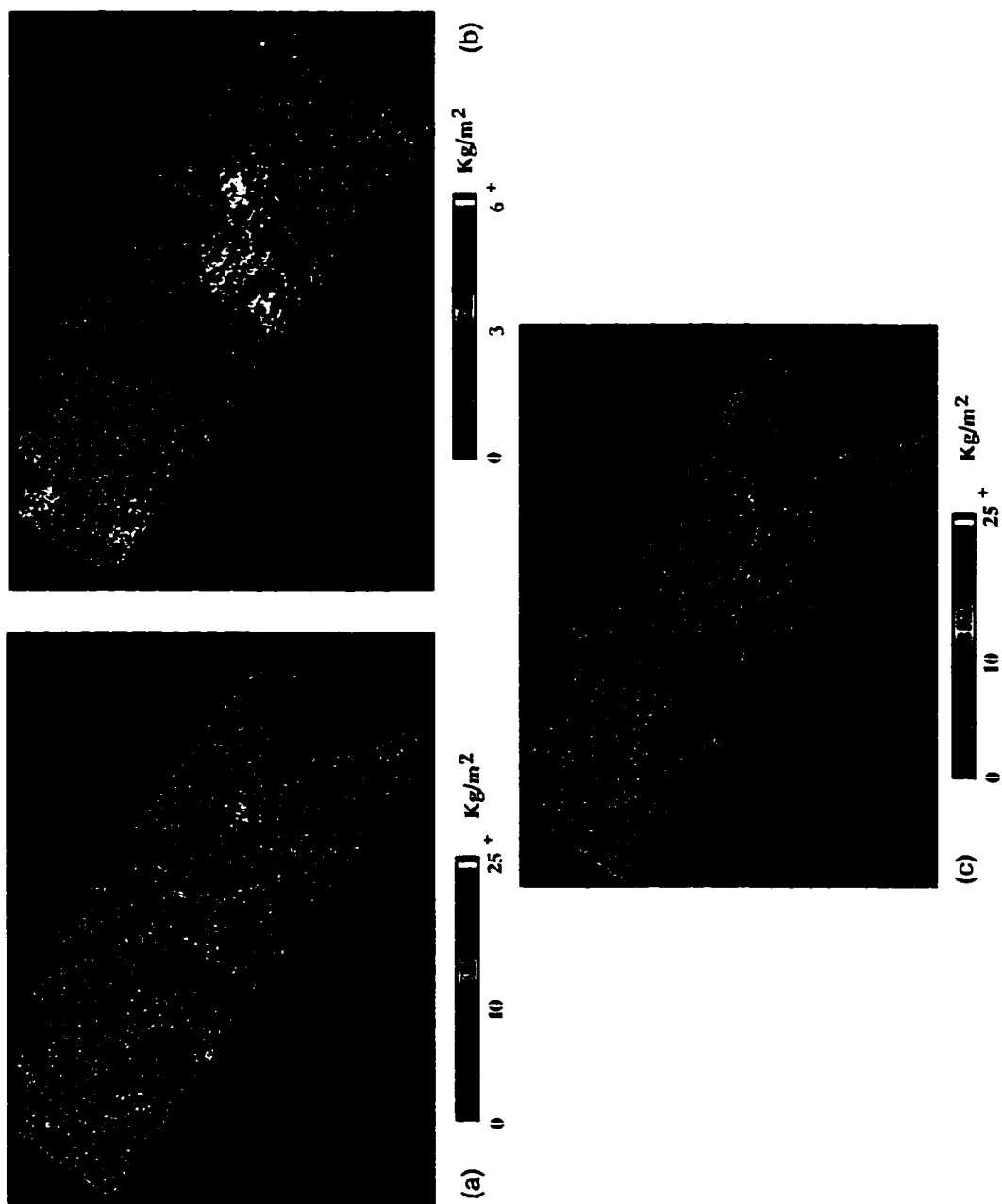
Figure 4.3: Images of SIR-C derived (a)trunk-layer dry biomass, (b) crown-layer dry biomass, and (c) total biomass.
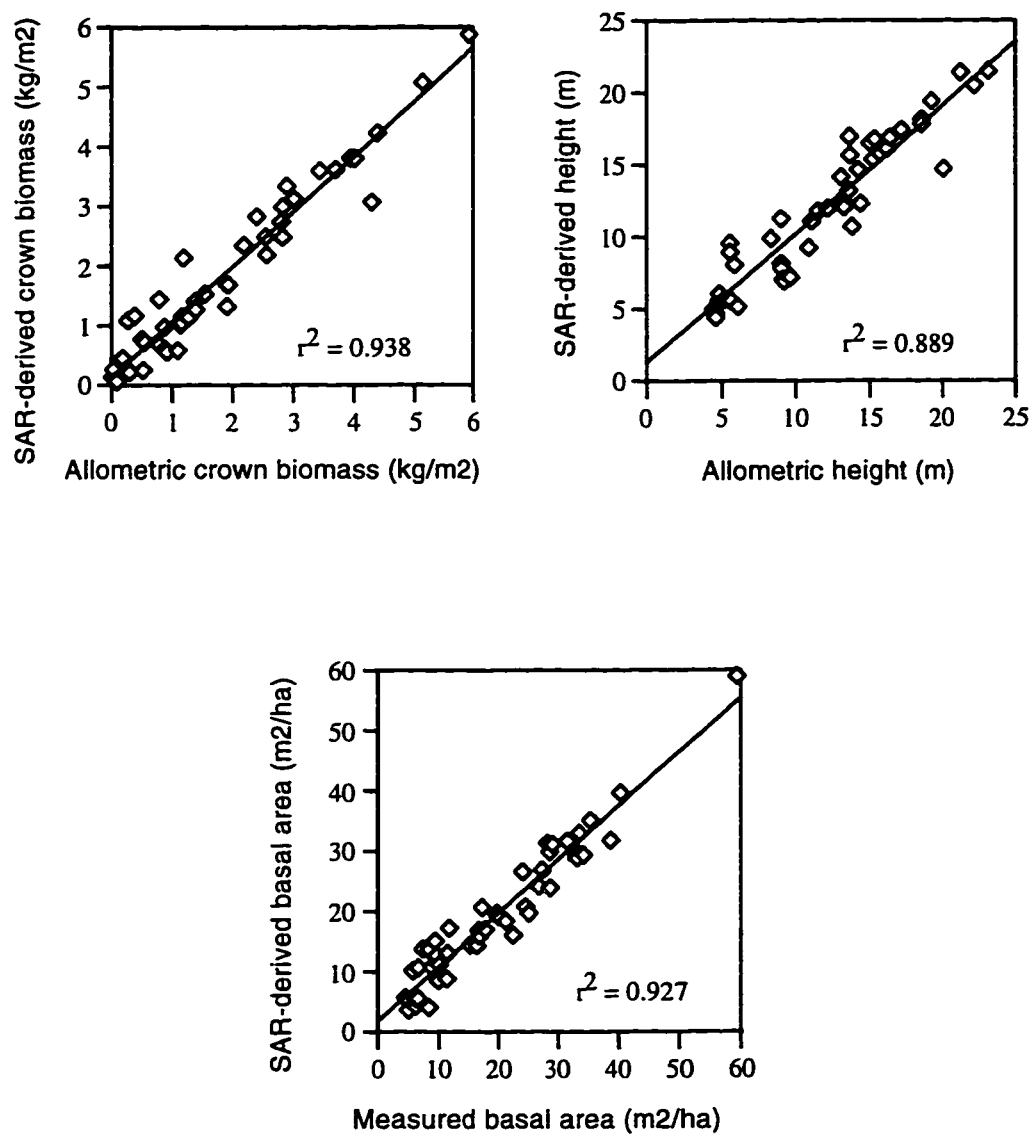
Figure 4.4: Accuracy of SIR-C-derived estimates of (a) crown (b) height and (c) basal area.

CHAPTER 5

CHARACTERIZATION OF CARBON STORAGE AND CHANGE

5.0.1 Goals of this Study

There are three goals in the present study to demonstrate that a primarily SAR-based methodology can be used to characterize components of both natural and human-induced forest C dynamics:

(1) Estimate C stored in above- and below-ground living forest vegetation at the site,

(2) Determine C gain from forest above-ground net primary productivity (ANPP) over one growing season, and

(3) Measure C removal due to managed forest disturbance in the form of clearcutting.

The following sections of this paper document and discuss the SAR-based methodology and results for the MFTS. An overview of the regional and test site ecology, reference data, and SAR data is provided. Following this the methodology and results are presented, first those for natural processes, and second those of human mitigated components of C dynamics. Each of these are discussed in terms of the input data sets, techniques/methods, and finally results in both the image domain and as numerical estimates are presented.

5.1 Regional Ecology and SIR-C/X-SAR Mission

Succession and forest age are important concepts in the NHCF. A frequently used model of succession is that of Bormann and Likens (1979). This model postulates that forests in a disturbed environment, such as most of the NHCF, proceed through several phases of stand development: (1) reorganization, (2) aggradation, (3) transition, and (4) steady-state. Depending on the type of disturbance, during reorganization there may be a net loss of total ecosystem dry matter (to decomposition) despite accumulation in initial sproutings of woody vegetation. The aggradation phase may last a century or more (depending on species composition) and is distinguished by ongoing accumulation of dry matter. The transition period is an undefined length of time during which total dry matter declines, and

the steady state occurs when total dry matter fluctuates about a mean.

A premise of this study asserts that capturing age/successional stages of terrestrial vegetation is key to increased accuracy in C modeling. A method to map forest age has importance as young ecosystems are allocating C to growth at faster relative rates than older forests. Theoretically, in young ecosystems the rate of primary production (PP) or total gross photosynthesis (P) exceeds the rate of community respiration (R) so that P/R is $\geq$ 1.0. P/R approaches 1.0 as succession proceeds where the energy fixed tends to be balanced by the energy cost of maintenance. This means that relative net community production in an annual cycle is large in young, smaller in maturing, and tending toward a zero C balance for old-growth forests. Both forest type and age/successional stage (using biomass and forest type in combination as a surrogate) are captured in the SAR-based methodology.

All forests in the test site are second-growth and are the result of late 19th century selective/total harvesting, or of continued clearcutting, the dominant managed harvesting pattern maintained in the lakes states national forests until recently. The pattern of recovery after disturbance in deciduous forests of the region is characterized by initial establishment of both early (aspen) and late successional species (maple/beech) and rapid early production of the early successional species. For deciduous forest in the region of this study, the aspen reorganization phase may last 5 years or less and quickly proceeds to the aggradation phase. Depending on site characteristics, aspen will eventually succeed to upland conifer or northern hardwoods in which form aggradation continues. For young conifers, planted seedlings following clearcutting may proceed more slowly through the reorganization phase, and the harvesting cycle precludes their proceeding beyond the aggradation phase. The aggradation phase in essence captures the stage of all but the youngest of the MFTS test stands. None of the forests in the test stands have reached old-growth steady state or fluctuating biomass (if that model is indeed the case). There are some scattered grassland areas in the test site; however, here we concentrate on forest land-cover.

The ecological processes in the region are an interaction of the differing forest communities and their age/successional state (or time since last disturbance). In a study to determine ecosystem parameters most influential in C storage in northern forests, Grigal and Ohmann (1992) found that forest type had the strongest effect on differing C storage, and that patterns of C storage in the NHCF are not as strongly influenced by climatic variables (except by its effect on vegetation composition) as is C storage in grasslands to the west (Grigal and Ohmann, 1992). A high proportion of the significance of forest type is attributed to wood specific gravity or wood density. In addition to forest type, results emphasize the importance of stand age (surrogate for time since last major disturbance) in affecting the size of C pools (Grigal and Ohmann, 1992).

Much of the C stored worldwide in living vegetation is below ground. The proportion of total biomass represented by roots is lowest for forests and rises to 90% for tundra and certain grassland vegetation types (Bazilevich and Rodin, 1968). In their summary of below-ground matter in terrestrial ecosystems, Bazilevich and Rodin published that broad-

leaved and subtropical forests are characterized by a maximum of 7.0 to 10.0 kg/m^2 of root biomass and 15-33% of total accumulated biomass. This is an important component of regional ecology and much research has been done in the NHCF to quantify the role of perennial and fine roots in C storage and change.

5.1.1 Test Site and Reference Data

Detailed measurements were made in each stand to quantify composition, structure, and biomass. Approximately 64,000 trees were measured for diameter and species and a subsample for height. Remaining heights were estimated by species-specific height prediction equations developed from the sample of measured heights (Table 2.11). Above-ground biomass for the stands was estimated using diameter and height measurements combined with allometric biomass equations developed on trees in the NHCF, primarily in the lake states (Perala and Alban, 1994). This data has been analyzed to have error rates of 15-20% or better. Total above-ground biomass for the 70 stands ranges from < 2.5 kg/m^2 for clear-cut seedling stands to 27.3 kg/m^2 for a mature northern hardwoods stand (Bergen et al., 1995a). The 70 stands were measured over the course of 1-3 years prior to the 1994 SIR-C overflights. In addition to these base measurements, a number of the stands were remeasured after the 1994 growing season had terminated. These remeasurements form a database of stand-level biomass/C accrual over 1-3 growing seasons, on which to validate ANPP estimates in this study. Refer to chapter 2 for more detailed information on MFTS reference data.

5.2 Carbon Dynamics: Modelling Natural Processes

Estimation of components of vegetative C using the methodology outlined below is predicated on the availability of SAR imagery from which to derive a classification of land cover at forest community level and biomass estimates in the image domain, plus allometric equations for parameters and species/communities of interest. All of these are readily available for the MFTS. The two SAR-derived datasets form the basis of the methodology to estimate C and given several potential scenes, priority is placed on using the classification and biomass estimation images with the highest accuracy. With this logic, it is reasonable to use images derived from a single data-take or different data-takes, provided that the latter option has included sufficient processing that the two are correctly orthorectified and thus registered to each other. The SAR-based methodology is discussed in terms of input datasets, techniques, and results.

5.2.1 Input Datasets

Land-Cover Classification: Land-cover was determined from classification of SIR-C imagery obtained in April 1994 during SRL-1 data-take 22.2 (Figure 5.1a). The classification procedure used a hybrid hierarchical methodology. Imagery was first classified to level I structural classes (tall vegetation, short vegetation, surfaces) using a simple decision tree. Tall vegetation was further classified to level II using a supervised maximum likelihood Bayesian classifier. The classes applied in the level II image were surfaces, short vegetation/agriculture, northern hardwood (decurrent-mesic), mixed aspen-birch-conifer (mixed-wet mesic), lowland conifer (excurrent-hydric), and upland conifer (excurrent-xeric). Details of the structural based classification process are covered in Bergen et al. (1996). The accuracy of the classification for the image used was 99% for level I and 93% for level II based on a test stand validation dataset. The classified image is shown as Figure 5.1b.

Above-ground Biomass: Estimates of above-ground biomass were derived from SIR-C imagery obtained during SRL-1 on data-take 102.41 (April 15). Height, basal area (BA), trunk biomass, crown biomass, and total above-ground biomass were empirically determined for each structural class in the land-cover classification image and then mapped as images. To arrive at biomass, relationships were developed between biomass of test stands on the ground and SAR backscatter (Dobson et al., 1995a). A set of equations was then developed for each structural type which related some combination of SIR-C/X-SAR channels and polarizations to components of stand biomass (Table 4.1). Height, basal area (BA), and crown biomass (branches and foliage) were directly related to backscatter values. Trunk biomass was arrived at by a simple biophysical model which used SAR-derived height and basal area with two readily available figures - wood dry density (by structural type) and trunk taper factor (by structural type). The rms error for total above-ground biomass $(0 - 25)$ kg/m^2 when validated on test stand data was 1.4 kg/m^2. An in-depth discussion of the biomass estimation procedure for the imagery used in the present study has been published by Dobson et al. (1995a). The total above-ground biomass image is shown as Figure 5.1c.

Below-ground allometric equations: Much work has been done by ecologists in the past several decades to advance understanding of below-ground C allocation in forest ecosystems. Toward this end, studies have been carried out in which equations to predict such parameters as below-ground biomass have been developed for various forest communities worldwide. Appropriate expressions from the literature are applied in this study. Regression analysis is the approach most widely used for estimating plant biomass. Logarithmic equations are widely accepted and are requisite for estimation of biomass and production in mixed and uneven-aged stands with a range of diameters and height. In such stands the plotted variance increases with age, violating the assumption of constant variance. A logarithmic transformation generally removes this (Santantonio et al., 1977), and most equations are of a double-logarithmic form.
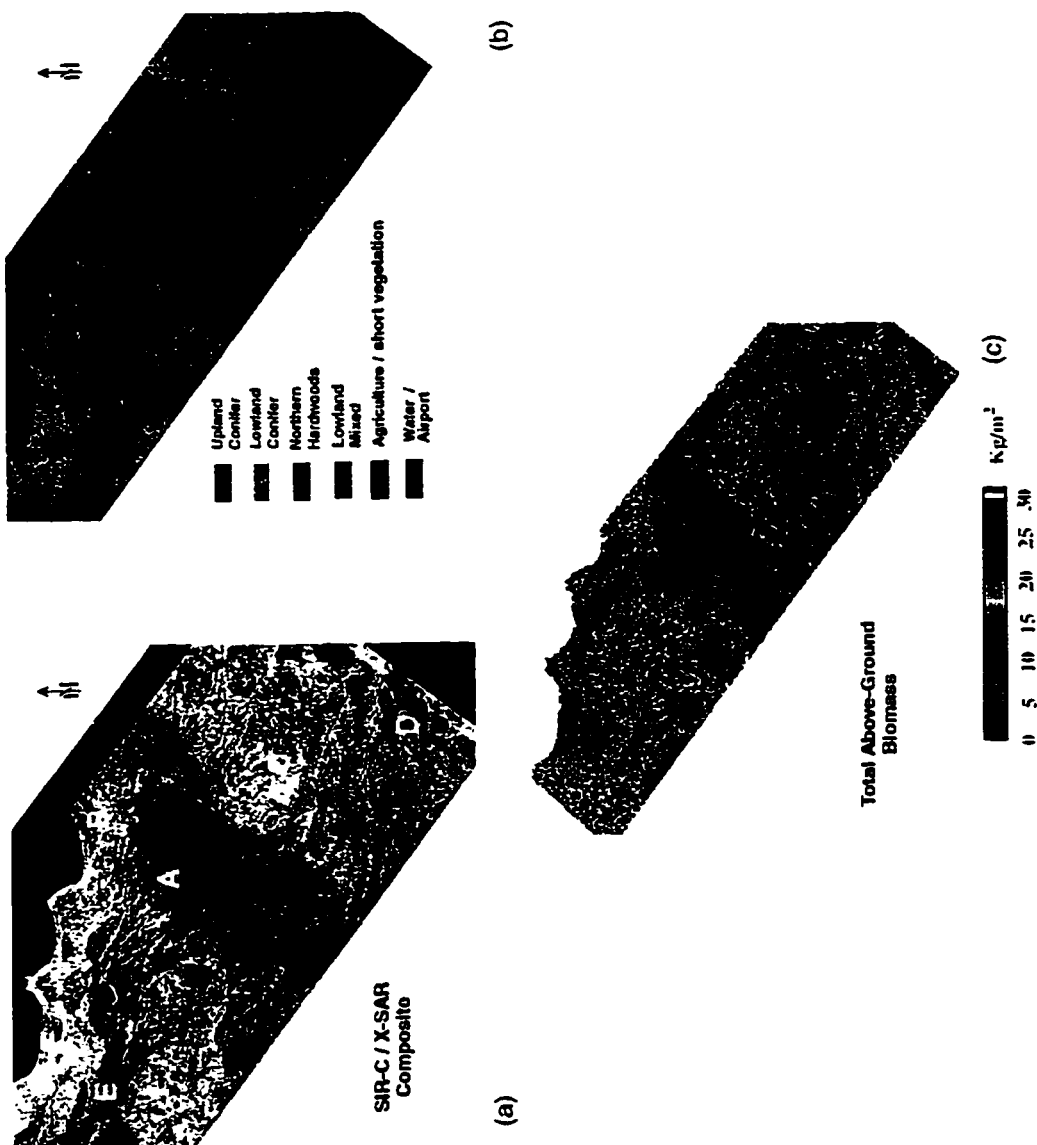
Figure 5.1: (a) Composite SIR-C/X-SAR image. Data-take 22.2, SRL-2, October 1, 1994. Incidence angle = 22.2°. Red = L-hv, Green = C-hv, Blue = X-vv. (b) Classified image. Multi-temporal classification of April and October SIR-C/X-SAR data-take 22.2. (c) Total above-ground biomass image. Derived from SIR-C/X-SAR April data-take 102.41.

Significant early work on root biomass was done by R.H. Whittaker for the Hubbard Brook Ecosystem Study. Among the many relationships published during this study were equations for root systems for several northern overstory species, both broadleaf and conifer, measured in the NHCF of New Hampshire and New York (Whittaker et al., 1974). Harris et al. (1977) developed and published root biomass equations for the southern pine and southern mixed deciduous ecosystems. Concurrently, Santantonio et al. (1977) carried similar work for the Douglas-fir (Pseudotsuga menziesii) ecosystems of the Pacific northwest and produced a major review article of published root biomass studies in forest ecosystems for species worldwide. These studies conclude that the published data show a remarkably consistent relation between root-system biomass and stem diameter for coniferous and deciduous trees over a wide range of diameters under widely differing environmental conditions. Over the long term, the broad generality of such allometric equations has been demonstrated repeatedly (Grigal and Kernik, 1984) for both above- and below-ground, and it is typical for researchers to apply them over the broader NHCF region with some consideration to site productivity and altitudinal differences when given a choice of equations.

In this study, root biomass equations developed specifically for the lake states portion of the NHCF are available in the work of Perala and Alban (1994). Perala's tree stratum root biomass equation was developed on woody roots (> 5 mm) plus the 15 cm stump from excavated roots systems of eight hardwoods and nine conifers at two different sites. This was a fairly small dataset because root systems of large trees are difficult to excavate. Thus tree root data was fit to one generic equation of the form:

$$\ln y = a + b \ln(dbh) + c \ln(ht) \tag{5.1}$$

where $\ln y = \ln$ component oven-dry wt. in kg, dbh = diameter (in cm) at 1.37 m height, and ht = height in m. The R^2 for tree equations was 0.93 (n=17).

Understory/shrub root data is significantly easier to collect. It was also pooled, but the residuals were averaged by species to create a new variable – Species. The value of Species was multiplied with the overall constant to obtain a species constant and thus separate equations were developed for most species and fit to an equation of the form:

$$\ln y = a + b \ln(D15) \tag{5.2}$$

where D15 is the diameter (in cm) at a 15 cm height. The coefficients of the root biomass allometric equations used in this study are given in Table 5.1.

Other research on lake states and northern forests in general quantifies such root characteristics as root:shoot (R/S) ratios (Alban and Perala, 1992; Ruark and Bockheim, 1988), total root production (Nadelhoffer et al., 1985), fine root production and percentage (Nadelhoffer and Raich, 1992), C and nitrogen content of roots (Grigal and Ohman, 1992; Nadelhoffer et al., 1985; Pregitzer et al., 1995), percentage of C fixation by roots (Harris et al., 1977). Reported results from these can be used as guides and for comparison purposes in

Species	a	b	c	Adj R^2
Stratum 1 (ht ≥ 5 m)				
All species	0.0918	2.498	-0.6471	0.93
Stratum 2 (1 m ≤ ht < 5 m)				
balsam fir larch red oak black cherry northern pin oak red pine black spruce northern white-cedar scotch pine choke cherry paper birch white pine hemlock pin cherry white spruce jack pine	0.1318	2.187		0.66
American basswood red maple sugar maple mountain maple striped maple	0.2026	2.187		0.66
speckled alder yellow birch	0.1011	2.187		0.66
serviceberry eastern-hop- elder hornbeam chokeberry	0.1826	2.187		
beaked hazel	0.1383	2.187		0.66
American beech winterberry mountain-holly alternate-leaf dog- wood	0.1084	2.187		0.66
American ash black ash	0.1203	2.187		0.66
fly-honeysuckle elder viburnum labrador-tea	0.3532	2.187		0.66
bigtooth aspen balsam poplar willow trembling aspen cottonwood	0.0977	2.187		0.66

Form of equation for Stratum 1 is: Root weight $= a \times Dbh^b \times Ht^c$

Form of equation for Stratum 2 is: Root weight $= a \times D15^b$

Where dbh $=$ diameter at 1.37 m height, and D15 $=$ basal diameter at height of 15 cm.

Source: Perala and Alban, 1994.

Table 5.1: Allometric root biomass prediction equations.

evaluating the results of the SAR estimated below-ground biomass/C.

ANPP allometric equations: Equations which predict ANPP as a function of stem diameter are available for the NHCF and other biomes as well. In the MFTS aspen and maple dominate the northern deciduous forest, and a choice of equations developed on the range of ages is available for each (Pastor and Bockheim, 1981; Ruark and Bockheim, 1988). For predicting ANPP, there is an advantage in having separate equations for aspen and maple because aspen is an early successional or pioneer species and has a higher relative rate of growth than the later successional species such as maple. These equations were developed on all but the smaller understory stratum stems in northern hardwood stands. For conifer, equations derived by Whittaker and Woodwell (1968) are used. All ANPP equations are of the double-logarithmic form and yield ANPP in g/yr or kg/yr.

$$\log_{10} \text{ANPP} = a + b \log_{10}(dbh) \tag{5.3}$$

105

Equations are inclusive of foliage and are given in Table 5.2. Plant losses by death, shedding, and consumption have been found by researchers to amount to a maximum of 3 - 4% and for the purposes of this study these were ignored. However, these could be modeled or estimated and included as an additional component of the methodology.

Ranges of ANPP in the NHCF have been evaluated in the studies cited in Table 5.2 and others, and these are useful for comparison purposes (Nadelhoffer et al., 1985, Nadelhoffer and Raich, 1992). Equations for many major species of interest in other global biomes can be found in Ruark and Bockheim (1988).

5.2.2 Techniques

Above-Ground Carbon: The first C component derived was that of above-ground living vegetation. The procedure is shown diagramatically in Figure 5.2. Only the SAR-derived biomass image was needed to estimate total C and this was done to a first approximation by applying a widely used allometric rule that biomass is approximately 47% C. This proportion has been generated independently by numerous researchers and found to be generally applicable (Linder and Axelsson, 1982). A recent study in northern lower Michigan, for example, found leaves of Populus *Populus x euramericana* cv. *Eugenei* to have a C concentration of 460 mg/g and stems to 490 mg/g. The whole tree (including roots which were 448 mg/g) had an average C concentration of 461 mg/g (Pregitzer et al., 1995).Thus each pixel value in the biomass estimation image classified as forest was multiplied by 0.47 to arrive at the total above-ground C as shown in Figure 5.4a. Co-registration of the SAR-derived land-cover classification to the above-ground C image permits retrieval of C sequestration by forest community type.

Below-Ground Carbon: Below-ground biomass, C, and R/S ratio were estimated for all forested areas in the portion of the region represented in the imagery. This procedure involved several steps as outlined in Figure 5.3. First, the selected species/stratum - specific below-ground allometric biomass equations were applied to each tree in the test stand database to predict below-ground biomass as a function of above-ground stem diameter; when summed by stand, this resulted in estimates of below-ground biomass in kg/ha for each test stand. Total above-ground biomass was already available for each of the test stands since it had been required for previous above-ground biomass estimation results (Dobson et al., 1995a). The test stand population (selected from 70 stands) was then divided into two populations - hardwood and conifer, and new equations were developed for each which predicted below-ground biomass as a function of above-ground biomass. The aspen and northern hardwoods communities were combined into one equation. The conifer population consists of lowland and upland conifer. The lowland conifer test stand population was not of sufficient size to construct a a separate equation, and plots showed that the several lowland conifer test stands which did exist fell within the distribution of the upland conifer stands, so these communities were merged as well. Recently clear-cut seedling test stands were not

106

Stratum 1 (ht $\geq$ 5m)					
Species			a	b	source	r

Stratum 1 (ht $\geq$ 5m)				
Species	**a**	**b**	**source**	**r**
Form of equation is: $\log_{10}$ANPP (g/yr) $= a + b \times \log_{10}$Dbh				
Conifers	0.9369	1.8667 (stem wood)	Whittaker and Woodwell, 1968	0.93
balsam fir larch scotch pine				
black spruce n. white-cedar white pine	0.4784	1.718 (stem bark)		0.97
hemlock red pine white spruce				
jack pine	0.8928	2.0078 (branch)		0.98
	1.3625	1.8772 (twig/leaf)		0.98
Birches	1.2763	2.1745	Whittaker et al. 1974	0.96
yellow birch paper birch				
Form of equation is: $\log_{10}$ANPP (kg/yr) $= a + b \times \log_{10}$Dbh				
Northern Hardwoods	-2.2650	2.678	Pastor and Bockheim 1981	0.98
American ash elder red oak				
basswood hazel serviceberry				
American beech mountain maple speckled alder				
black ash northern pin oak striped maple				
chokeberry red maple sugar maple				
E. hop-hornbeam				
Aspen/Cherry	-0.7722	1.418	Pastor and Bockheim 1981	0.87
balsam poplar choke cherry trembling aspen				
bigtooth aspen cottonwood willow				
black cherry pin cherry				

r= correlation coefficient as provided by source.

Table 5.2: Allometric above-ground net primary production prediction equations.

Stratum 2 (1 m $\leq$ ht $<$ 5 m)						
Species			a	b	source	r
Form of equation is: $\log_{10}$ANPP (g/yr) $= a + b \times \log_{10}(0.8 \times D15)$						
Conifers			0.9369	1.8667	Whittaker and	0.98
balsam fir	larch	scotch pine		(stem wood)	Woodwell, 1968	
black spruce	n. white-cedar	white pine	0.4784	1.718		
hemlock	red pine	white spruce		(stem bark)		
jack pine			0.8928	2.0078		
				(branch)		
			1.3625	1.8772		
				(twig/leaf)		
Form of equation is: $\log_{10}$ANPP (kg/yr) $= a + b \times \log_{10}(0.8 \times D15)$						
Northern Hardwoods			-2.2650	2.678	Pastor and	0.98
dogwood	fly-honeysuckle	red oak			Bockheim, 1981	
American ash	hazel	serviceberry				
basswood	labrador-tea	speckled alder				
American beech	mountain-holly	striped maple				
black ash	mountain maple	sugar maple				
black cherry	northern pin oak	willow				
chokeberry	red maple	winterberry				
choke cherry	paper birch	yellow birch				
elder	red maple	viburnum				
E. hop-hornbeam						
Aspens			-0.7720	1.418	Pastor and	0.86
balsam poplar	cottonwood	trembling aspen			Bockheim, 1981	
bigtooth aspen						

Table 5.2 cont'd.

r= correlation coefficient as provided by source.
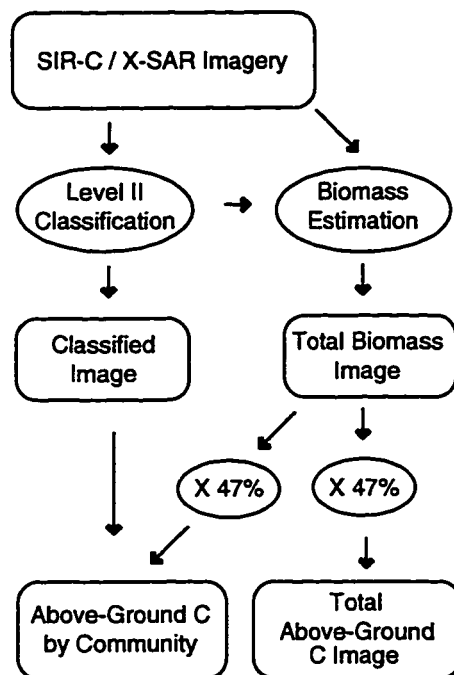
Figure 5.2: Model for estimating C storage and change: above-ground total C and by community.

Below-ground biomass						
Community	**constant**	**a**	**b**	**c**	$\mathbf{R^2}$	**n of cases**
[1]Conifer	-1.712	1.0675			0.91	38
[1]Deciduous	1.1688	0.7528			0.97	20
ANPP						
[2]Conifer	0.3479	0.7747			0.97	38
[3]Deciduous	3981.8482	0.0861	-4.09E-7	1.5987E-12	0.92	20

[1] *Form of equation is:*

$\log_{10}$root weight $=$ constant $+$ a($\log_{10}$above-ground biomass)

[2] *Form of equation is:*

$\log_{10}$ANPP $=$ constant $+$ a($\log_{10}$above-ground biomass)

[3] *Form of equation is:*

ANPP $=$ constant $+$ a(above-ground biomass) $+$ b(above-ground biomass)^2 $+$ c(above-ground biomass)^3

Table 5.3: Below-ground biomass and ANPP prediction equations.

used as they were classified as short vegetation. Table 5.3 lists the prediction equations developed and used in this study.

Below-ground biomass was mapped in the image domain on a pixel-by-pixel basis using as inputs (1) the SAR-derived above-ground biomass image, (2) the SAR-derived land-cover classification, and (3) the equations given in Table 5.3. Finally, below-ground C was estimated as 47% of below-ground biomass. This can be stated as:

$$W_{bg_i} = f(W_{ag_i} \text{ and } C_i), \qquad (5.4)$$

where W_{bg} = below-ground biomass, W_{ag} = above-ground biomass, C = class, and i = ith forest pixel. Another ecologically meaningful image to derive is that of the R/S ratio. This was accomplished by dividing the pixel values of the below-ground biomass by the above-ground biomass image.

ANPP: The method of estimating ANPP is also shown diagramatically in Figure 5.3. Like the below-ground biomass/C estimation, species/community – specific allometric ANPP equations were applied to each tree in the test stand database and from this totals of ANPP in kg/ha were summed for each stand. Equations were then developed which predicted ANPP as a function of test stand total above-ground biomass. As with below-ground biomass, two equations, one for conifer and one for deciduous were developed. These were applied on a pixel-by-pixel basis using the biomass and classified images to arrive at a new image of absolute ANPP using the appropriate equations in Table 5.3 and the simple model:

$$ANPP_i = f(W_{ag_i} \text{ and } C_i), \qquad (5.5)$$

110
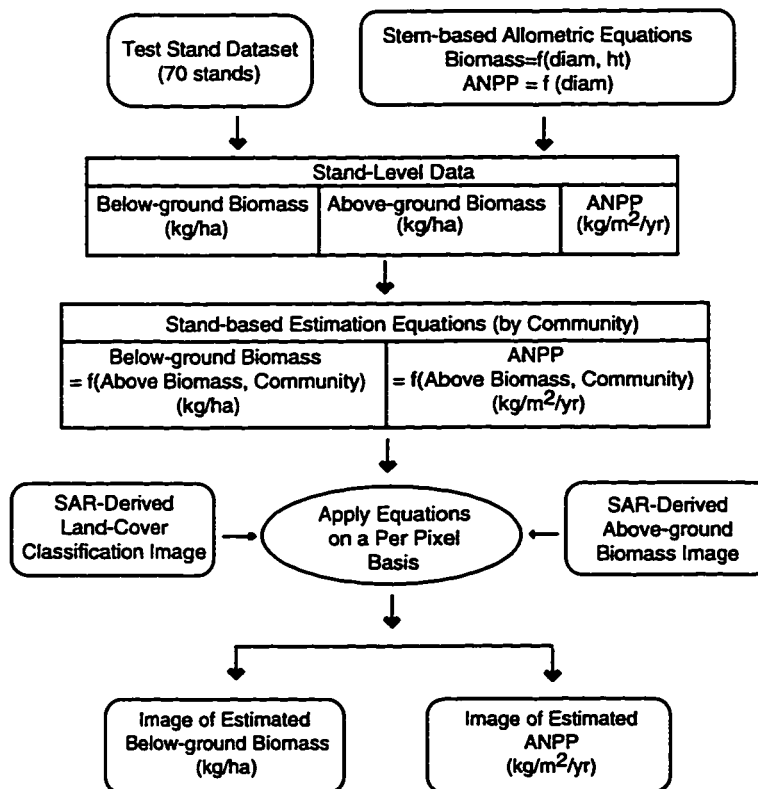
Figure 5.3: Model for estimating C storage and change: below-ground C
and ANPP.

where $ANPP$ = above-ground NPP, W_{ag} = above-ground biomass, C = class, and i = ith forest pixel.

Where there is interest in future C sequestering, the relative growth rate of the differing forest communities and successional stages is a key measure. ANPP as a percent of current above-ground biomass is computed by dividing ANPP by total biomass and generating an output image of ANPP percent or relative rate of accrual.

5.2.3 Results

Above-ground Carbon: Results of the SAR-based methodology for above-ground C are obtainable in both tabular or image form. Overview results show that the imaged region contains 5.96×10^9 kg biomass or 2.80×10^9 kg C stored in above-ground vegetative C. Image results are shown in Figure 5.4a. Tabular results by forest community are given in Table 5.4 where the total area, total biomass, total above-ground C, and average value of C stored are given for each community. Within the 70 test stands, which are representative of the range of conditions found at the site, above-ground C stored ranges from < 0.025 kg/m^2 for new clear-cut seedling conifer sites to 11.8 kg/m^2 for a mature northern hardwoods stand.

Comparison of these results with others obtained for the U.S. and the NHCF in particular confirms that they fall where expected given the published ranges. Birdsey (1990) estimated that the average forest in the U.S. (across many bioregions) stored about 5.5 kg/m^2 of C. In a survey of biomass/C data from forests in the lake states, Crow (1978) stated that above-ground C storage in most closed canopy forest in the lake states is approximately 5 to < 15 kg/m^2. Recently harvested forest areas are, of course, much lower, and scattered old-growth forest (not found in the MFTS) in the lake states may contain as much as 25 kg/m^2 C at the upper bound (Crow, 1978).

Ecological interpretations can be drawn from the SAR-based results of above-ground C allocation in the region. For example, although one-quarter of the region represented in the scene is in managed plantations of upland conifer, this community type contains only 15% of

Community	Total Biomass (kg)	Total Carbon (kg)	Average Carbon (kg/m^2)	Area (ha)
Upland Conifer	9.14×10^8	4.57×10^8	3.75	12,252
Upland Hardwood	2.32×10^9	1.16×10^9	6.90	16,809
Lowland Mixed (birch/conifer)	1.36×10^9	6.81×10^8	5.9	11,606
Lowland Conifer	1.20×10^9	6.00×10^8	5.6	10,781

Table 5.4: Above-ground C storage by forest community.

the C. Conversely the upland deciduous northern hardwoods type comprises 32% of the area but 40% of the C. The other two forest communities (lowland mixed and lowland conifer) have an area to C ratio of 1.0. These numbers show that the area of second-growth northern hardwood forest is the greatest pool of sequestered C in the region. This can be attributed to several things. First, and most significant, the deciduous community is a natural forest - its density and complexity of layers is much greater than in the managed conifer plantations. The conifer plantations are not only less dense, but more frequent harvesting has resulted in many stands of young age and low biomass, or significantly thinned stands also with lower biomass. Additionally, the deciduous community occupies the richer sites of moraine clay till substrate while the upland conifers are found on more xeric outwash sands and in comparison the two are subject to site productivity differences.

Below-ground Carbon: Image results for below-ground biomass/C (exclusive of fine roots), and total C (above- and below-ground) are presented as Figures 5.4b and 5.4c. R/S ratio is displayed in 5.4d. The images of above- and below-ground C show that the pattern of greater amounts of C stored in the northern hardwoods communities and less in the upland conifer communities holds for below-ground as well. The total amount of C stored in the perennial (woody roots > 3mm) below-ground component in the imaged portion of the test site is 5.15×10^8. This is approximately 18% of above-ground C storage and 15% of the total. In comparison, Alban and Perala (1992) found that roots of mature lake states trees are approximately 20% of aboveground biomass, and other studies have found similar results (Baskerville, 1965).

An expected phenomenon is observed when the R/S ratio image is compared with the total above-ground biomass image. It is seen that the R/S ratio in the test site is higher (as high as 45%) in young forests and lower (as low as 16%) in maturing second-growth forests. This curve was observed in early root biomass studies (Rodin and Bazilevich, 1967; Harris et al., 1977; Whittaker et al., 1974), and since that time other researchers have repeatedly confirmed that R/S ratio declines with stand age (Ruark and Bockheim, 1988). In their study of below-ground biomass of natural deciduous forest and loblolly pine plantations, Harris et al. (1977) published a figure plotting the ratio of below- to above-ground biomass against above-ground biomass, and this is reproduced in Figure 5.5a. The dashed line is a hand-fitted approximation of a trend noted by Rodin and Bazilevich (1967) for broad-leaved deciduous forests. The plotted points are observed values in three forest areas measured by Harris et al. Note that a loblolly pine plantation of a much lower density, and thus lower above-ground biomass, is displaced far to the left on the X axis. A plot of the MFTS test stand R/S ratios is given in Figure 5.5b and displays a very similar pattern of biomass allocation. R/S ratios range from 0.16 to 0.52. Points on the right-hand side which level off asymptotically as expected at about 0.16 - 0.21 are pole to mature second-growth northern hardwood stands. Like Harris' Loblolly pine, the cluster on the left is composed of conifer stands of various age and density combinations. For example, those with low biomass - low R/S ratios are pole to mature conifer stands of low density (selectively thinned). The
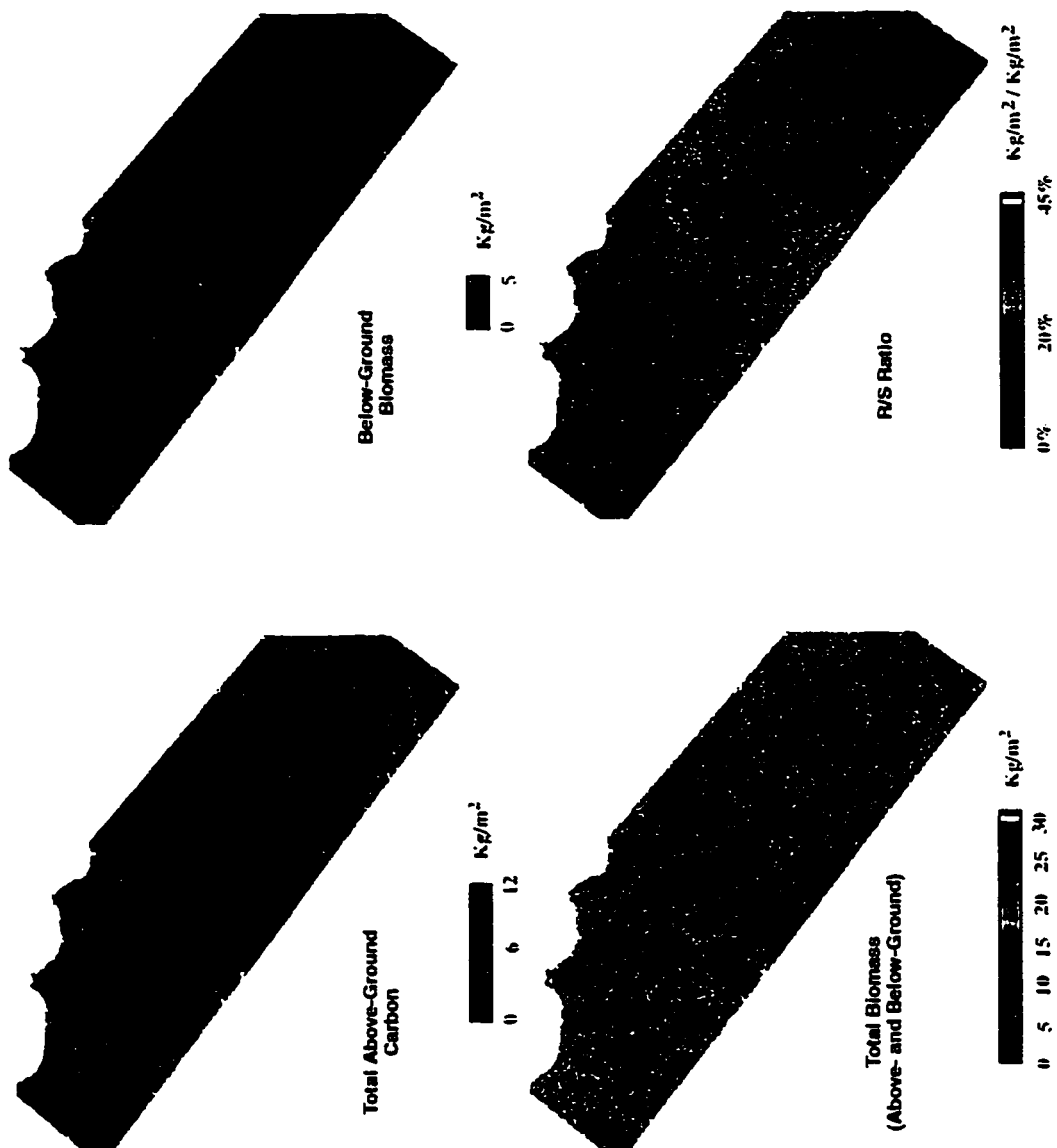
Figure 5.4: (a) Total above-ground C. (b) Below-ground biomass. (c) Total biomass (above- and below-ground). (d) Image results of R/S ratio.

114

Average ANPP ($kg/m^2/yr$)			
Upland Conifer	Lowland Conifer	Upland Hardwood	Lowland Mixed
0.75	1.06	1.31	1.12

Table 5.5: Average ANPP for forest classes.

R/S estimates for the MFTS test stands are also comparable to those of equivalent age and diameter reported in the literature on lake states forests (Young et al., 1980; Perala and Alban, 1992). For example, an average figure for R/S ratios of pole to mature trees in the lake states is given as 0.21 (Crow, 1978). Thus while young forest stands have less total biomass/C in their root systems, the relative importance and allocation of underground biomass/C is greater and this is captured in the current methodology. This interaction of age and below-ground C component is an example of the importance of not ignoring forest age when modeling future C sequestering.

ANPP: ANPP results on an absolute basis are presented in the image domain as Figure 5.6a. As with below-ground biomass, it is seen that, in general, absolute ANPP scales with total biomass/C in aggrading forests. The pole to mature second-growth northern hardwood forests are acquiring the most biomass/C in $kg/m^2/yr$. The younger stands have less mass to which to add C. It can be clearly seen, however, from the ANPP percent image (Figure 5.6b), that the relative growth rate is higher for the young stands - for example, note the young conifer stands on the Raco Plains have a higher relative rate of C accumulation than the older northern hardwoods stands to the west. Here too predictions into the future for C accumulation are dependent not only on total biomass, but the age of the stands, as this variable affects the relative rate of current and future C accumulation.

Results show that ANPP ranges from 0.5 to 2.7 $kg/m^2/yr$ in the imaged portion of the MFTS with an average of 1.09 $kg/m^2/yr$. Averages by level II forest class are given in Table 5.5. These ANPP estimates produced by the SAR-based methodology were evaluated in two ways: first by comparison with values obtained by other reseachers, and second, through ground measurements made at the MFTS to quantify ANPP for a selection of the younger test stands. Overall productivity figures for north-temperate forests have a fairly narrow range. Westlake (1963) gave 1.2 $kg/m^2/yr$ as the average and 1.0 to 2.5 $kg/m^2/yr$ as the range for total ANPP for pole to maturing temperate forests. Based on 10 regional stands, Crow (1978) estimated an average total production for similar age forests in the lake states as 1.07 $kg/m^2/yr$. While Crow's figure is at the lower bound of the temperate forest estimate given by Westlake, it is reasonable for forests on the edge of the biome such as those of the NHCF, which have a cooler, shorter growing season.

There are also reference figures for specific forest communities; e.g., aspen. The SAR-based methodology gave test stand aspen ANPP with a range of 0.4 to 1.0 $kg/m^2/yr$. Based on traditional ground measurements, other lake states researchers have also found the ANPP

ORNL-DWG 73-2560A
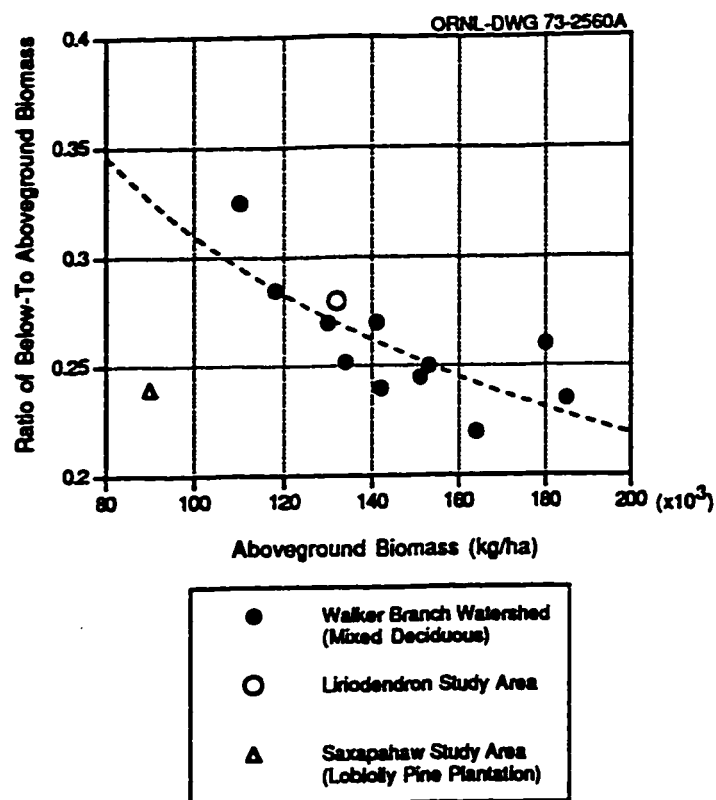
Relationship of Root:Shoot Ratio and Total Above-Ground Biomass for Michigan Forests Test Stands
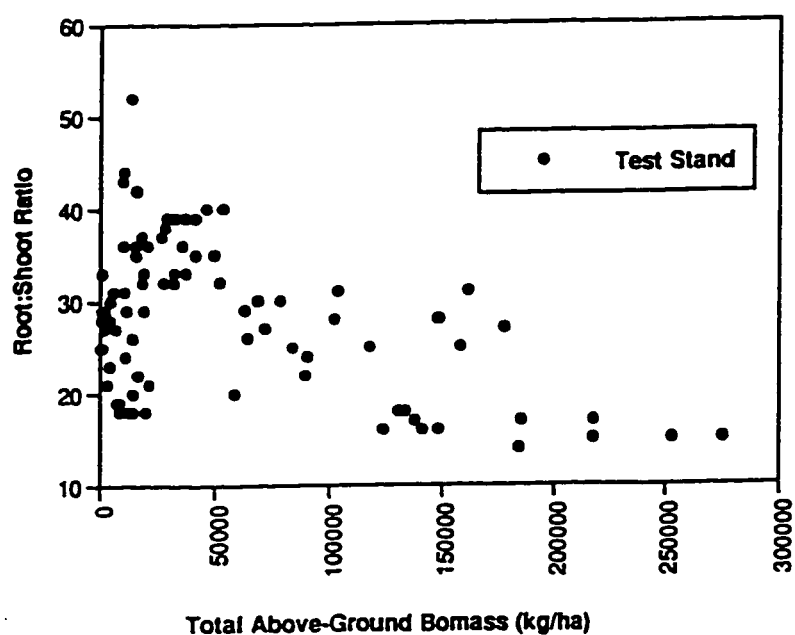
Figure 5.5: Plots of the ratio of below- to above-ground biomass vs. above-ground biomass. (a) Harris et al., (1977), and (b) MFTS.

116
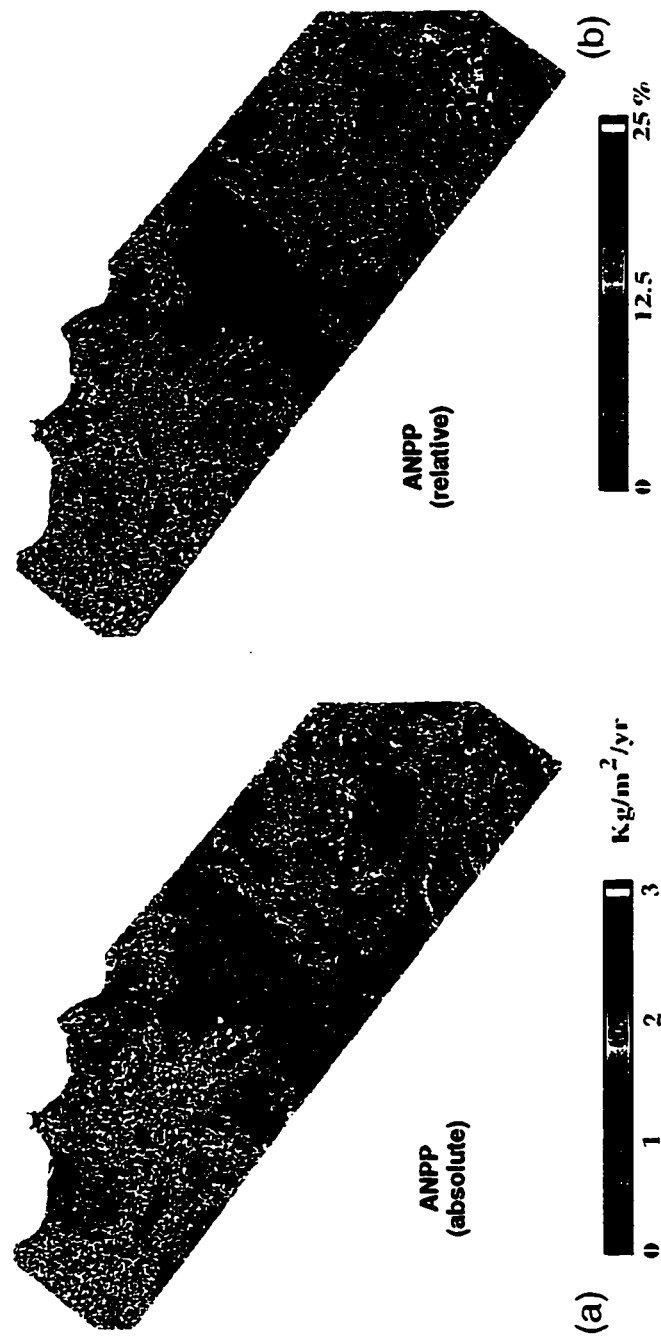
Figure 5.6: (a) ANPP on absolute basis. (b) ANPP on relative (percent of above-ground biomass) basis.

of aspen stands to have a similar range. Pastor and Bockheim (1981) published results also showing a range of 0.4 kg/m^2/yr to 1.0 kg/m^2/yr. Koerper and Richardson's (1980) measurements of pole to mature *Populus grandidentata* growing on high quality sites in Michigan showed an ANPP of 1.1 kg/m^2/yr. Ruark and Bockheim (1988) measured aspen stands aged 8 to 63 years and determined a range of 0.59 to 1.11 kg/m^2/yr. Crow's (1978) analysis of primary production in aspen, birch-maple forests found that ANPP in the lake states had a narrow range of 0.7 to 1.04 kg/m^2/yr. Similar matches to published figures were obtained for the other communities in the MFTS.

In addition to comparisons with published data of generally accepted values for ANPP in the region, test stand remeasurement of several younger stands at the MFTS provided a database of ANPP validation figures. These are given in Table 5.6. Columns 1 and 2 give stand and community, and column 3 reports the annual ANPP in kg/ha ($\pm$ a 20% uncertainty about the mean from measurement error plus any biomass prediction model error) measured by our field crews. The fourth column contains the estimated total ANPP for each stand based on applying the individual tree allometric equations given in Table 5.2, and then summing over that test stand. This gives a measure of the applicability of the allometric ANPP equations. The final column gives the ANPP as mapped in the image domain, and is an integration of the SAR classification, biomass estimation, and one of two (conifer or hardwood) equations developed for this site to provide ANPP for the entire image. Figure 5.7 also provides a comparison of the measured, allometric, and image estimations. Some larger values (e.g., stands 37 and 78) in the image estimation compared with measured ANPP are directly attributable to the presence of large standing residual overstory trees in a number of otherwise clear-cut young seedling stands which we know have been adequately accounted for in ground sampling at different dates, but dominate the pixel values. Another source of error is random over- or underestimation in the biomass image used in the ANPP methodology. This is partly related to the effects of fading and can skew individual pixel or stand values, but when taken over a region, the values stabilize, and the previous comparsion with published data shows very good agreement with mean values.

The preceeding results account for above-ground C, below-ground C, and that added to above-ground biomass on an annual basis as ANPP. These are the most obvious of the major components of vegetative C at the site. Another major change component is in the form of forest harvesting, and this is included in the methodology and discussed below. Two other components - fine roots and soil C/detritus - which would complete the picture of C dynamics were not estimated for this study, but are reviewed in the discussion section.

Stand	Community & Age	Measured ANPP (kg/ha)	Equation Estimation (kg/ha)	Image Estimation (kg/ha)
36	jack pine - sapling	1554	1934	2090
37	jack pine - seedling	332	276	860
38	jack pine - sapling	2352	2005	2240
58	jack pine - sapling	3116	2174	2208
66	jack pine - seedling	383	556	580
81	jack pine - sapling	6928	4630	5880
40	red pine - sapling	1968	1225	1379
41	red pine - sapling	2412	2793	2410
78	red pine - seedling	460	386	730
82	red pine - sapling	1711	2945	1220
33	aspen - sapling	7368	10519	5793
45	aspen - sapling	2913	2815	4484
49	aspen - sapling	3180	4042	5050

Table 5.6: ANPP estimates.
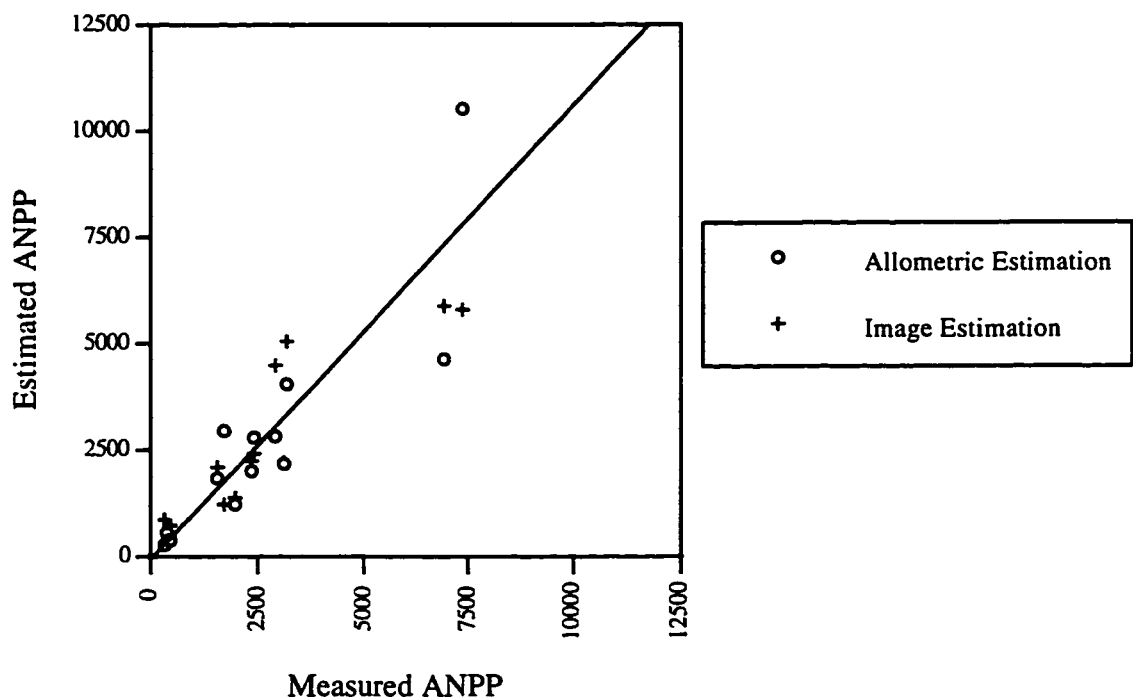
Figure 5.7: Plot of measured vs. estimated ANPP.

5.3 Carbon Dynamics: Modeling Human-Induced Disturbance

Estimation of C removal due to clearcutting was done using multi-temporal SIR-C/X-SAR imagery classified to level I and a procedure involving image differencing and decision rules. The goal was to locate clearcuts which were made between SIR-C/X-SAR SRL-1 (April) and SRL-2 (October) and extract these from the imagery. C removal was then estimated by orthorectifying and overlaying the clearcut image on the biomass image and segmenting out the amount of biomass/C stored in those portions of the image.

5.3.1 Input Datasets

Quantifying the amount of C removed by clearcutting involved: (1) identifying the location of clearcuts and (2) determining the amount of C at those locations. Because identifying the location of clearcuts involved information solely on the presence/absence of trees, two SAR images of different dates classified to level I were sufficient. They were matched to the ANPP methodology by including one from before the annual growing season (April), and one from the conclusion (October). The level I classifier outputs the categories of tall vegetation (trees), short vegetation, and surfaces using the following decision rules:

$$
\begin{array}{llll}
\text{If} & \text{(L-hv} > (-0.91 * \text{L-hh} - 25.0) & \text{then trees} & \\
\text{Elseif} & \text{(C-hv} > -20.0) & \text{then shortveg} & \\
\text{Elseif} & \text{(C-hv} < -20.0 \text{ and L-hv} < -20.0) & \text{then surface} & (5.6) \\
\text{Else shortveg} & & &
\end{array}
$$

These rules are the same for both April and October. The level I classification achieved a mean accuracy of 99% based on training and testing regions. Details of the classification are reported elsewhere (Bergen et al., 1996).

The biomass image used was the biomass estimation from SRL-1 datatake 102.41 shown in Figure 5.1c (Dobson et al., 1995a). The three images were orthorectified to each other so that they could be overlaid accurately (better than 50 m).

5.3.2 Techniques

A general model of the clear-cut identification method is given in Figure 5.8. Because level I classified results are highly accurate, clearcutting activity can be reliably located and measured using an image differencing methodology. This was done in several steps. First, April level I classified imagery was further post-processed to sieve out any small clusters of pixels erroneously classified as trees in the level I classification. In the sieving process, the software used (PCI) reads an image channel, and merges image value polygons smaller than a user specified threshold with the largest neighboring polygon. This is typically used to filter small classification polygons from a classification result. In the present study this was

120

done to assure location of only major clearcuts which were tall vegetation (trees) in April and short vegetation (clear-cut) in October. A spatial threshold smaller than the known lower bound of clearcut patch size of approximately 4 ha. was established.

The same was done for short vegetation classification errors in the October imagery. After this was done, the two images were differenced. The resulting image showed a number of obvious and known completed clearcuts. Results also produced a number of isolated pixels or groups of pixels much smaller than the lower bound which were known to be slight errors (generally edge pixels) not sieved out of the original classification or slight orthorectification mismatches. Again these were sieved from the imagery. The output clearcut areas were then co-located with the biomass image to determine the amount of biomass/C removed.

5.3.3 Results

The location of the clear-cuts identified by the SAR-based methodology are shown in Figures 5.9a and 5.9b. Figure 5.8a displays trees and clearcuts in green and red respectively, and non-forested areas are represented by the background SAR image. Figure 5.8b gives just the clearcuts overlain on the October SAR image. The process shows that approximately 300 ha of forest was removed during the period between April 10 and October 6, 1994. Most of this occurred in the Raco Plains area, the area of highly xeric sandy outwash supporting plantations of primarily jack pine, but also red pine. Due to jack pine budworm infestation, there is an active salvage clear-cutting program. From the biomass imagery it was determined that this clear-cutting amounted to 12.82×10^6 kg of biomass removed. Applying the allometric relationship, approximately 6.02×10^6 kg of C was removed (see Table 5.7). Location of clear-cuts was validated by comparison to reference data including airborne video photography.

	Stored (April, 1994)	Removed (April - Oct., 1994)
Biomass (ha)	5.96×10^9	12.82×10^6
Carbon (kg)	2.80×10^9	6.022×10^6
Area (ha)	56,111	300

Table 5.7: Total above-ground biomass and C storage and removal.

121
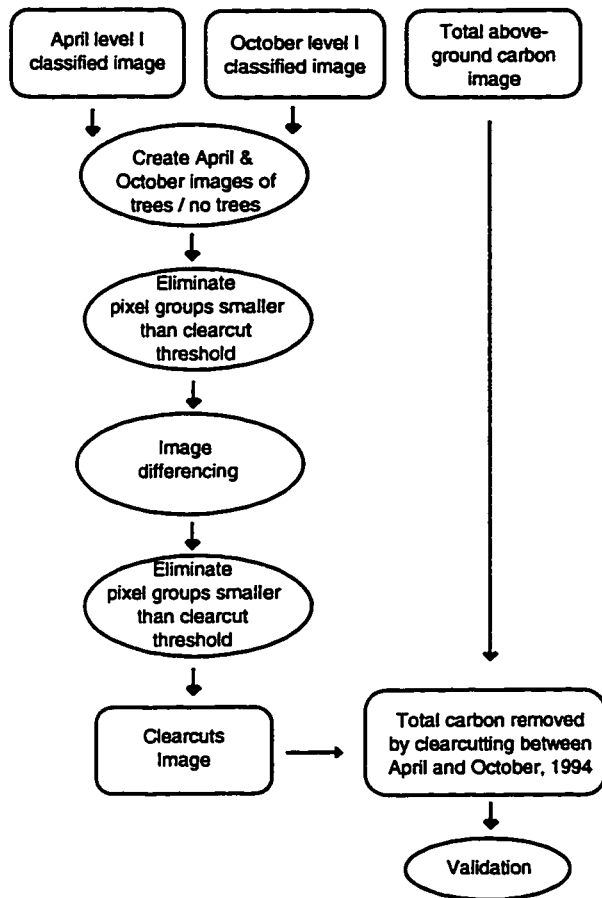
Figure 5.8: Model for SAR-derived estimation of C removed by forest clearcutting.

Figure 5.9: (a) Forest harvesting during the period April 10, to October 1, 1994 MFTS. SIR-C/X-SAR data-takes 22.2 SRL-1 and SRL-2. Clearcuts (red) and forest vegetation (green) with background SAR image visible in non-forested areas (short vegetation and old clearcuts). (b) New MFTS clearcuts overlain on the October 1 SIR-C L-hv image.

5.4 Discussion on Ecosystem Carbon Estimation

The SAR-based methodology was implemented to include above-ground C storage, below-ground C storage, ANPP, and removal due to land-cover change. These parameters were chosen because they are key terrestrial vegetative C components typically of interest to be measured or modeled. They do not, however, represent total ecosystem C, due to not accounting for soil C and fine and coarse root production. While this project could have been extended to develop inclusion of these additional components, such exhaustiveness was not the goal. This study was undertaken to demonstrate that a SAR-based methodology could be implemented to quantify key vegetative C components in a region with more efficiency than ground measurements and to a greater degree of specificity than other empirical or process-based models which have been based on general potential vegetation databases or coarse resolution data such as AVHRR which does not account for forest age. A discussion of the additional C components is useful, however, including some suggestions as to how they might be included.

5.4.1 Fine and Coarse Root Production

Annual production of below-ground C (BNPP) is quite difficult to measure using field techniques, and compared to ANPP, community specific BNPP equations are not as widely available. Below-ground production has often been estimated using the ratio relationship proposed by Whittaker and Marks (1975) which assumes that above-ground and below-ground relative production rates are equal:

$$\frac{\text{above-ground biomass}}{\text{above-ground production}} = \frac{\text{below-ground biomass}}{\text{below-ground production}} \tag{5.7}$$

Other lake states researchers have relied on using this simple model in their published predictions of total vegetation production. From this, Nadelhoffer et al. (1985) assumed BNPP to be 13% of ANPP in their study on fine roots, NPP and nitrogen availability in Wisconsin. Another lake states study assumed net root production to be 11% of total stand production, with a statement from the authors that this was probably somewhat conservative (Pastor and Bockheim, 1981). Recently, in addition to applying a ratio relationship, some studies have measured both coarse and fine root NPP, and published figures of rates are available such as those for red pine at 0.09 kg /m^2/yr by Haynes and Gower (1995).

Considering both perennial and fine roots, the latter pose the greatest difficulty in quantification. Fine roots are generally defined as the ephemeral, non-woody, small diameter roots (< 3 mm) and mycorrhizae portion of the root system which absorb growth limiting moisture and nutrients (Pregitzer et al., 1995). Fine roots are believed to be a small percentage of standing biomass/C at any given time, about 5% in a study of closed canopy forests in the lake states (Grigal and Ohman, 1992). Keyes and Grier (1981) also found fine

roots to be approximately 5% of the total root mass, so ignoring them has minor effects on the overall estimate of C stored. In contrast, because they turn over relatively rapidly, it is suggested that fine root turnover may account for some of the C gap between estimates of rates of photosynthesis and those of net assimilation by destructive sampling (Pregitzer et al., 1995). Nadelhoffer and Raich (1992) collected the results of 43 studies worldwide which measured fine root production (FRP). Their compilation shows that fine root production may account for approximately 20 to 30% of total ANPP in most deciduous and coniferous NHCF communities. Researchers agree, however, that figures are still generally inconclusive regarding the magnitude of fine root production and often depend on which of several measurement methods were used. Nevertheless, this is an area of active research as fine roots are an important consideration in the C balance, and in the potential effects of rising CO_2 on productivity. In a study on the latter topic, it was found that as CO_2 rose, so did the rate of fine root production and mortality (Pregitzer et al., 1995), although rates of mortality also increased as soil nitrogen availability increased, regardless of CO_2 concentration, and N influenced the relative allocation of C to leaves vs. fine roots. With the continuation of such efforts it should become more feasible to include fine root production in C models of all types, including that discussed in this study.

5.4.2 Soil and Forest Floor/Detritus

Field experiments in other lake states test sites have found soil C to be quite stable, and estimates show an average of about 55% of total ecosystem C in the region is stored in soil organic matter (Grigal and Ohman, 1992). The average for the U.S. is estimated to be 59%. Other researchers have found soil C to be stable through both age series and timber harvesting (Alban and Perala, 1992). It has been found to vary somewhat by forest community based on the different soil substrates. C in the mineral soil has been found to be lowest in jack pine ecosystems (3.2 kg/m^2) and highest in sugar maple (5.1 kg/m^2) and balsam fir (5.2 kg/m^2). C in the forest floor (leaves and woody debris) was less variable by community and averaged approximately 1.5 kg/m^2 (Grigal and Ohman, 1992). Forest trees are subject to mortality in addition to growth, and it would be possible to incorporate a simple stand dynamics model to account for death of trees on an annual basis. This was not done here due to the negligiable change - annual tree mortality averages approximately 3% of above-ground C stored. Balanced against the effort to incorporate the adjustment and the fact that this percentage is much smaller than the expected 10-15% error inherent in the overall process, it was decided to ignore this for purposes of this demonstration study. In sum, the aforementioned relationships and models could be added in implementations of the SAR-based methodology proposed in this study to further characterize C stored in a region in addition to the present system of interest of that stored in living vegetation.

5.5 Carbon Estimates and Process-based Models

In addition to using empirical models such as done in this study, there is also great interest in building and parameterizing complex process-based models which can be used to predict changes in C storage and flux due to outside forcings such as changing CO_2 concentrations and climatic variables. In their 1993 "Global Climate Change and Terrestrial Net Primary Production," Melillo et al. used a process-based model (Terrestrial Ecosystems Model, TEM) to estimate global net primary production under current CO_2 concentrations and under doubled CO_2. An excellent methodology is presented but is acknowledged to be constrained, as per discussed earlier in this paper, by the fact that consistent input datasets for land cover are not available. It was necessary for the authors to use different databases for the several continents, vegetation was potential, mature-state vegetation only, agricultural and urban incursions were generally poorly accounted for, and some types (wetlands) are missing altogether due to scarce source data. A regional to global dataset which would correct for the lacking information is needed; and the ideal would be a dataset which not only mapped the correct land cover classes, but one which provided the amount of living vegetation.

The biomass, C, and NPP results from the SAR-based empirical methodology can be used as stand-alone datasets, as inputs to process-based models, and to evaluate and calibrate global process-based models such as the that (TEM) invoked by Melillo et al. (1993) It is interesting to consider the latter. If general categories presented by Melillo et al. are associated with the roughly corresponding classes in the MFTS, a comparison can be made between ANPP predicted by the SAR methodology, intensive field measurements, and minimum, mean, and max ANPP predicted by the TEM in Melillo et al. Some adjustment must be made in the MFTS ANPP results to be equivalent to the NPP results of the field measurements and to Melillo et al. which included below-ground NPP. This was roughly estimated using the 13% figure employed by other lake states researchers (Nadelhoffer et al., 1985). The comparisons are given in Table 5.8.

There is relatively good agreement between the SAR, field, and TEM *maximum* predictions for upland conifer and upland hardwoods, with the SAR and field results consistently somewhat higher than the maximum for the TEM. While the species composition is the same, production rates for Melillo's lowland conifer equivalent – Boreal Forest – are lower. In part, this is probably due to the fact that the MFTS is on the extreme southern end of the Boreal forest, and thus Boreal communities are at their highest productivity in this region. If the rough community equivalencies are reasonable, overall, the SAR-based methodology results, along with the field-based results, potentially show a larger amount of C sequestered in the region of the Boreal–North Temperate ecotone than those of the process-based TEM. Such results, on a regional basis, can be used to evaluate process-based models and to suggest modifications of parameterization.

126

NPP (kg/m²/yr)						
	SAR	Field	TEM			
Reference	This study	Nadelhoffer et al., 1985	Melillo et al., 1993			
SAR class			Min	Mean	Max	TEM class
Upland Conifer	0.84	0.85 (red pine)	0.21	0.47	0.70	Temperate Coniferous
Lowland Conifer	1.19	0.91 (spruce)	0.12	0.23	0.43	Boreal Forest
Upland Hard woods	1.48	1.33 (maple)	0.081	0.62	0.98	Temperate Mixed

Table 5.8: Comparison of NPP estimates.

CHAPTER 6

CONCLUSIONS AND DIRECTIONS
FOR FUTURE WORK

This study has sought to demonstrate that a primarily SAR-based methodology can contribute significantly to the study and solution of fundamental questions in landscape to global scale vegetation ecology. These include the distribution of vegetation types (land-cover classification), the amount of vegetation (biomass estimation), and its contribution to the C cycle (estimation of C storage and change). In turn, each of these may be examined at several different scales (i.e., local, regional, and global) and for different reasons (i.e., management, monitoring, and modelling). The following offers some conclusions on the implications of the SAR-based methodologies discussed in this dissertation in these various scale and impetus configurations.

6.1 SAR-Derived Land-Cover Classification

Land-cover classification is an important issue at local to regional levels, and improvement in accuracy and efficiency is an ongoing objective. Wolter et al. (1995) state, "Forest cover type mapping in the northern lake states using spaceborne sensors has been a forest management goal since the launch of Landsat-1 July 1972. Forest classification of large regions with Anderson Level III (species level) are especially needed to assist with landscape scale analyses and management objectives." Good land-cover classifications provide the information for management issues such as habitat identification and analysis, forest inventory, inputs to comprehensive ecological classifications, wetland deliniation and management, forest harvesting, natural disturbance such as windthrow and fire, human settlement impacts, and much more.

The classification results from this study show that multi-frequency, multi-polarimetric SAR can be useful in local to regional forest type classification to at least Level II. Additional work at the Microwave Image Processing Laboratory, using the same data used for this study, has shown that forest may be classified to Level III. Preliminary results show good discrimination between red pine and jack pine conifer plantations, and between northern

128

white-cedar and black spruce lowland conifer communities. In fact, classification to Level III may result in higher classification accuracies as groupings into human-derived Level-II categories may be contrary to the structural based discrimination capabilities of the sensor, and thus introduce confusion into the multivariate statistical analysis.

In addition this study has shown that SAR is well-suited to studying forest disturbance. Because of it direct sensitivity to the presence and absence of large structure, mapping of forest clearcutting is a natural application of SAR. By extension, natural disturbance such as fire or severe windthrow can also be successfully mapped.

At global scales there exists the need for consistent, updatable land-cover databases. As would be expected this is an ultimate goal of researchers working with a number of different spaceborne sensor systems; SAR is only one of these. The SIR-C/X-SAR space shuttle missions, which were limited in time and space, were in part a demonstration project to show that multi-band, fully polarimetric, SAR imagery could contribute significantly to this goal. The advantages of SAR, in general, are its independence of solar illumination, ability to map through cloud cover, and potential for absolute calibration on which classification algorithms which work across many scenes and regions may be based. Other researchers are exploring such algorithms with single-frequency single-polarization sensors such as ERS-1/2 and JERS-1 (Kellndorfer, et al., 1996).

Remote sensing systems also offer the possibility of efficient repeatability, and of capturing terrain states at different times of the year. In this study, results of a comparison of classification methodologies show that multi-temporal classifications can be successfully developed to derive more information from SAR imagery than may be possible at a single date, depending, however, on what information is included in the classifier. A multi-temporal classification resulted in highly improved results for imagery from early spring. Multi-temporal classification also resulted in a somewhat improved classification for the fall fully-foliated scene and in high unbiased overall classification accuracy (97%). Therefore, we conclude that at least for spring scenes, the addition of more features from imagery at full-foliation results in an improved classification accuracy. Multi-temporal also consistently out-performed the pooled methodology. Table 6.1 summarizes the unbiased overall accuracies of the single-date optimized, pooled, and multi-temporal classifications discussed in Chapter 3.

Image	Single-date	Pooled	Multi-temporal
April 9	90%	90%	97%
April 15	90%	-	-
Sept. 30	95%	77%	97%
Oct. 6	98%	-	97%

Table 6.1: Comparison of unbiased overall accuracies.

6.2 SAR-Derived Biomass Estimation

At local to regional scales, quantification of vegetation biomass is an increasingly important parameter in management and monitoring activities. For example, quantification of above-ground biomass as an alternative to volume estimates is becoming more widespread in the forest management community due to whole tree harvesting. With the identification of clearcuts, SAR may be used to quantify the amount of vegetation removed over a region and this may be of interest to both forestry and environmental groups. Additionally, forest biomass may play a key role in some habitat identification and analysis where certain populations may be correlated with paticular biomass levels.

On a regional to global scale, an expanded SAR-derived dataset of land-cover classes and biomass would form a greatly enhanced input dataset for process-based models due to its incorporation of the actual *quantity and functional state* of each vegetation type, as opposed to simply type of terrestrial vegetation.

6.3 SAR-Derived Carbon Estimation

This study described a primarily SAR-based methodology to estimate key components of vegetative C storage and change: above-ground C in forest vegetation, forest below-ground C in perennial roots, annual forest ANPP, and managed C removal due to clearcutting. Results of the empirical SAR-based C estimations showed a very close agreement to those produced by intensive field measurements - both those published in the literature by other researchers and data produced specifically for the MFTS. This leads to the conclusion that given SAR imagery equivalent to the resolution of SIR-C/X-SAR and good classification and biomass algorithms, that it is entirely feasible to map C with a high degree of efficiency and accuracy using this empirical methodology. For local to regional scales, the efficiency of the remote sensing-based method is much greater than that of traditional field techniques. For regional to global scales C estimations based on actual land cover and biomass stand to greatly enhance methodologies which cannot account for one or both.

On the basis of the preceding results, it is believed that this technique to estimate C could be extended to a number of other bioregions worldwide via one of two currently possible implementational scenarios. The first uses the existing database of SIR-C/X-SAR data; the second uses composite datasets of ERS-1/2, Radarsat, and JERS-1. Each scenario currently imposes certain limitations. The two SIR-C/X-SAR missions conducted in 1994 provide polarimetric SAR data at L- and C-bands which are crucial for high accuracy land-cover classification and above-ground biomass estimation because of the structural information embedded in the SAR signal. However, SIR-C/X-SAR was never intended as a global mapping mission, and hence the available coverage is a series of non-contiguous 20 to 40 km wide swaths that subsample terrestrial ecoregions. As a consequence, the classification, biomass and C dynamics algroithms could be adapted to test sites in other

130

regions, but at best could only provide local subsampling. Extension of subsequent results to regional and continental scales could be enlightening, but would be dependent upon the assumptions inherent in the subsampling scheme.

The second scenario would adapt the given techniques to the global coverage provided by a suite of orbital SARs (ERS-1/2, Radarsat and JERS-1), none of which are likely to be coincident at any given location. Thus the structural information that is the basis for SAR-derived classification and biomass estimation is composited over time. While studies to date have shown that this may be adequate for simplified land-cover classification (Dobson et al., 1996; Kellndorfer et al., 1996), most of the C dynamics is also dependent upon SAR-derived estimation of above-ground biomass. It is not realistic to expect that this can be done to a high level of specificity using a multi-temporal, multi-sensor "virtual" SAR approach because temporal changes in the scene dielectrics (a moisture related quantity) become confused with structural attributes that are presumed to be static over the compositing period. Even ignoring the confounding factor of temporal dynamics, the use of non-polarimetric like-polarized SAR data at L- and C-bands will generally limit biomass retrivals to regenerating forests with above-ground dry biomass less than about 10 kg/m^2 due to signal "saturation." However, it is important to note that even the limited capability to quantize biomass into several levels would be a major improvement over current techniques using potential vegetation and assuming mature growth stage.

APPENDICES

APPENDIX A

Stand Summary Statistics

UPPER STRATUM DRY BIOMASS (kg/ha)

Stand	Year Measured	Dominant Species	Structural Type	Level 1 Category	Level 2 Category	Level 3 Category	Summer Total	Winter Total	Trunk	Crown summer	Crown winter	Branch	Foliage
22	1991	red pine	excurrent	tall	upcon	pinres	45620	45620	27740	17880	17880	13789	4091
23	1991	red pine	excurrent	tall	upcon	pinres	176946	176701	136779	40167	39923	23628	16539
24	1991	jack pine	excurrent	tall	upcon	pinban	70656	70523	51453	19203	19070	13654	5549
25	1991	red pine	excurrent	tall	upcon	pinres	147095	146938	110070	37024	36868	21913	15111
26	1991	black spruce	excurrent	tall	lowcon	picmar	62899	62826	51218	11681	11608	8953	2728
27	1991	jack pine	excurrent	tall	upcon	pinban	89531	89459	70200	19331	19259	13773	5558
28	1991	beech	decurrent	tall	decid	nharwd	250591	247911	199144	51447	48767	47884	3562
29	1991	red maple	decurrent	tall	decid	nharwd	214760	212221	170777	43984	41444	40973	3011
31	1991	red maple	decurrent	tall	decid	nharwd	140535	138278	112264	28271	26014	26014	2257
32	1991	N. white-cedar	excurrent	tall	lowcon	thuocc	162453	162356	103187	59266	59169	40609	18657
33	1991	trembling aspen	decurrent	tall	decid	popspp	36115	34580	31105	5011	3476	3476	1535
34	1991	red maple	decurrent	tall	decid	nharwd	145947	143612	120441	25506	23171	23108	2398
35	1991	jack pine	excurrent	tall	upcon	pinban	31837	31830	20855	10982	10975	8157	2824
36	1991	jack pine	excurrent	tall	upcon	pinban	6463	6463	3476	2987	2987	2545	442
37	1992	jack pine	excurrent	short	supcon	supcon	20	20	13	6	6	5	1
38	1992	jack pine	excurrent	short	supcon	supcon							
39	1992	jack pine	excurrent	short	supcon	supcon	548	548	301	247	247	206	41
40	1992	red pine	excurrent	short	supcon	supcon							
41	1992	red pine	excurrent	tall	upcon	pinres	2611	2608	1595	1016	1013	806	210
42	1992	jack pine	excurrent	tall	upcon	pinban	496	495	325	172	170	144	28
43	1992	red pine	excurrent	tall	upcon	pinres	147510	147442	104500	43009	42941	25390	17620
44	1992	black spruce	excurrent	tall	lowcon	picmar	116204	115611	94354	21850	21257	17928	3922
45	1992	trembling aspen	decurrent	tall	decid	popspp	1837	1793	1227	609	566	473	136
47	1992	trembling aspen	decurrent	tall	decid	popspp	88767	87054	74805	13962	12249	11414	2548
48	1992	red maple	decurrent	tall	decid	nharwd	135142	133194	106843	28299	26352	24324	3976
49	1992	trembling aspen	decurrent	tall	decid	popspp	640	619	575	65	44	44	22
50	1992	red pine	excurrent	tall	upcon	pinres	101176	100656	73130	28046	27526	19750	8296
51	1992	red pine	excurrent	tall	upcon	pinres	35372	35331	20737	14635	14594	11545	3090
46	1993	beech	decurrent	tall	decid	nharwd	272884	270224	214752	58132	55472	53767	4365
52	1993	red pine	excurrent	tall	upcon	pinres	77488	77488	53484	24004	24004	16329	7674
53	1993	bigtooth aspen	decurrent	tall	decid	popspp	128941	126913	105487	23455	21426	20319	3136
54	1993	jack pine	excurrent	tall	upcon	pinban	273	273	156	116	116	99	17
55	1993	jack pine	excurrent	tall	upcon	pinban	129	129	75	54	54	46	8
56	1993	jack pine	excurrent	tall	upcon	pinban	15475	15475	10046	5430	5430	4101	1329
57	1993	bigtooth aspen	decurrent	tall	decid	popspp	141428	139222	112444	28985	26778	24386	4599
58	1993	jack pine	excurrent	tall	upcon	pinban							
59	1993	jack pine	excurrent	tall	upcon	pinban	4114	4114	2277	1837	1837	1564	273

UPPER STRATUM DRY BIOMASS (kg/ha)

Stand	Year Measured	Dominant Species	Structural Type	Level 1 Category	Level 2 Category	Level 3 Category	Summer Total	Winter Total	Trunk	Crown summer	Crown winter	Branch	Foliage
60	1993	jack pine	excurrent	tall	upcon	pinban	11252	11252	6269	4983	4983	4103	880
61	1993	jack pine	excurrent	tall	upcon	pinban	62244	62244	46325	15919	15919	11386	4533
62	1993	jack pine	excurrent	tall	upcon	pinban	40376	40376	28717	11658	11658	8928	2730
63	1993	jack pine	excurrent	tall	upcon	pinban	26459	26459	17307	9153	9153	6883	2269
64	1993	jack pine	excurrent	tall	upcon	pinban	35277	35277	23771	11506	11506	8375	3131
65	1993	jack pine	excurrent	tall	upcon	pinban	51755	51755	37854	13901	13901	10126	3775
66	1993	jack pine	excurrent	short	supcon	supcon							
67	1993	jack pine	excurrent	tall	upcon	pinban	83200	83200	64068	19132	19132	13433	5699
68	1993	red pine	excurrent	tall	upcon	pinres	103069	103069	72934	30135	30135	19479	10655
69	1993	pin cherry	decurrent	tall	decid	popspp	4486	4316	3895	591	421	421	170
70	1993	trembling aspen	decurrent	tall	decid	popspp	1681	1620	1491	190	129	129	60
71	1993	red pine	excurrent	tall	upcon	pinres	37254	37254	21723	15531	15531	10873	4659
72	1993	red pine	excurrent	tall	upcon	pinres	32005	32003	19219	12786	12784	8853	3933
73	1993	red pine	excurrent	tall	upcon	pinres	68073	68072	42439	25634	25634	17641	7994
74	1993	white pine	excurrent	tall	upcon	pinstr	159489	158483	133285	26204	25197	21095	5109
75	1993	white pine	excurrent	tall	upcon	pinstr	161338	161109	138189	23149	22920	16713	6436
76	1993	sugar maple	decurrent	tall	decid	nharwd	220567	217972	146237	74330	71736	71736	2595
77	1993	red pine	excurrent	tall	upcon	pinres	23918	23869	13906	10011	9962	7995	2016
78	1993	red pine	excurrent	short	supcon	supcon	4202	4195	2526	1677	1670	1131	546
79	1993	red pine	excurrent	short	supcon	supcon	564	564	418	145	145	85	60
80	1993	red pine	excurrent	short	supcon	supcon	2114	2110	1407	707	703	443	264
81	1993	jack pine	excurrent	tall	upcon	pinban	25681	25667	15687	9994	9981	8025	1968
82	1993	red pine	excurrent	tall	upcon	pinres	11461	11461	6492	4969	4969	4130	839
83	1993	red pine	excurrent	tall	upcon	pinres	2741	2737	1937	804	801	654	150
85	1993	sugar maple	decurrent	tall	decid	nharwd	184028	180765	144530	39498	36234	36130	3368
86	1993	red maple	decurrent	tall	decid	nharwd	183362	180668	148951	34411	31717	31717	2693
87	1993	trembling aspen	decurrent	tall	decid	popspp	54532	53288	46650	7882	6638	6638	1244
88	1993	n. white cedar	excurrent	tall	lowcon	thuocc	173288	173288	112779	60509	60509	40918	19592
91	1993	sugar maple	decurrent	tall	decid	nharwd	122080	120297	95906	26174	24391	24387	1787

135

UPPER STRATUM DRY BIOMASS (kg/ha)

Stand	Year Measured	Dominant Species	Structural Type	Level 1 Category	Level 2 Category	Level 3 Category	Summer Total	Winter Total	Trunk	Crown summer	Crown winter	Branch	Foliage
22	1994	red pine	excurrent	tall	upcon	pinres	53122	53122	33203	19919	19919	15029	4890
33	1994	trembling aspen	decurrent	tall	decid	popspp	59155	57149	50448	8707	6700	6700	2006
36	1994	jack pine	excurrent	tall	upcon	pinban	12086	12086	6921	5165	5165	4291	874
37	1994	jack pine	excurrent	short	supcon	supcon	161	161	96	64	64	54	10
38	1994	jack pine	excurrent	short	supcon	supcon							
39	1994	red pine	excurrent	short	supcon	supcon							
40	1994	red pine	excurrent	short	supcon	supcon							
41	1994	red pine	excurrent	tall	upcon	pinres	9888	9873	6117	3771	3756	3077	694
42	1994	jack pine	excurrent	tall	upcon	pinban	8104	8079	5469	2636	2610	2167	468
45	1994	trembling aspen	decurrent	tall	decid	popspp	6276	6202	4485	1791	1717	1533	258
49	1994	trembling aspen	decurrent	tall	decid	popspp	7167	6888	6344	822	544	544	279
51	1994	red pine	excurrent	tall	upcon	pinres	48002	47995	36072	11930	11923	8011	3919
54	1994	jack pine	excurrent	tall	upcon	pinban	1774	1774	1085	689	689	582	107
55	1994	jack pine	excurrent	tall	upcon	pinban	863	863	552	311	311	260	51
58	1994	jack pine	excurrent	tall	upcon	pinban							
59	1994	jack pine	excurrent	tall	upcon	pinban	6316	6316	3846	2470	2470	2052	418
66	1994	jack pine	excurrent	short	supcon	supcon							
77	1994	red pine	excurrent	tall	upcon	pinres	24153	24051	15374	8779	8677	6890	1889
78	1994	red pine	excurrent	tall	upcon	pinres	6351	6339	3989	2363	2351	1426	937
79	1994	red pine	excurrent	short	supcon	supcon	1401	1401	981	420	420	248	172
80	1994	red pine	excurrent	short	supcon	supcon	4012	4004	2665	1347	1339	847	500
81	1994	jack pine	excurrent	tall	upcon	pinban	27551	27529	19698	7854	7831	5892	1961
82	1994	red pine	excurrent	tall	upcon	pinres	14857	14857	9499	5358	5358	4300	1058
83	1994	red pine	excurrent	tall	upcon	pinres	8571	8568	5697	2874	2871	2371	503

Middle Stratum Totals (Conifer and Broadleaf Combined)

Stand	Year Measured	Summer Total	Winter Total	Trunk	Crown summer	Crown winter	Branch	Foliage
22	1991	548	448	448				101
23	1991	627	485	485				142
24	1991	493	388	388				105
25	1991	1456	1133	1133				324
26	1991	5033	3682	3682				1351
27	1991	329	266	266				63
28	1991	2081	1734	1734				348
29	1991	2796	2259	2259				537
31	1991	351	287	287				65
32	1991	1612	1287	1287				325
33	1991	5417	4321	4321				1096
34	1991	2232	1892	1892				340
35	1991	768	614	614				155
36	1991	3608	2918	2918				689
37	1992	946	702	702				243
38	1992	8473	6771	6771				1703
39	1992	160	133	133				27
40	1992	2868	2223	2223				645
41	1992	13527	11032	11032				2495
42	1992	19134	15724	15724				3410
43	1992	277	201	201				76
44	1992	2378	1779	1779				599
45	1992	3825	3063	3063				761
47	1992							
48	1992	2334	1817	1817				517
49	1992	10741	8635	8635				2106
50	1992	860	688	688				173
51	1992	1725	1380	1380				344

Stand	Year Measured	Middle Stratum Totals (Conifer and Broadleaf Combined)						
		Summer Total	Winter Total	Trunk	Crown summer	Crown winter	Branch	Foliage
46	1993	1991	1646	1646				345
52	1993	190	153	153				37
53	1993	1708	1372	1372				336
54	1993	11439	9323	9323				2115
55	1993	14027	11299	11299				2728
56	1993	115	89	89				26
57	1993	3248	2624	2624				625
58	1993	8297	6705	6705				1591
59	1993	5723	4666	4666				1058
60	1993	4107	3404	3404				703
61	1993	175	141	141				34
62	1993	1079	867	867				212
63	1993	1708	1466	1466				241
64	1993	354	284	284				70
65	1993	25	20	20				6
66	1993	447	322	322				125
67	1993	55	43	43				12
68	1993	369	305	305				64
69	1993	10742	8569	8569				2173
70	1993	8499	7136	7136				1363
71	1993	108	89	89				19
72	1993	225	185	185				41
73	1993	300	237	237				63
74	1993	420	331	331				89
75	1993	69	53	53				16

Middle Stratum Totals (Conifer and Broadleaf Combined)

Stand	Year Mea-sured	Summer Total	Winter Total	Trunk	Crown sum-mer	Crown winter	Branch	Foliage
76	1993	368	284	284				83
77	1993	4021	3309	3309				712
78	1993	105	83	83				22
79	1993	5	4	4				1
80	1993							
81	1993	3281	2730	2730				551
82	1993	6340	5249	5249				1091
83	1993	18202	14987	14987				3215
85	1993	1061	839	839				222
86	1993	727	587	587				140
87	1993	3629	3079	3079				549
88	1993	1240	984	984				256
91	1993	1560	1275	1275				285

Middle Stratum Totals (Conifer and Broadleaf Combined)

Stand	Year Measured	Summer Total	Winter Total	Trunk	Crown summer	Crown winter	Branch	Foliage
22	1994	110	87	87				23
33	1994	4480	3654	3654				826
36	1994	1060	876	876				184
37	1994	4044	3052	3052				993
38	1994	13017	10554	10554				2463
39	1994	56	41	41				15
40	1994	7090	5656	5656				1434
41	1994	8128	6664	6664				1464
42	1994	7125	5911	5911				1214
45	1994	7475	6073	6073				1403
49	1994	11485	9379	9379				2107
51	1994	1456	1173	1173				282
54	1994	8947	7290	7290				1657
55	1994	13198	10728	10728				2469
58	1994	13828	11175	11175				2652
59	1994	3254	2661	2661				593
66	1994	1702	1232	1232				470
77	1994	3311	2745	2745				566
78	1994	217	175	175				42
79	1994	7	5	5				2
80	1994							
81	1994	4515	3779	3779				736
82	1994	5435	4492	4492				943
83	1994	10207	8385	8385				1822

DRY BIOMASS (kg/ha)

Stand	Year Measured	Stand Totals — Summer Total	Winter Total	Trunk (Upper Stratum only)	Crown summer	Crown winter	Branch	Foliage	Stand BA-weighted Avg. Height	Upper Stratum (H≥5m) — Height (calculated) Mean (m)	Height S.D. (m)	Diameter at DBH Mean (cm)	Diameter at DBH S.D. (cm)
22	1991	46168	45620	28188	17880	17880	13789	4192	8.51	7.91	1.63	13.57	3.06
23	1991	177573	176701	137264	40167	39923	23628	16681	23.14	14.56	8.10	17.95	13.79
24	1991	71149	70523	51841	19203	19070	13654	5654	13.02	11.26	3.09	15.28	6.23
25	1991	148551	146938	111203	37024	36868	21913	15435	22.18	12.31	8.04	16.02	14.50
26	1991	67932	62826	54900	11681	11608	8953	4079	11.54	10.25	3.61	12.08	5.51
27	1991	89860	89459	70466	19331	19259	13773	5621	13.18	11.87	3.03	14.26	4.56
28	1991	252672	247911	200878	51447	48767	47884	3910	21.27	16.20	7.68	21.78	14.73
29	1991	217556	212221	173035	43984	41444	40973	3548	19.23	13.99	6.83	17.37	12.30
31	1991	140886	138278	112551	28271	26014	26014	2321	16.37	12.00	4.85	11.83	6.83
32	1991	164065	162356	104473	59266	59169	40609	18982	13.59	11.41	3.68	17.46	8.08
33	1991	41532	34580	35426	5011	3476	3476	2631	5.74	5.57	1.70	4.31	1.58
34	1991	148178	143612	122332	25506	23171	23108	2738	17.14	10.76	5.85	10.76	8.17
35	1991	32605	31830	21469	10982	10975	8157	2979	9.64	7.82	2.54	13.47	6.37
36	1991	10071	6463	6394	2987	2987	2545	1132	4.70	4.55	1.01	8.18	2.27
37	1992	966	20	716	6	6	5	245	1.38	5.60		7.20	
38	1992	8473	6771	6771				1703	3.01				
39	1992	709	548	435	247	247	206	68	6.59	7.31	1.31	12.10	2.69
40	1992	2868	2223	2223				645	1.46				
41	1992	16138	2608	12626	1016	1013	806	2705	4.23	5.64	1.63	8.18	3.29
42	1992	19630	495	16049	172	170	144	3438	4.01	5.25	0.19	8.34	1.23
43	1992	147787	147442	104702	43009	42941	25390	17695	20.06	18.28	4.33	26.18	9.26
44	1992	118582	115611	96133	21850	21257	17928	4521	15.21	13.08	3.91	15.14	6.52
45	1992	5661	1793	4291	609	566	473	897	2.72	7.79	2.18	8.66	4.11
47	1992	88767	87054	74805	13962	12249	11414	2548	13.27	8.64	3.85	7.90	4.53
48	1992	137476	133194	108660	28299	26352	24324	4492	16.18	10.38	5.57	10.82	7.71
49	1992	11381	619	9210	65	44	44	2127	3.05	5.80	0.92	4.34	0.82
50	1992	102036	100656	73818	28046	27526	19750	8469	15.03	13.08	3.90	17.05	7.60
51	1992	37097	35331	22117	14635	14594	11545	3434	7.69	6.97	1.96	12.17	4.44

DRY BIOMASS (kg/ha)

Stand	Year Measured	Stand Totals							Stand BA-weighted Avg. Height	Upper Stratum (H≥5m)			
		Summer Total	Winter Total	Trunk (Upper Stratum only)	Crown summer	Crown winter	Branch	Foliage		Height (calculated)		Diameter at DBH	
										Mean (m)	S.D. (m)	Mean (cm)	S.D. (cm)
46	1993	274875	270224	216398	58132	55472	53767	4710	20.72	12.59	8.16	16.85	14.93
52	1993	77678	77488	53637	24004	24004	16329	7712	14.23	12.53	3.18	19.59	6.80
53	1993	130649	126913	106859	23455	21426	20319	3471	16.57	12.29	5.12	13.21	7.85
54	1993	11711	273	9479	116	116	99	2133	3.87	4.97	0.54	7.91	1.61
55	1993	14156	129	11375	54	54	46	2736	3.90	4.78	0.61	7.47	1.51
56	1993	15590	15475	10134	5430	5430	4101	1355	9.05	7.86	2.18	13.82	4.66
57	1993	144677	139222	115068	28985	26778	24386	5223	15.72	11.99	5.00	12.61	7.13
58	1993	8297	6705	6705				1591	3.44				
59	1993	9837	4114	6942	1837	1837	1564	1331	4.41	4.59	0.95	8.09	1.97
60	1993	15358	11252	9673	4983	4983	4103	1583	5.87	5.53	1.32	10.00	3.11
61	1993	62419	62244	46465	15919	15919	11386	4567	12.06	10.75	2.59	15.01	4.48
62	1993	41455	40376	29584	11658	11658	8928	2942	8.34	7.40	1.91	10.12	3.04
63	1993	28167	26459	18773	9153	9153	6883	2511	9.16	7.98	2.39	13.93	5.45
64	1993	35632	35277	24055	11506	11506	8375	3202	10.88	9.90	2.40	17.87	5.53
65	1993	51780	51755	37874	13901	13901	10126	3780	11.08	9.98	2.32	14.40	3.98
66	1993	447	322	322				125	1.20				
67	1993	83255	83200	64111	19132	19132	13433	5711	13.80	12.76	2.54	16.82	4.18
68	1993	103438	103069	73239	30135	30135	19479	10720	15.34	13.82	3.11	19.73	6.30
69	1993	15228	4316	12464	591	421	421	2343	3.52	4.94	1.26	4.19	1.15
70	1993	10180	1620	8628	190	129	129	1423	3.70	5.04	1.06	4.41	1.06
71	1993	37363	37254	21812	15531	15531	10873	4678	13.62	13.17	1.94	26.37	5.03
72	1993	32230	32003	19404	12786	12784	8853	3974	13.65	12.52	3.05	23.70	7.54
73	1993	68373	68072	42675	25634	25634	17641	8057	14.38	12.52	3.40	22.30	8.92
74	1993	159909	158483	133616	26204	25197	21095	5198	18.21	15.81	4.50	19.21	7.24
75	1993	161407	161109	138242	23149	22920	16713	6451	18.98	16.85	3.97	21.82	7.33

DRY BIOMASS (kg/ha)

Stand	Year Measured	Stand Totals							Stand BA-weighted Avg. Height	Upper Stratum (H≥5m)			
		Summer Total	Winter Total	Trunk (Upper Stratum only)	Crown summer	Crown winter	Branch	Foliage		Height (calculated)		Diameter at DBH	
										Mean (m)	S.D. (m)	Mean (cm)	S.D. (cm)
76	1993	220935	217972	146521	74330	71736	71736	2678	18.11	16.59	4.66	18.59	9.18
77	1993	27939	23869	17216	10011	9962	7995	2728	7.34	6.87	2.04	12.70	4.66
78	1993	4308	4195	2609	1677	1670	1131	568	13.95	10.81	5.21	17.27	12.47
79	1993	568	564	422	145	145	85	61	18.67	19.50		26.50	
80	1993	2114	2110	1407	707	703	443	264	18.56	12.71	6.28	18.52	13.89
81	1993	28961	25667	18416	9994	9981	8025	2519	7.13	6.63	1.81	11.38	3.21
82	1993	17801	11461	11741	4969	4969	4130	1930	5.53	5.76	1.15	10.58	2.07
83	1993	20943	2737	16924	804	801	654	3365	4.85	5.61	2.24	9.05	4.88
85	1993	185089	180765	145369	39498	36234	36130	3590	18.55	12.44	6.46	11.35	7.73
86	1993	184089	180668	149538	34411	31717	31717	2834	18.55	15.58	4.93	16.35	7.27
87	1993	58161	53288	49730	7882	6638	6638	1793	13.06	10.74	5.15	10.77	6.00
88	1993	174528	173288	113763	60509	60509	40918	19848	12.12	9.62	3.46	13.43	6.27
91	1993	123641	120297	97181	26174	24391	24387	2072	17.31	13.57	5.05	15.18	9.13

143

DRY BIOMASS (kg/ha)

Stand	Year Measured	Stand Totals							Stand BA-weighted Avg. Height	Upper Stratum (H,5m)			
		Summer Total	Winter Total	Trunk (Upper Stratum only)	Crown summer	Crown winter	Branch	Foliage		Height (calculated) Mean (m)	S.D. (m)	Diameter at DBH Mean (cm)	S.D. (cm)
22	1994	53232	53122	33290	19919	19919	15029	4914	9.32	8.74	1.62	14.59	3.08
33	1994	63635	57149	54103	8707	6700	6700	2832	9.03	7.27	2.89	5.02	2.24
36	1994	13146	12086	7796	5165	5165	4291	1059	5.63	5.03	1.39	8.81	2.82
37	1994	4044	3052	3052				993	1.99				
38	1994	13177	161	10650	64	64	54	2473	4.45	5.10	0.14	7.93	1.20
39	1994	56	41	41				15	1.49				
40	1994	7090	5656	5656				1434	2.56				
41	1994	18016	9873	12781	3771	3756	3077	2158	5.57	5.44	1.64	8.38	2.54
42	1994	15229	8079	11380	2636	2610	2167	1682	5.55	5.72	0.98	7.58	1.44
45	1994	13751	6202	10557	1791	1717	1533	1661	4.84	6.62	4.04	7.71	9.02
49	1994	18652	6888	15723	822	544	544	2385	4.59	5.39	1.15	4.10	1.09
51	1994	49458	47995	37246	11930	11923	8011	4201	12.17	11.58	2.60	13.68	4.01
54	1994	10721	1774	8375	689	689	582	1764	4.58	5.01	0.59	7.54	1.04
55	1994	14061	863	11281	311	311	260	2520	4.83	5.20	0.59	7.09	1.48
58	1994	13828	11175	11175				2652	3.62				
59	1994	9570	6316	6507	2470	2470	2052	1011	5.19	5.25	0.93	8.43	1.92
66	1994	1702	1232	1232				470	1.34				
77	1994	27464	24051	18119	8779	8677	6890	2455	9.23	8.04	2.97	13.00	5.90
78	1994	6568	6339	4164	2363	2351	1426	979	17.68	9.98	7.15	15.67	15.93
79	1994	1408	1401	986	420	420	248	174	19.47	20.00		31.50	
80	1994	4012	4004	2665	1347	1339	847	500	18.80	13.27	6.20	19.48	13.87
81	1994	32066	27529	23477	7854	7831	5892	2697	9.03	8.86	2.23	12.05	3.19
82	1994	20292	14857	13991	5358	5358	4300	2002	6.58	6.67	1.72	10.61	2.49
83	1994	18779	8568	14083	2874	2871	2371	2325	6.09	5.69	2.03	8.61	2.78

144

Stand	Year Measured	Middle Stratum (1m⩽H⩽5m)		Basal Diameter (15cm)		Crown Depth (in m) upper stratum		Density (live stems/ha)		
		Height (calculated) Mean (m)	S.D. (m)	Mean (cm)	S.D. (cm)	Mean (m)	S.D. (m)	Stand Total	Upper Stratum	Middle Stratum
22	1991	2.53	1.50	3.69	3.09	5.79	1.05	1313	1173	141
23	1991	1.87	0.96	1.32	0.87	8.11	3.31	4143	948	3195
24	1991	1.89	0.68	1.56	0.97	6.54	2.83	2496	903	1594
25	1991	2.13	1.06	1.94	1.19	9.27	4.12	3638	873	2766
26	1991	1.66	0.76	1.81	1.10	7.62	3.65	10509	1213	9297
27	1991	1.76	0.79	1.40	0.82	6.13	2.38	3147	1405	1742
28	1991	1.93	0.85	1.79	0.84	10.31	4.67	7478	705	6773
29	1991	1.83	0.84	1.91	1.01	10.31	4.57	7636	925	6711
31	1991	2.04	1.13	1.78	1.06	8.02	3.44	2895	1840	1055
32	1991	1.83	0.87	2.40	1.68	5.76	2.57	3547	2008	1539
33	1991	2.53	1.02	1.72	0.73	3.04	1.47	31017	9227	21790
34	1991	1.91	0.98	1.34	1.74	8.49	4.37	6218	1911	4307
35	1991	2.34	0.98	3.19	2.04	7.02	2.79	1000	625	375
36	1991	3.05	1.21	4.08	2.49	5.12	0.91	1542	565	977
37	1992	1.21	0.23	2.05	0.77	2.10		2010	3	2008
38	1992	2.80	0.61	5.31	1.46			1844		1844
39	1992	4.80		10.00		5.19	0.92	25	18	8
40	1992	1.37	0.28	3.69	1.06			1555		1555
41	1992	2.36	1.14	3.17	2.69	4.84	1.15	5015	183	4832
42	1992	2.66	1.31	4.42	3.08	4.51	0.71	3808	43	3766
43	1992	1.95	0.72	1.47	0.63	8.62	3.54	1750	561	1189
44	1992	1.83	0.79	1.88	0.93	7.23	3.91	6979	1245	5734
45	1992	1.63	0.54	1.53	0.65	4.71	1.73	21442	70	21372
47	1992					5.38	2.98	3693	3693	
48	1992	2.06	0.94	1.92	1.08	7.52	3.99	7041	1893	5148
49	1992	2.35	0.91	2.01	0.89	3.27	0.91	30744	205	30540
50	1992	1.51	0.50	1.27	0.71	7.59	3.17	6771	943	5828
51	1992	1.97	0.89	2.08	1.17	5.83	1.98	4523	1015	3508

Stand	Year Measured	Middle Stratum (1mjlfj5m) Height (calculated) Mean (m)	S.D. (m)	Basal Diameter (15cm) Mean (cm)	S.D. (cm)	Crown Depth (in m) upper stratum Mean (m)	S.D. (m)	Density (live stems/ha) Stand Total	Upper Stratum	Middle Stratum
46	1993	1.90	0.87	1.64	0.86	7.87	3.75	8267	1040	7227
52	1993	3.53	1.25	4.58	2.53	8.27	2.30	674	628	47
53	1993	1.96	1.18	1.60	1.35	7.32	3.14	5111	1393	3719
54	1993	3.20	1.04	6.06	2.39	4.70	0.46	1582	28	1555
55	1993	3.29	1.02	5.41	1.94	4.65	0.13	2671	15	2656
56	1993	2.03	1.05	2.86	1.65	7.92	2.02	423	338	86
57	1993	1.90	1.06	1.45	1.18	6.12	2.86	10356	1770	8586
58	1993	2.63	0.99	4.82	2.30			1789		1789
59	1993	2.72	1.33	4.64	2.78	4.96	0.46	1526	385	1141
60	1993	3.39	1.45	6.08	3.52	5.34	0.95	1002	573	430
61	1993	3.99	1.05	5.70	1.87	7.09	2.23	1006	975	31
62	1993	3.64	1.18	4.87	2.21	5.92	1.86	2055	1813	242
63	1993	2.54	1.47	4.13	2.46	6.95	2.29	882	530	352
64	1993	2.70	1.27	4.24	2.27	8.29	2.49	512	410	102
65	1993	1.95	1.69	2.27	2.20	6.89	2.17	976	953	23
66	1993	1.08	0.24	1.66	0.54			1788		1788
67	1993	1.87	0.38	2.54	1.55	6.84	1.95	1007	953	55
68	1993	3.05	1.26	7.20	3.55	7.89	1.73	876	845	31
69	1993	2.11	0.93	1.68	0.91	2.52	0.68	40850	1433	39417
70	1993	2.33	1.12	1.98	1.11	3.24	0.40	21450	513	20938
71	1993	2.20	1.41	4.50	5.80	9.51	1.23	193	178	16
72	1993	2.42	1.43	2.76	2.44	9.41	1.63	305	180	125
73	1993	2.17	1.08	2.19	1.76	9.26	2.50	687	390	297
74	1993	1.81	0.73	1.33	0.68	7.50	2.47	3680	1125	2555
75	1993	1.52	0.53	0.90	0.45	5.74	2.15	2226	1022	1204

| Stand | Year Measured | Middle Stratum (1m¡H¡5m) | | | | Crown Depth (in m) upper stratum | | Density (live stems/ha) | | |
| | | Height (calculated) | | Basal Diameter (15cm) | | | | | | |
		Mean (m)	S.D. (m)	Mean (cm)	S.D. (cm)	Mean (m)	S.D. (m)	Stand Total	Upper Stratum	Middle Stratum
76	1993	1.58	0.62	1.21	0.52	8.58	4.04	4181	970	3211
77	1993	2.17	1.03	2.74	2.04	5.57	1.40	2956	613	2344
78	1993	1.20	0.28	1.12	0.34	8.36	3.57	1436	29	1406
79	1993	1.09	0.17	1.11	0.32	10.00		65	3	63
80	1993					10.83	3.33	13	13	
81	1993	2.58	1.32	3.63	3.08	6.25	1.45	1773	938	836
82	1993	3.40	1.50	7.11	3.39	5.16	1.09	1086	563	523
83	1993	2.72	1.34	4.10	3.25	5.00	1.41	3848	138	3711
85	1993	2.28	1.83	1.89	1.52	7.01	2.83	3924	2205	1719
86	1993	1.56	0.67	1.30	0.66	9.26	3.47	6140	1283	4857
87	1993	2.19	1.24	1.76	1.25	5.69	2.48	11267	1100	10167
88	1993	1.93	1.32	2.54	1.85	5.68	2.13	4703	3813	891
91	1993	1.72	0.90	1.32	0.97	8.60	2.78	7193	880	6313

147

Stand	Year Measured	Middle Stratum (1m¡H¡5m)				Crown Depth (in m) upper stratum		Density (live stems/ha)		
		Height (calculated) Mean (m)	S.D. (m)	Basal Diameter (15cm) Mean (cm)	S.D. (cm)	Mean (m)	S.D. (m)	Stand Total	Upper Stratum	Middle Stratum
22	1994	2.23	0.96	2.80	2.34	6.58	1.14	1207	1142	65
33	1994	2.30	1.48	1.65	0.93	3.27	1.32	24555	8430	16125
36	1994	2.40	1.08	3.26	1.98	5.52	0.92	1376	842	534
37	1994	1.34	0.53	2.08	1.01			7096		7096
38	1994	3.98	1.03	6.22	1.84	4.77	0.25	1866	17	1849
39	1994	1.36	0.26	2.26	0.77			104		104
40	1994	2.19	0.82	5.04	1.54			1706		1706
41	1994	2.51	1.43	2.78	2.56	5.25	2.52	4310	729	3581
42	1994	2.48	1.66	2.80	2.61	4.31	0.50	3802	833	2969
45	1994	2.11	0.94	1.66	0.91	7.43	5.60	30037	115	29922
49	1994	2.87	1.31	1.96	1.00	3.59	0.78	33476	2447	31029
51	1994	2.93	1.52	2.19	1.30	7.31	2.45	3517	1004	2513
54	1994	3.72	1.21	6.03	2.33	4.75	0.44	1441	204	1237
55	1994	3.94	1.41	5.81	2.33	4.33	0.78	2088	108	1979
58	1994	2.78	1.07	4.82	2.30			1883		1883
59	1994	3.62	0.97	5.87	2.58	5.13	0.49	980	531	449
66	1994	1.13	0.31	1.80	0.65			5288		5288
77	1994	2.54	1.28	2.97	2.18	5.62	2.35	2033	483	1549
78	1994	1.28	0.27	1.22	0.42	11.17	6.83	2254	35	2219
79	1994	1.17	0.18	1.17	0.45	12.00		82	4	78
80	1994					12.47	4.50	22	22	
81	1994	3.05	1.71	4.04	3.60	6.89	1.92	1585	817	768
82	1994	3.72	1.51	6.57	3.41	6.07	0.95	1196	675	521
83	1994	2.93	1.46	3.76	3.06	4.89	0.60	3083	583	2500

Stand	Year Measured	Basal Area (m²/ha)										
		Stand Total Living	Stand Total Dead	Upper Stratum Live	Middle Stratum Live	Conifer BA Live	Conifer BA Percent	Red Pine BA	Jack Pine BA	Red BA cent	Red Pine Per-cent	Jack Pine BA Percent
22	1991	18.06	0.01	17.81	0.25	18.05	1.00	17.98	0.00	1.00		0.00
23	1991	38.70	2.06	38.07	0.62	35.67	0.92	19.84	0.00	0.51		0.00
24	1991	19.72	4.24	19.29	0.42	18.42	0.93	1.31	16.85	0.07		0.85
25	1991	33.06	0.92	31.94	1.12	31.06	0.94	17.26	0.00	0.52		0.00
26	1991	20.05	4.57	16.78	3.27	18.21	0.91	0.08	0.55	0.00		0.03
27	1991	25.08	8.59	24.72	0.36	24.24	0.97	0.00	24.24	0.00		0.97
28	1991	40.33	3.88	38.26	2.08	4.08	0.10	0.00	0.00	0.00		0.00
29	1991	35.34	2.59	32.88	2.46	2.72	0.08	0.00	0.00	0.00		0.00
31	1991	27.33	1.87	26.98	0.35	0.02	0.00	0.00	0.00	0.00		0.00
32	1991	59.36	8.06	58.32	1.04	58.18	0.98	0.00	0.00	0.00		0.00
33	1991	21.27	4.39	15.27	6.00			0.00	0.00	0.00		0.00
34	1991	29.03	5.17	27.40	1.63	0.18	0.01	0.00	0.00	0.00		0.00
35	1991	11.32	0.73	10.90	0.42	11.22	0.99	0.00	11.21	0.00		0.99
36	1991	4.95	0.20	3.20	1.75	4.93	1.00	0.71	4.22	0.14		0.85
37	1992	0.77	0.02	0.01	0.76	0.77	1.00	0.05	0.72	0.06		0.94
38	1992	4.39	0.01		4.39	4.39	1.00	0.00	4.39	0.00		1.00
39	1992	0.27	0.04	0.21	0.06	0.27	1.00	0.21	0.06	0.78		0.22
40	1992	1.80			1.80	1.80	1.00	1.58	0.22	0.88		0.12
41	1992	7.67	0.29	1.11	6.55	6.73	0.88	4.45	2.12	0.58		0.28
42	1992	8.82	0.30	0.24	8.59	7.95	0.90	0.00	8.00	0.00		0.91
43	1992	34.19	0.11	33.95	0.24	33.10	0.97	32.75	0.22	0.96		0.01
44	1992	28.53	4.56	26.55	1.98	21.68	0.76	0.12	0.00	0.00		0.00
45	1992	5.15	0.11	0.50	4.66	0.24	0.05	0.00	0.00	0.00		0.00
47	1992	24.04	3.60	24.04		1.81	0.08	0.00	0.00	0.00		0.00
48	1992	28.17	2.21	26.21	1.95	5.37	0.19	0.00	0.00	0.00		0.00
49	1992	11.89	1.29	0.31	11.58			0.00	0.00	0.00		0.00
50	1992	26.75	0.81	25.78	0.97	19.76	0.74	19.44	0.00	0.73		0.00
51	1992	14.95	0.89	13.38	1.57	13.40	0.90	11.14	2.25	0.75		0.15

Basal Area (m²/ha)

Stand	Year Measured	Stand Total Living	Stand Total Dead	Upper Stratum Live	Middle Stratum Live	Conifer BA Live	Conifer BA Percent	Red Pine BA	Jack Pine BA	Red BA cent	Pine Per-	Jack Pine BA Percent
46	1993	43.30	2.84	41.36	1.94	8.77	0.20	0.00	0.00	0.00		0.00
52	1993	21.27	1.21	21.17	0.10	21.27	1.00	11.99	9.28	0.56		0.44
53	1993	27.09	1.70	25.81	1.28	3.25	0.12	0.10	0.64	0.00		0.02
54	1993	5.31	0.11	0.14	5.17	5.31	1.00	0.00	5.31	0.00		1.00
55	1993	6.96	0.13	0.07	6.89	6.96	1.00	0.00	6.96	0.00		1.00
56	1993	5.70	4.97	5.63	0.07	5.70	1.00	0.26	5.44	0.05		0.95
57	1993	31.51	2.02	29.15	2.36	6.19	0.20	0.99	0.25	0.03		0.01
58	1993	4.00	0.01		4.00	4.00	1.00	0.00	4.00	0.00		1.00
59	1993	4.71	0.02	2.10	2.62	4.69	1.00	0.04	4.65	0.01		0.99
60	1993	6.59	0.20	4.93	1.66	6.56	1.00	1.83	4.73	0.28		0.72
61	1993	18.86	1.79	18.78	0.09	18.86	1.00	0.30	18.56	0.02		0.98
62	1993	16.43	1.98	15.88	0.54	16.42	1.00	0.26	16.16	0.02		0.98
63	1993	9.94	0.63	9.31	0.63	9.94	1.00	0.33	9.58	0.03		0.96
64	1993	11.44	0.43	11.26	0.18	11.44	1.00	0.00	11.43	0.00		1.00
65	1993	16.71	3.85	16.69	0.02	16.71	1.00	0.29	16.42	0.02		0.98
66	1993	0.43	0.18		0.43	0.40	0.94	0.00	0.40	0.00		0.94
67	1993	22.52	5.80	22.48	0.04	22.51	1.00	0.10	22.41	0.00		1.00
68	1993	28.62	0.43	28.47	0.15	28.62	1.00	25.43	3.20	0.89		0.11
69	1993	13.40	3.64	2.12	11.28	0.25	0.02	0.00	0.00	0.00		0.00
70	1993	9.32	1.26	0.83	8.50			0.00	0.00	0.00		0.00
71	1993	10.09	0.26	10.05	0.05	10.09	1.00	9.76	0.33	0.97		0.03
72	1993	8.86	0.51	8.73	0.13	8.79	0.99	8.13	0.65	0.92		0.07
73	1993	17.84	0.20	17.65	0.18	17.81	1.00	12.29	5.52	0.69		0.31
74	1993	37.67	6.70	37.22	0.44	25.51	0.68	0.00	0.00	0.00		0.00
75	1993	42.63	7.22	42.53	0.10	39.72	0.93	0.00	0.42	0.00		0.01

Stand	Year Measured	Basal Area (m²/ha)										
		Stand Total Living	Stand Total Dead	Upper Stratum Live	Middle Stratum Live	Conifer BA Live	Conifer BA Per-cent	Red Pine BA	Jack Pine BA	Red BA cent	Red Pine Per-	Jack Pine BA Percent
76	1993	33.19	1.31	32.75	0.44			0.00	0.00	0.00		0.00
77	1993	10.95	0.55	8.80	2.15	9.77	0.89	6.67	3.10	0.61		0.28
78	1993	1.16	0.12	1.01	0.15	0.93	0.80	0.93	0.00	0.80		0.00
79	1993	0.14	0.20	0.14	0.01	0.14	0.95	0.14	0.00	0.95		0.00
80	1993	0.49	0.03	0.49		0.44	0.91	0.44	0.00	0.91		0.00
81	1993	11.78	0.27	10.30	1.48	11.38	0.97	5.53	5.84	0.47		0.50
82	1993	7.67	0.06	5.13	2.55	7.67	1.00	4.08	3.59	0.53		0.47
83	1993	9.12	0.14	1.14	7.98	8.34	0.91	5.82	2.11	0.64		0.23
85	1993	33.43	2.61	32.63	0.79	0.42	0.01	0.00	0.00	0.00		0.00
86	1993	33.05	3.16	32.24	0.82	0.06	0.00	0.00	0.00	0.00		0.00
87	1993	16.85	9.05	13.12	3.73			0.00	0.00	0.00		0.00
88	1993	66.40	8.22	65.72	0.69	66.40	1.00	0.00	0.00	0.00		0.00
91	1993	23.00	1.07	21.67	1.33	0.36	0.02	0.00	0.00	0.00		0.00

Stand	Year Measured	Basal Area (m²/ha)										
		Stand Total Living	Stand Total Dead	Upper Stratum Live	Middle Stratum Live	Conifer BA Live	Conifer BA Percent	Red Pine BA	Jack Pine BA	Red BA cent	Red Pine Per-cent	Jack Pine BA Percent
22	1994	20.00		19.94	0.06	20.00	1.00	20.00	0.00	1.00		0.00
33	1994	24.54	3.47	20.00	4.54			0.00	0.00	0.00		0.00
36	1994	6.27	0.61	5.66	0.60	6.11	0.98	1.17	4.94	0.19		0.79
37	1994	2.99	0.46		2.99	2.99	1.00	0.10	2.89	0.03		0.97
38	1994	6.18	0.05	0.08	6.10	6.18	1.00	0.00	6.18	0.00		1.00
39	1994	0.05			0.05	0.04	0.97	0.00	0.04	0.00		0.97
40	1994	3.72	0.03		3.72	3.72	1.00	3.31	0.40	0.89		0.11
41	1994	8.40	0.18	4.39	4.01	7.47	0.89	4.88	2.34	0.58		0.28
42	1994	7.32	1.03	3.90	3.42	6.31	0.86	0.00	6.29	0.00		0.86
45	1994	9.63	1.03	1.24	8.39	0.30	0.03	0.00	0.00	0.00		0.00
49	1994	15.21	0.44	3.45	11.76			0.00	0.00	0.00		0.00
51	1994	17.29	0.03	16.01	1.28	16.19	0.94	14.90	1.28	0.86		0.07
54	1994	4.99	0.10	0.93	4.06	4.99	1.00	0.00	4.99	0.00		1.00
55	1994	6.53	0.02	0.45	6.08	6.53	1.00	0.00	6.53	0.00		1.00
58	1994	4.23			4.21	4.21	1.00	0.00	4.21	0.00		1.00
59	1994	4.56	0.42	3.12	1.44	4.56	1.00	0.00	4.56	0.00		1.00
66	1994	1.52	0.33		1.52	1.52	1.00	0.00	1.52	0.00		1.00
77	1994	9.37	0.13	7.73	1.65	8.02	0.86	5.40	2.76	0.58		0.29
78	1994	1.56	0.09	1.27	0.29	1.14	0.73	1.14	0.00	0.73		0.00
79	1994	0.33	0.05	0.32	0.01	0.32	0.97	0.32	0.00	0.97		0.00
80	1994	0.91	0.54	0.91		0.81	0.89	0.81	0.00	0.89		0.00
81	1994	11.72	0.05	9.97	1.75	11.43	0.97	5.89	5.59	0.50		0.48
82	1994	8.52	0.12	6.29	2.23	8.50	1.00	4.35	4.15	0.51		0.49
83	1994	8.35		3.75	4.60	7.78	0.93	5.61	1.75	0.67		0.21

Stand	Year Measured	Ground Cover%				Error % (upper and middle)	
		Year measured	Avg. Cover %	Stdev	N of Plots	BA	Density
22	1991					16.80	15.79
23	1991					12.88	22.99
24	1991					12.95	31.86
25	1991					16.87	27.30
26	1991					10.55	15.90
27	1991					5.03	36.81
28	1991					14.43	15.06
29	1991					11.90	11.65
31	1991					8.79	13.52
32	1991					9.24	23.43
33	1991					15.23	18.19
34	1991					17.71	13.49
35	1991					16.97	24.39
36	1991					24.74	30.08
37	1992	1992	54.74	22.52	114	41.85	37.85
38	1992	1992	61.95	20.97	104	17.16	13.49
39	1992	1992	66.07	19.05	120	126.96	34.96
40	1992	1992	86.97	14.86	108	24.34	15.40
41	1992	1992	66.23	24.33	120	17.09	18.70
42	1992	1992	74.01	20.83	118	14.90	21.02
43	1992	1992	48.87	25.71	62	12.33	36.88
44	1992	1992	60.98	30.87	120	16.42	20.68
45	1992	1994	70.70	20.93	20	19.88	15.00
47	1992	1993	63.95	28.44	84	11.22	21.57
48	1992	1992	32.71	21.99	120	12.69	14.25
49	1992	1992	75.19	23.899	66	26.30	21.74
50	1992	1992	32.69	23.85	120	9.89	21.58
51	1992	1992	53.11	29.34	120	15.46	34.69

Stand	Year Measured	Ground Cover%				Error % (upper and middle)	
		Year measured	Avg. Cover %	Stdev	N of Plots	BA	Density
46	1993	1993	29.43	17.45	120	14.09	16.89
52	1993	1993	51.43	25.03	120	17.27	15.83
53	1993	1993	41.65	17.85	120	15.86	17.84
54	1993	1993	67.11	15.76	120	16.44	22.92
55	1993	1993	62.54	19.46	120	14.86	19.14
56	1993	1993	83.21	16.33	120	22.74	25.37
57	1993	1993	43.78	17.86	120	11.27	17.25
58	1993	1993	85.08	17.72	120	21.37	21.66
59	1993	1993	76.79	17.95	120	22.56	36.21
60	1993	1993	72.04	19.74	120	16.38	22.59
61	1993	1993	65.62	19.16	120	10.24	13.70
62	1993	1993	72.12	15.83	120	10.86	12.62
63	1993	1993	70.08	20.76	120	13.60	18.96
64	1993	1993	69.88	21.44	120	19.80	21.67
65	1993	1993	74.46	17.46	120	13.57	16.03
66	1993	1993	83.31	17.81	120	39.27	42.78
67	1993	1993	67.19	16.12	120	9.95	11.52
68	1993	1993	35.76	20.51	120	11.96	12.73
69	1993	1993	62.16	19.93	45	13.02	18.08
70	1993	1993	86.5	19.2	24	28.61	48.71
71	1993	1993	26.43	29.49	120	25.24	24.30
72	1993	1993	27.97	31.11	120	21.47	50.86
73	1993	1993	56.23	24.84	120	18.57	24.50
74	1993	1993	39.84	16.25	120	9.12	38.04
75	1993	1993	33.67	21.68	81	9.45	30.07

Stand	Year Measured	Ground Cover%				Error % (upper and middle)	
		Year measured	Avg. Cover %	Stdev	N of Plots	BA	Density
76	1993	1993	28.26	17	120	10.12	27.53
77	1993	1993	60.77	21.18	120	16.71	21.15
78	1993	1993	60.72	18.97	120	114.19	37.83
79	1993	1993	46.2	26.16	120	127.27	86.91
80	1993	1993	32.9	22.38	120	79.62	80.00
81	1993	1993	88.76	12.2	120	14.03	26.75
82	1993	1993	86.53	12.88	120	18.87	21.46
83	1993	1993	49.15	20.37	120	13.73	16.78
85	1993	1993	23.16	16.27	120	8.00	14.17
86	1993	1993	37.25	19.62	105	9.93	26.34
87	1993	1993	92.97	13.2	90	15.59	20.79
88	1993	1993	42.15	25.28	120	6.51	25.27
91	1993	1993	30.88	16.76	120	11.27	36.97

Stand	Year Measured	Ground Cover%				Error % (upper and middle)	
		Year measured	Avg. Cover %	Stdev	N of Plots	BA	Density
22	1994	1994	65.76	34.35	72		
33	1994	1994	44.17	23.38	24		
36	1994	1994	86.93	12.10	71		
37	1994	1994	70.95	25.27	73		
38	1994	1994	70.73	17.71	48		
39	1994	1994	62.34	21.68	71		
40	1994	1994	68.17	13.29	24		
41	1994	1994	73.28	28.44	54		
42	1994	1994	84.06	18.18	72		
45	1994	1994	70.70	20.93	20		
49	1994	1994	69.44	26.73	50		
51	1994	1994	61.85	26.93	72		
54	1994	1994	71.04	18.03	72		
55	1994	1994	78.56	18.57	72		
58	1994	1994	92.34	13.82	71		
59	1994	1994	86.14	17.98	69		
66	1994	1994	88.14	14.45	70		
77	1994	1994	62.60	32.44	72		
78	1994	1994	81.23	17.04	61		
79	1994	1994	47.02	25.68	47		
80	1994	1994	53.33	25.90	72		
81	1994	1994	88.96	12.87	72		
82	1994	1994	88.86	10.75	71		
83	1994	1994	73.11	22.06	72		

Stand	Year Measured	UTM COORDINATES			
		SW X	SW Y	NE X	NE Y
22	1991	667521.8	5135412.5	667820.0	5135645.0
23	1991	669386.9	5130535.0	669650.8	5130808.5
24	1991	673629.3	5138048.5	673826.4	5138262.0
25	1991	669398.8	5130725.5	669580.2	5131006.0
26	1991	676233.3	5133015.5	676390.8	5133338.5
27	1991	662780.4	5135912.0	663020.3	5136121.0
28	1991	661538.3	5139469.5	661738.7	5139694.5
29	1991	661647.8	5139805.5	661861.8	5140015.0
31	1991	660905.3	5143976.5	661109.2	5144177.5
32	1991	656007.3	5147767.5	656203.3	5147983.0
33	1991	660439.2	5143750.0	660818.8	5143976.0
34	1991	660543.3	5143507.0	660796.1	5143756.5
35	1991	670117.2	5135924.0	670311.0	5136173.5
36	1991	666660.3	5136079.0	666904.9	5136271.5
37	1992	667959.8	5139207.5	668164.2	5139413.5
38	1992	669440.2	5139490.5	669710.7	5139683.5
39	1992	668050.5	5139879.0	668300.7	5140099.5
40	1992	672560.4	5139640.5	672959.5	5139832.5
41	1992	671385.9	5135536.0	671727.1	5135743.0
42	1992	668034.9	5132472.0	668246.3	5132752.5
43	1992	658474.1	5134080.5	658742.7	5134277.0
44	1992	657865.9	5137720.0	658188.8	5137887.0
45	1992	659897.4	5144299.5	660131.8	5144620.5
47	1992	655088.5	5146510.0	655400.1	5146768.0
48	1992	655528.3	5145666.0	655861.4	5145808.0
49	1992	661165.4	5143632.5	661445.1	5143842.0
50	1992	661312.9	5143262.5	661535.6	5143541.5
51	1992	674289.1	5139404.5	674555.6	5139599.0

Stand	Year Measured	UTM COORDINATES			
		SW X	SW Y	NE X	NE Y
46	1993	649908.9	5148313.5	650229.4	5148562.0
52	1993	671515.9	5137512.0	671722.6	5137729.5
53	1993	673429.1	5141082.0	673745.7	5141207.5
54	1993	669036.0	5138940.0	669246.7	5139153.5
55	1993	669267.5	5140453.5	669496.3	5140713.0
56	1993	669054.7	5138413.5	669263.0	5138612.0
57	1993	669615.5	5141957.5	669773.6	5142210.0
58	1993	671252.4	5137709.0	671458.6	5137909.5
59	1993	668649.5	5136817.0	668847.0	5137018.5
60	1993	666890.8	5136312.5	667058.4	5136648.0
61	1993				
62	1993	668310.1	5136535.5	668509.3	5136753.0
63	1993	668630.3	5137065.0	668821.0	5137266.0
64	1993	669216.4	5136833.5	669416.8	5137036.0
65	1993	668654.0	5137900.0	668856.1	5138108.5
66	1993	668550.4	5138722.0	668857.6	5138925.0
67	1993	668344.7	5139487.5	668546.3	5139692.5
68	1993	670203.3	5137129.5	670423.4	5137337.0
69	1993	673804.4	5141280.5	673939.7	5141601.5
70	1993				
71	1993	671806.2	5139581.5	671998.9	5139785.0
72	1993	671998.9	5139585.0	672205.3	5139795.5
73	1993	670106.5	5140329.0	670413.4	5140558.5
74	1993	666143.3	5141916.0	666376.1	5142152.5
75	1993	666417.5	5141759.5	666534.1	5142160.5

Stand	Year Measured	UTM COORDINATES			
		SW X	SW Y	NE X	NE Y
76	1993	666264.9	5142955.0	666498.5	5143148.5
77	1993	664039.9	5137771.0	664239.1	5138006.5
78	1993	661131.1	5134797.0	661389.3	5135128.0
79	1993	660921.1	5133597.0	661119.9	5133830.5
80	1993	660858.3	5134149.0	661108.1	5134352.0
81	1993	665172.9	5135674.0	665421.8	5135869.0
82	1993	665688.9	5135026.5	665887.6	5135293.5
83	1993	672055.0	5135539.0	672253.4	5135776.0
85	1993	655787.4	5139630.0	655996.6	5139831.5
86	1993	660400.8	5141600.0	660557.9	5141918.5
87	1993	658838.3	5147164.5	659143.2	5147494.0
88	1993	656279.8	5148144.5	656476.0	5148363.5
91	1993	646641.8	5145553.5	646838.5	5145872.0

Stand	Year Measured	UTM COORDINATES			
		SW X	SW Y	NE X	NE Y
22	1994	667521.8	5135412.5	667820.0	5135645.0
33	1994	660439.2	5143750.0	660818.8	5143976.0
36	1994	666660.3	5136079.0	666904.9	5136271.5
37	1994	667959.8	5139207.5	668164.2	5139413.5
38	1994	669440.2	5139490.5	669710.7	5139683.5
39	1994	668050.5	5139879.0	668300.7	5140099.5
40	1994	672560.4	5139640.5	672959.5	5139832.5
41	1994	671385.9	5135536.0	671727.1	5135743.0
42	1994	668034.9	5132472.0	668246.3	5132752.5
45	1994	659897.4	5144299.5	660131.8	5144620.5
49	1994	661165.4	5143632.5	661445.1	5143842.0
51	1994	674289.1	5139404.5	674555.6	5139599.0
54	1994	669036.0	5138940.0	669246.7	5139153.5
55	1994	669267.5	5140453.5	669496.3	5140713.0
58	1994	671252.4	5137709.0	671458.6	5137909.5
59	1994	668649.5	5136817.0	668847.0	5137018.5
66	1994	668550.4	5138722.0	668857.6	5138925.0
77	1994	664039.9	5137771.0	664239.1	5138006.5
78	1994	661131.1	5134797.0	661389.3	5135128.0
79	1994	660921.1	5133597.0	661119.9	5133830.5
80	1994	660858.3	5134149.0	661108.1	5134352.0
81	1994	665172.9	5135674.0	665421.8	5135869.0
82	1994	665688.9	5135026.5	665887.6	5135293.5
83	1994	672055.0	5135539.0	672253.4	5135776.0

BIBLIOGRAPHY

BIBLIOGRAPHY

[1] Aber, J.D., and J.M. Melillo, *Terrestrial Ecosystems*. Holt, Rinehart and Winston Inc., Orlando, FL, 1991.

[2] Alban, D.H. and D.A. Perala, "C storage in Lake States aspen ecosystems," *Canadian Journal of Forest Research*, Vol. 22, pp. 1107-1110, 1992.

[3] Anderson, J.R., E.E. Hardy, J.T. Roach, and R.E. Witmer, "A land use and land cover classification system for use with remote sensor data," *U.S. Geological Survey Professional Paper 964*, Washington, D.C., 28 pp. 1976.

[4] Barnes, B.V. *Michigan Trees*. Ann Arbor: The University of Michigan Press, 1981.

[5] Baskerville, "Estimation of dry weight of tree components and total standing crop in conifer stands," *Ecology*, Vol. 46, pp. 867-869, 1965.

[6] Bazilvich,N.I., and L.E. Rodin, "Reserves of organic matter in under-ground of terrestrial phytocoenoses," *International Symposium, USSR. Methods of Productivity in Root Systems and Rhizosphere Organisms* Guildford, U.K.: Biddles, Ltd., 1968.

[7] Bergen, K.M., L.E. Pierce, M.C. Dobson, F.T. Ulaby, "A multi-temporal classifier for SIR-C/X-SAR imagery," *IGARSS '96: International Geoscience and Remote Sensing Symposium*, Lincoln, NB, pp. 1996.

[8] Bergen, K.M., M.C. Dobson, T.L. Sharik, I.J. Brodie, *Structure, Composition, and Above-ground Biomass of SIR-C/X-SAR and ERS-1 Forest Test Stands 1991-1994, Raco, Michigan Site*. Radiation Laboratory Technical Report, 026511-7-T, Radiation Laboratory, EECS Dept. The University of Michigan, Ann Arbor, MI, Oct. 1995a.

[9] Bergen, K.M., M.C. Dobson, L.E. Pierce, J. Kellndorfer, and P. Siqueira, *October 1994 SIR-C/X-SAR Mission: Ancillary Data Report Raco, Michigan Site*, Radiation Laboratory Technical Report 036511-6T, Radiation Laboratory, EECS Dept. The University of Michigan, Ann Arbor, MI, Dec. 1995b.

[10] Bergen, K.M., M.C. Dobson, L.E. Pierce, J.L. Kendra, J. Kellndorfer, and P. Siqueira, *April 1994 SIR-C/X-SAR Mission: Ancillary Data Report Raco, Michigan Site*, Radiation Laboratory Technical Report 036511-5-T, Radiation Laboratory, EECS Dept. The University of Michigan, Ann Arbor, MI, Dec. 1994.

[11] Birdsey, R.A., "Inventory of C storage and accumulation in U.S. forest ecosystems," in H.E. Burkhart et al. (ed.), *Research in Forest Inventory, Monitoring, Growth and Yield*. Proc. IUFRO World Congr. Montreal. 5-11 Aug. 1990. School of Forestry and Wildlife Resources, Publ. FWS-2-90. Virginia Polytechnic Institute and State University, Blacksburg.

[12] Bonan, G.B., "Seasonal and annual carbon fluxes in a boreal forest landscape," *Journal of Geophysical Research*, Vol. 96 pp. 17329-17338, 1991.

[13] Bormann, F.H., and G.E. Likens, *Pattern and Process in a Forested Ecosystem.* New York: Springer-Verlag, 1979.

[14] Ciais, P., P. Tans, M. Trolier, J.W. White, R.J. Francey, "A large northern hemisphere terrestrial CO^2 sink indicated by the 13C/12C ratio of atmospheric CO^2. *Science*, Vol. 269, pp. 1089-1102, 1995.

[15] Clark, W.C., *Carbon Dioxide Review*, New York: Oxford University Press, 1982

[16] Crow, T.R., "Biomass and production in three contiguous forests in northern Wisconsin," *Ecology*, Vol. 59 No. 2, pp. 265-273, 1978.

[17] Crow, T.R. and G.G. Erdmann, *Weight and volume equations and tables for red maple in the Lake States.* USDA For. Serv. Res. Pap. NC-242. 14 pp., 1983

[18] Dai, A., I.Y. Fung, "Can climate variability contribute to the "missing" CO_2 sink? *Global Biogeochemical Cycles*, No. 7, pp. 599-610, 1993.

[19] Denning, A.S., I.Y. Fung, D. Randall, "Latitudinal gradient of atmospheric CO_2 due to seasonal exchange with land biota, *Nature*, Vol. 376, pp. 240-243, 1995.

[20] Dobson, M.C., F.T. Ulaby, L.E. Pierce,T.L. Sharik, K.M. Bergen, et al., "Estimation of forest biophysical characteristics in northern Michigan with SIR-C/X-SAR," *IEEE Transactions on Geosciences and Remote Sensing*, Vol. 33, No. 4, pp. 877-895, July, 1995a.

[21] Dobson, M.C., L.E. Pierce, F.T. Ulaby, "Knowledge-based land-cover classification using ERS-1/JERS-1 SAR Composites," *IEEE Transactions Geosciences and Remote Sensing*, Vol. 34, No. 1, pp. 83-99, 1996.

[22] Dobson, M.C., F.T. Ulaby, T. LeToan, A. Beaudoin, and E.S. Kasischke, "Dependence of radar backscatter on conifer forest biomass," *IEEE Transactions on Geosciences and Remote Sensing*, Vol. 30, No. 2, pp. 412-415, 1992a.

[23] Dobson, M.C., K. McDonald, F.T. Ulaby, and T. Sharik, "Relating the temporal change observed by AIRSAR to surface and canopy properties of mixed conifer and hardwood forests of northern Michigan," *Proc. 3rd Airborne Synthetic Aperture Radar (AIRSAR) Workshop*, May 23-24, 1991, Jet Propulsion Laboratory, Pasadena, CA, JPL Pub. 91-30, pp. 34-43, Aug. 1991.

[24] Dobson, M.C., L.E. Pierce, and F.T. Ulaby, "Semi-empirical method for estimation of forest biophysical properties from multifrequency polarimetric SAR," *IEEE Transactions on Geosciences and Remote Sensing*, pp. 2466, 1994.

[25] Dobson, M.C., L. Pierce, K. Sarabandi, F.T. Ulaby and T.L. Sharik, "Preliminary analysis of ERS-1 SAR for forest ecosystem studies," *IEEE Transactions on Geosciences and Remote Sensing*, Vol. 30, No. 2, pp. 203-211, 1992b.

[26] Dobson, M.C. E. Wilcox, and F.T. Ulaby, "Effects of forest structure on radar response to forest biomass," *International Geoscience and Remote Sensing Symposium*, August 18-21, 1993, Tokyo, Japan.

[27] Dobson, M.C., F.T. Ulaby, and L.E. Pierce, "Land-cover classification and estimation of terrain attributes using synthetic aperture radar," *Remote Sensing of Environment*, Vol. 51, No. 1, pp. 199-214, 1995b.

[28] ERDAS Corp., *ERDAS System Documentation*, Atlanta, GA.

[29] Field, C.B., J.T. Randerson, and C.M. Malmstrom, "Global net primary production: combining ecology and remote sensing," *Remote Sensing of Environment*, Vol. 51, pp. 74-85, 1995.

[30] Friedlingstein, P., I.Y. Fung, E. Holland, J. John, G. Brasseur, D. Erickson, D. Schimel, "On the contribution of CO^2 fertilization to the missing biospheric sink," *Global Biogeochemical Cycles*, Vol. 9, pp. 541-556, 1995.

[31] Grigal, D.F. and L.K. Kernik, "Generality of black spruce biomass estimation equations," *Canadian Journal of Forest Research*, Vol. 14, pp. 468-479, 1984.

[32] Grigal, D.F. and L.F. Ohmann, "C storage in upland forests of the lake states," *Soil Science Society of America Journal*, Vol. 56 pp. 935-943, 1992.

[33] Hagg, W., M. Sties, "Efficient Speckle Fltering of SAR Images," *IGARSS '94: Proceedings of the 1994 International Geoscience and Remote Sensing Symposium*, Pasadena, California, USA. Vol. 4, pp. 2140-2142.

[34] Harris, W.F., R.S. Kinerson, Jr., and N.T. Edwards, "Comparison of belowground biomass of natural deciduous forest and loblolly pine plantations," *Pedobiologia*, Bd. 17, S. pp. 369-381, 1977.

[35] Haynes, R.E. and S.T. Gower, "Belowground C allocation in unfertilized and fertilized red pine plantations in northern Wisconsin," *Tree Physiology*, Vol. 15 pp. 317-325, 1995.

[36] Keyes, M.R. and C.C. Grier, "Above- and below-ground net production in 40-year-old Douglas-fir stands on low and high productivity sites," *Canadian Journal of Forest Research*, Vol. 11, pp. 599-605, 1981.

[37] Kasischke, E. S., and Bourgeau-Chavez, L. L., "Observations on the sensitivity of ERS-1 SAR image intensity to changes in aboveground biomass in young loblolly pine forests", *International Journal of Remote Sensing*, Vol. 15, No. 1, pp. 3-16, 1994.

[38] Kasischke, E. S., *Monitoring changes in aboveground biomass in Loblolly Pine forests using multichannel synthetic aperture radar data* Ann Arbor, MI: The University of Michigan (Dissertation), 1992.

[39] Kellndorfer, J.M., M.C. Dobson, F.T. Ulaby, "Geocoding for Classification of ERS/JERS-1 SAR Composites. *IGARSS '96: Proceedings of the 1996 International Geoscience and Remote Sensing Symposium*, Lincoln, NB, pp. 2335-2337, 1996a.

[40] Kellndorfer, J.M., M.C. Dobson, F.T. Ulaby, "Regional stability of and ERS/JERS-1 classifier," *IGARSS '96: Proceedings of the 1996 International Geoscience and Remote Sensing Symposium*, Lincoln, NB, pp. 1093-1095, 1996b.

164

[41] Ker, M.F., "Tree biomass equations for seven species in southwestern New Brunswick," *Can. For. Serv. Maritime Forest. res. Center Inf. Rep.*, M-X-114.

[42] Koerper, G.J. , and C.J. Richardson, "Biomass and net annual production regressions for Populus grandidentata on three sites in northern lower Michigan," *Canadian Journal of Forest Research*, Vol. 10, pp. 92-101, 1980.

[43] Leith, H. "Modelling the primary productivity of the world," *Nature and Resources*, Vol. 8, pp. 5-10, 1972.

[44] LeToan, T., A. Beaudoin, J. Riom, and D. Guyon, "Relating forest biomass to SAR data," *IEEE Transactions on Geosciences and Remote Sensing*, Vol. 30 No. 2 pp. 403-411, 1992.

[45] Linder, S., and B. Axelsson, "Changes in C uptake and allocation patterns as a result of irrigation and fertilization in a young it Pinus sylvestris stand," in R.H. Waring (ed.) *C Uptake and Allocation in Subalpine Ecosystems as a Key to Management.* IUFRO Workshop, 2-3 Aug. 1982, Corvallis, OR. Oregon State University, Corvallis, 1982.

[46] Lozano-Garcia, D.F. and Hoffer, Roger M., "Hierarchical classification of multitemporal/multispectral scanner data," *Eleventh International Symposium; Machine Processing of Remotely Sensed Data with Special Emphasis on Quantifying Global Process: Models, Sensor Systems, and Analytical Methods.* W Lafayette, IN, 1985.

[47] Melillo, J.M., McGuire, D., Kicklighter, D.W., et al., "Global climate change and terrestrial net primary production," *Nature*, Vol. 363, pp. 234-239, 1993.

[48] Michigan State Dept. of Natural Resources, *Michigan Resource Information System (MIRIS)*, 1985.

[49] McDonald, K.C., M.C. Dobson, and F.T. Ulaby, "Using MIMICS to model L-band multiangle and multitemporal backscatter for a walnut orchard", *IEEE Trans. Geosci. Remote Sensing*, Vol. 28, pp. 477-491, July, 1990.

[50] Mladenoff, D.J., and J. Pastor, "Sustainable forest ecosystems in the northern hardwood and conifer forest region: concepts and management," in *Defining Sustainable Forestry*, ed. by G.H. Aplet, N. Johnson, J.T. Olson, and V.A. Sample, Island Press, Washington, D.C., 1993.

[51] Moghaddam, M. and A. Freeman, "Modifications to the three-component classification algorithm for SAR data," *Progress in Electromagnetics Research Symposium (PIERS '93)*, July, 1993, Jet Propulsion Laboratory, California Institute of Technology.

[52] Nadelhoffer, K.J. and J.W. Raich, "Fine root production estimates and belowground C allocation in forest ecosystems," *Ecology*, Vol. 73, No. 4, pp. 1139-1147, 1992.

[53] Nadelhoffer, K.J., Aber, J.D., and Melillo, J.M., "Fine roots, net primary production, and soil nitrogen availability: a new hypothesis," *Ecology*, Vol. 66 No. 4, pp. 1377-1390, 1985.

[54] PCI Remote Sensing Corp., *PCI System Documentation*, Arlington, VA, 1995.

[55] Pastor, J. and J.G. Bockheim, "Biomass and production of an aspen - mixed hardwood - spodosol ecosystem in northern Wisconsin," National Research Council of Canada, 1981.

[56] Perala, D.A., and D.H. Alban. *Allometric biomass estimators for aspen-dominated ecosystems in the upper great lakes*. USDA North Central Forest Experiment Station, Research Paper NC-314, 1994.

[57] Pierce, L.E., F.T. Ulaby, K. Sarabandi, and M.C. Dobson, "Knowledge-based classification of polarimetric SAR images," *IEEE Transactions on Geosciences and Remote Sensing*, Vol. 32, pp. 1081-1086, Sept. 1994a.

[58] Pierce, L.E., M.C. Dobson, and F.T. Ulaby, "Knowledge-based land-cover classification using ERS-1/JERS-1 composites," *IGARSS '94: Proceedings of the 1994 International Geoscience and Remote Sensing Symposium*, 1994b.

[59] Pierce, L.E., K.M. Bergen, M.C. Dobson, F.T. Ulaby, "Land-Cover Classification using SIR-C/X-SAR Data," *Proceedings of the 1995 International Geoscience and Remote Sensing Symposium*, Florence, Italy, Vol. , pp. 918-919.

[60] Pregitzer, K.S., D.R. Zak, R.S. Curtis, M.E. Kubiske, J.A. Teeri, and C.S. Vogel, "Atmospheric CO_2, soil nitrogen, and turnover of fine roots," *New Phytologist*, Vol. 129, No. 4, pp. 579-585, 1995.

[61] Ranson, J.K., and G. Sun, "Northern forest classification using temporal multifrequency and multipolarimetric SAR images," *Remote Sensing of Environment*, Vol. 47, No. 2 pp. 142-153, 1994.

[62] Rhode, W.G. and C.E. Olson, "Estimating leaf moisture content from infrared reflectance data," *Proceedings of the third biennial workshop on color aerial photography in the plant sciences*, Bethesda, MD: American Society of Photogrammetry and Remote Sensing, pp. 144-164, 1971.

[63] Rignot, E. and J. van Zyl, "Change detection techniques for ERS-1 SAR data," *IEEE Transactions on Geoscience and Remote Sensing*, Vol. 31, No. 4, pp. 896-906, July 1993.

[64] Rignot, E., J. Way, C. Williams, and L. Viereck, "Radar estimates of aboveground biomass in boreal forests of interior Alaska," *IEEE Transactions on Geoscience and Remote Sensing*, Vol. 32, No. 5, pp. 1117-1124, September 1993.

[65] Rodin, L.E., and N.I. Bazilevich, *Production and Mineral Cycling in Terrestrial Vegetation*, [English translation edited by G.E. Fogg], Oliver and Boyd, London, 1967.

[66] Ruark, G.A. and J.G. Bockheim, "Biomass, net primary production, and nutrient distribution for an age sequence of Populus tremuloides ecosystems," *Canadian Journal of Forest Research* Vol. 18 pp. 435-443, 1988.

[67] SAS Institute, *SAS System Documentation*, Cary, NC.

[68] Samson, S.A., "Two indices to characterize temporal patterns in the spectral responses of vegetation", *Photogrammetric Engineering & Remote Sensing*, Vol. 59 No. 4, pp. 511-517, 1993.

[69] Santantonio, D., R.K. Hermann and W.S. Overton, "Root biomass studies in forest ecosystems," *Pedobiologia*, Bd. 17, pp. 1-21, 1977.

[70] Sarabandi, K., Pierce, L., Dobson, M.C., Ulaby, R.T., Stiles, J. et al., "Polarimetric calibration of SIR-C using point and distributed targets," *IEEE Transactions on Geosciences and Remote Sensing*, Vol. 33, No. 4, July 1995.

[71] Schimel, D.S., "Terrestrial biogeochemical cycles: global estimates with remote sensing," *Remote Sensing of Environment* Vol. 51 pp. 49-56, 1995.

[72] Schowengerdt, Robert A., *Techniques for image processing and classification in remote sensing*, New York : Academic Press, 1983.

[73] Schriever, J.R. and R.G. Congalton, "Mapping forest cover-types in New Hampshire using multi-temporal Landsat Thematic Mapper data", *ASPRS/ACSM Annual Convention and Exposition*, 15-19 February (New Orleans, Louisiana), Vol. 3, pp. 333-342, 1993.

[74] Sedjo, R.A., "Temperate forest ecosystems in the global C cycle," *Ambio*, Vol. 21, pp. 274-277, 1992.

[75] Sellers, P.J., B.W. Meeson, F.G. Hall, G. Asrar, R.E. Murphy, R.A. Schiffer, F.P. Bretherton, R.E. Dickinson, R.G. Ellingson, C.B. Field, K.F. Huemmrich, C.O. Justice, J.M. Melack, N.T. Roulet, D.S. Schimel, and P.D. Try, "Remote sensing of the land surface for studies of global change: models-algorithms-experiments," *Remote Sensing of Environment*, Vol. 51, pp. 3-26, 1995.

[76] Sellers, P. J. (ed.), *ISLSCP Workshop Report: Remote Sensing of the Land Surface for Studies of Global Change*, International Satellite Land Surface Climatology Project Workshop, June 23-26, 1992, Columbia, MD, NASA Goddard Space Flight Center, Greenbelt, MD, May 1993.

[77] *A Systems Analysis of the Global Boreal Forest*, ed. by H.H. Shugart, R. Leemans, and G.B. Bonan, Cambridge University Press, Cambridge, U.K., 1992.

[78] Stofan, E.R., D.L. Evans, C. Schmullius, B. Holt, J.J. Plaut, et al, "Overview of Results of Spaceborne Imaging Radar-C, X-Band Synthetic Aperture Radar (SIR-C/X-SAR)", *IEEE Trans. Geosci. Remote Sensing*, Vol. 33, No. 4, pp. 817-827, 1995.

[79] Tans, P.P., I.Y. Fung, and T. Takahashi, "Observational constraints on the global atmosphericCO_2 budget," *Science* (Washington, DC), Vol. 247, pp. 1431-1438, 1990.

[80] Tou, J.T., and R.C. Gonzalez, *Pattern Recognition Principles*. Addison-Wesley Publishing Co., 1974.

[81] Townshend, J., C. Justice, W. Li, C. Gurney, and J. McManus, "Global land cover classification by remote sensing: Present capabilities and future possibilities," *Remote Sensing of Environment*, Vol. 35 pp. 243-255, 1991.

[82] Ulaby, F.T., K. Sarabandi, K. McDonald, M. Whitt, and M.C. Dobson, "Michigan Microwave Canopy Scattering Model (MIMICS)," *International Journal of Remote Sensing*, Vol. 11, pp. 1223-1253, 1990.

[83] Ulaby, F.T., R.K. Moore, and A.K. Fung, *Microwave Remote Sensing*, Vol. III "From Theory to Applications," Artech, Dedham, MA, 1981.

[84] *Prototype 1990 conterminous US land cover characteristics data set CD-ROM*, USGS EROS Data Center, Sioux Falls, SD, 1993.

[85] Van Zyl, J.J., "Unsupervised classification of scattering behavior using radar polarimetry data", *IEEE Transactions on Geosciences and Remote Sensing*, Vol. 27, pp. 36-45, 1989.

[86] Vitousek, P.M., "Can planted forests counteract increasing atmospheric C dioxide?," *Journal of Environmental Quality*, Vol. 20, pp. 348-354, 1991.

[87] Way, J.B., E. Rignot, K. McDonald, R. Oren, R. Kwok, G. Bonan, M.C. Dobson, L. Viereck, and J.E. Roth, "Evaluating the type and state of Alaska taiga forests with imaging radar for use in ecosystem flux models", *IEEE Transactions on Geoscience and Remote Sensing*, Vol. 32, No. 2, pp. 353-370, 1994.

[88] Westlake, D.F., "Comparisons of plant productivity," *Biological Review*, Vol. 38, pp. 385-425, 1963.

[89] Whittaker, R.H., F.H. Bormann, G.E. Likens, and T.G. Siccama, "The Hubbard Brook ecosystem study: forest biomass and production," *Ecological Monographs*, Vol. 44 pp. 233-252, 1974.

[90] Whittaker, R.H. and P.L. Marks, "Methods of assessing terrestrial productivity," in *Primary productivity of the biosphere*, ed. by H. Lieth and R.H. Whittaker, Springer-Verlag, New York, NY. pp. 55-118, 1975.

[91] Whittaker, R.H. and G.E. Likens, "Primary production: the biosphere and man," in *Primary productivity of the biosphere*, ed. by H. Lieth and R.H. Whittaker, Springer-Verlag, New York, NY. pp. 305-328, 1975.

[92] Whittaker, R.H. and G.M. Woodwell, "Dimension and production relations of trees and shrubs in the Brookhaven Forest, New York," *Journal of Ecology*, Vol. 56 pp. 1-25, 1968.

[93] Willstäter, R. and A. Stoll, *Untersuchungen über die assimilation der kohlensaure*, Berlin: Springer-Verlag, 1918.

[94] Wolter, P.T., D.J. Mladenoff, G.E. Host, and T.R. Crow, "Improved Forest Classification in the Northern Lake States Using Multi-Temporal Landsat Imagery," *Photogrammetric Engineering and Remote Sensing*, Vol. 61, no. 9, pp. 1129-1143, 1995.

[95] Young, H.E., J.H. Ribe, and K. Wainwright. *Weight Tables for Tree and Shrub Species in Maine*, University of Maine, Orono, Life Sciences and Agricultural Experiment Station, Misc. Report No. 230, 1980.